PV Reference Cells for Outdoor Use: An Investigation of Calibration Factors

Anton Driesse
PV Performance Labs

NREL Technical Monitors: Peter Gotseff and Manajit Sengupta

NREL is a national laboratory of the U.S. Department of Energy
Office of Energy Efficiency & Renewable Energy
Operated by the Alliance for Sustainable Energy, LLC

This report is available at no cost from the National Renewable Energy Laboratory (NREL) at www.nrel.gov/publications.

Contract No. DE-AC36-08GO28308

Subcontract Report
NREL/SR-5D00-80437
September 2021

PV Reference Cells for Outdoor Use: An Investigation of Calibration Factors

Anton Driesse
PV Performance Labs

NREL Technical Monitors: Peter Gotseff and Manajit Sengupta

Suggested Citation
Driesse, Anton. 2021. *PV Reference Cells for Outdoor Use: An Investigation of Calibration Factors*. Golden, CO: National Renewable Energy Laboratory. NREL/SR-5D00-80437. https://www.nrel.gov/docs/fy21osti/80437.pdf.

NREL is a national laboratory of the U.S. Department of Energy
Office of Energy Efficiency & Renewable Energy
Operated by the Alliance for Sustainable Energy, LLC

This report is available at no cost from the National Renewable Energy Laboratory (NREL) at www.nrel.gov/publications.

Contract No. DE-AC36-08GO28308

Subcontract Report
NREL/SR-5D00-80437
September 2021

National Renewable Energy Laboratory
15013 Denver West Parkway
Golden, CO 80401
303-275-3000 • www.nrel.gov

NOTICE

This work was authored in part by the National Renewable Energy Laboratory, operated by Alliance for Sustainable Energy, LLC, for the U.S. Department of Energy (DOE) under Contract No. DE-AC36-08GO28308. Funding provided by U.S. Department of Energy Office of Energy Efficiency and Renewable Energy Solar Energy Technologies Office. The views expressed herein do not necessarily represent the views of the DOE or the U.S. Government.

Acknowledgments

This work was authored by Anton Driesse of PV Performance Labs Germany for Alliance for Sustainable Energy, LLC, the manager and operator of the National Renewable Energy Laboratory for the U.S. Department of Energy (DOE) under Contract No. DE-AC36-08GO28308.

The author gratefully acknowledges the contributions of the National Renewable Energy Laboratory's (NREL's) Solar Radiation Research Laboratory Afshin Andreas, who spent countless hours on acquiring, mounting, wiring, configuring, and ensuring the correct operation of the many sensors before, during, and after the Broadband Outdoor Radiometer Calibration events; as well as Manajit Sengupta and Aron Habte for providing funding, organization, and many strategic discussions.

The contribution of Tao Song at NREL's Cell Lab was also much appreciated. Without their many measurements, this comparison would not have been possible.

List of Acronyms

BORCAL	Broadband Outdoor Radiometer Calibration
BORCAL-SW	Broadband Outdoor Radiometer Calibration, short-wave
IAM	incidence angle modifier
IEC	International Electrotechnical Commission
NREL	National Renewable Energy Laboratory
PTB	Physikalisch-Technische Bundesanstalt
PV	photovoltaic
R@45	BORCAL responsivity for a horizontal instrument, 45° zenith
R'@30	BORCAL adjusted responsivity for a horizontal reference cell, 30° zenith
SMARTS	Simple Model of the Atmospheric Radiative Transfer for Sunshine
SMM	spectral mismatch factor
SRRL	Solar Radiation Research Laboratory
TC	temperature coefficient
TCOR	temperature correction
WPVS	World Photovoltaic Scale
WRR	World Radiometric Reference

Executive Summary

Reference cells are widely used in the photovoltaic (PV) industry to measure irradiance. For field applications and outdoor use, a variety of products are on the market, and they are often perceived as a low-cost alternative to thermopile radiometers. But reference cell characteristics differ substantially from the latter, therefore measurements made by one category of instrument cannot be substituted for or directly compared with the other.

The National Renewable Energy Laboratory's (NREL's) Solar Radiation Research Laboratory is currently in a multiyear effort to develop guidance and recommendations for the design and use of outdoor reference cells, with a view to reducing inconsistencies and measurement uncertainty of the solar PV resource. The core of this effort is the long-term deployment of 39 units of 10 distinct types made by 6 manufacturers. This report compares the calibration factors provided by manufacturers—which most users rely upon—to those measured at a high level of accuracy by NREL's Cell Lab. It also reports on the application of the Broadband Outdoor Radiometer Calibration (BORCAL) method to reference cells.

As a group, the factory calibrations for the crystalline silicon cells when compared to the Cell Lab showed a small positive bias of +0.7%, with a tight distribution around this value. This is a very good result for the manufacturers. The two World Photovoltaic Scale cells constituted outliers, with a mean deviation of −0.8%, which is still within the reported uncertainty ranges.

The data collected during the BORCAL procedures show a strong and systematic fluctuation of the apparent responsivity of the reference cells over the course of a day, which was anticipated. Consequently, the standard BORCAL *R@45* calibration factors underestimated the reference cell responsivities by 1%–4%. An alternate responsivity indicator was developed, *R'@30*, incorporating adjustments for temperature response, spectral response, and directional response. This reduced the mean deviation to −0.4% compared to the Cell Lab. Further, two independent BORCAL events were able to produce the same values to within ±0.2%. This could be a viable approach for verifying reference cells using existing BORCAL infrastructure, for example, to evaluate their long-term stability.

The daily profiles of responsivity obtained during the BORCAL events (provided in Appendix B) show clear patterns of differences between models, which provides evidence that their directional responses differ from each other; thus, two sensors that are calibrated correctly might give the same reading at 30° zenith angle but systematically different readings at 60°. The impact of these inconsistencies in field operation will be quantified using the long-term observations started in 2020.

Table of Contents

List of Figures

List of Tables

1 Introduction

The National Renewable Energy Laboratory's (NREL's) Solar Radiation Research Laboratory (SRRL) is expanding its effort to deploy, measure, and evaluate various photovoltaic (PV) reference cells and pyranometers at different plane-of-array orientations and at multiple locations. The purpose is to develop new methods/processes and to improve the accuracy (based on using standard thermopile radiometers) from the current uncertainty levels by investigating methods to (1) calibrate reference cells and (2) accurately quantify the PV resource by considering various sources of uncertainty, such as the spectral response and directional response or angle-of-incidence effects (Habte et al. 2018). In general, better PV resource measurements enable stakeholders to more accurately estimate PV power production as well as better define its uncertainty. This, in turn, leads to improvements in the return on investment of PV projects and reductions in the price of solar electricity.

Commercial reference cells tend to be low-cost devices (with exceptions) and adhere to fewer standards than pyranometers. In this overall effort, we aim to develop recommendations for moving toward more standardized devices and procedures. To gain the needed insight into current reference cell products, SRRL has purchased and deployed 39 sensors of 10 distinct types produced by 6 different manufacturers. This first report explores the topic of calibration through a comparison of calibration factors (also referred to as *responsivity*) obtained from three different sources by different methods. The first set of values are the calibration factors provided by the manufacturers; the second set were determined by NREL's PV Cell Performance Calibration Lab (Cell Lab; also referred to as CellCal); and several additional calibration factors were obtained during three Broadband Outdoor Radiometer Calibration (BORCAL) events using two different data processing methods. The outdoor BORCAL method (Andreas and S. M. Wilcox 2016) has been used for many years to calibrate broadband thermopile pyranometers, and it is also used for photodiode pyranometers that are designed to emulate the former. Because reference cells are expressly designed to have different characteristics, BORCAL is not ideally suited for calibrating reference cells; nonetheless, we carried out the procedure to see what we could learn. In the process, we developed an alternate BORCAL data processing method that substantially improves the agreement with the Cell Lab calibrations.

The accuracy of calibration factors directly influences the accuracy of irradiance measurements; hence, the observations in this report make an important contribution to our understanding of reference cell measurement uncertainty.

2 Devices Tested

Over the course of 2019, SRRL acquired a substantial number of commercial reference cell products of varying designs and from different manufacturers. (See Table 1.) They were purchased from six different manufacturers from the United States, United Kingdom, and Germany. Although in principle they are sold for the same purpose—to measure solar irradiance in a PV system context—they differ substantially in the size and type of cells, style and materials of the enclosure, mounting method, temperature sensing, and electrical interface. Nevertheless, most used monocrystalline silicon cells and most were laminated under smooth, low-iron float glass. Several polycrystalline cells were also included to investigate to what extent these might perform differently, whereas the filtered cell from Atonometrics and the amorphous cell from IKS Photovoltaik were included to see whether they offer any unique benefits. These cells are flagged by the letters P, F, and A, respectively, where relevant. Four of these models were evaluated in a previous study (Driesse and Zaaiman 2015), which creates additional opportunities for comparison.

Table 1. Sensor Types Under Evaluation

Company	Model	Subtype	Flag
Atonometrics	810226-02	Mono	
Atonometrics	810226-03	Filtered (for CdTe)	F
EETS	RC01	Mono	
Fraunhofer	511311102	Mono	
IKS Photovoltaik	ISET	Mono	
IKS Photovoltaik	ISET-aSi	Amorphous	A
IKS Photovoltaik	ISET-poly	Poly	P
IMT	Si-mV-85-PT1000	Mono	
NES	SOZ-03	Mono	
NES	SOZ-03-P	Poly	P

2.1 Preconditioning

It is well-known that mono- and multicrystalline silicon PV modules can exhibit an initial degradation during a short period of initial exposure to light, a phenomenon called light-induced degradation (LID). The same is possible for reference cells made using these materials; therefore, all units, before any calibrations or measurements at NREL, were placed outdoors on the calibration benches for several full days until the accumulated radiation reached or exceeded 5 kWh/m^2. The amorphous cells received the same preconditioning, but they are not expected to reach the same degree of stability that the crystalline cells can achieve because of their inherently metastable characteristics.

3 Calibration Procedures

The calibration factor, or *responsivity*, for a reference cell is defined at standard test conditions with a cell temperature of 25°C, with normally incident illumination having the AM1.5G spectral distribution and an intensity of 1000 W/m². Under those conditions, a pyranometer and a reference cell produce the same reading of 1000 W/m^2, and traceability to the World Radiometric Reference (WRR) is thus made possible, as described in International Electrotechnical Commission (IEC) 60904-4.

3.1 Manufacturers

The manufacturers of the commercial reference cells use a variety of procedures to calibrate their products. Most often a working reference device is sent for calibration at a specialized lab—such as NREL, Fraunhofer ISE, or Physikalisch-Technische Bundesanstalt (PTB)—and the manufacturer then performs a calibration transfer to their products, in some cases indoors and in other cases outdoors. Conformity with IEC 60904-2 (IEC 2015) is claimed by some manufacturers, and calibration uncertainties quoted in their documentation range from 1.4%−3.0%.

3.2 NREL Cell Lab (Indoor)

NREL's Cell Lab follows standardized procedures to provide reference cell calibrations with the lowest possible uncertainty (IEC 2015; IEC 2019). The relative spectral response of each cell is measured separately to make individual spectral mismatch corrections. The final uncertainty of these calibrations is assessed at 0.9% (k=2) (Emery 2009).

3.3 BORCAL-SW (Outdoor)

The NREL BORCAL-SW (Broadband Outdoor Radiometer calibration, Short-Wave) procedure is an established method to calibrate broadband thermopile pyranometers in a horizontal position with traceability to the WRR. The reference irradiance is calculated from a DNI measurement using an absolute cavity radiometer and a diffuse horizontal measurement using the best available instrument and correction techniques.

The procedure produces a single calibration factor, which equals the responsivity at a solar zenith angle 45° (R@45) as well as a table of responsivities for a range of zenith angles (R@Z). R@45 is optimal for horizontal diffuse irradiance measurements because in an isotropic sky, the largest contribution comes from the sky dome at an elevation of 45°, but R@45 is also routinely used for global horizontal irradiance measurements when the data acquisition system cannot accommodate multiple responsivity values. The expanded uncertainty for R@45 varies by instrument and calibration conditions, but it can be as low as 1% for high-quality Class A pyranometers.

The use of the BORCAL procedure for reference cells is experimental, and the resulting calibration factors are not formally traceable to the WRR.

4 Comparison of Factory Calibrations to NREL's Cell Lab

This section examines the difference between the factory calibrations and those of NREL's Cell Lab. Figure 1 shows these results color-coded by manufacturer. The largest outliers are the two amorphous cells from IKS (marked by the A), which are at the upper end of the scale at +6.6 and +9.3%. Not having investigated their initial stability or metastability, it is best to interpret these differences as suspect. Also, the date on the original factory calibrations is in 2012.

The second largest outliers are the pair of filtered monocrystalline cells from Atonometrics (marked by the F). The factory calibration certificates indicate that they were calibrated outdoors using a monocrystalline cell as reference; therefore, the difference is probably a result of spectral mismatch.

The cells marked by the P are polycrystalline cells. The one NES polycrystalline cell could be considered a minor outlier, but it was retested and found to be in line with its sister cell. The IKS poly cells lie within the range observed for the IKS mono cells.

The next two visual outliers are the two World Photovoltaic Scale (WPVS) cells from Fraunhofer ISE. The difference between the NREL and Fraunhofer calibrations is not excessive, but it is the negative sign of the difference that makes them outliers: The Fraunhofer calibrations are 0.6 and 1.0% *lower* than those from NREL, whereas most factory calibrations are *higher* than those from NREL. Note that IKS and NES obtain their reference calibrations from Fraunhofer, but their deviations with respect to the NREL calibrations are in the opposite direction from the Fraunhofer deviation. It is not evident how such a bias could have arisen.

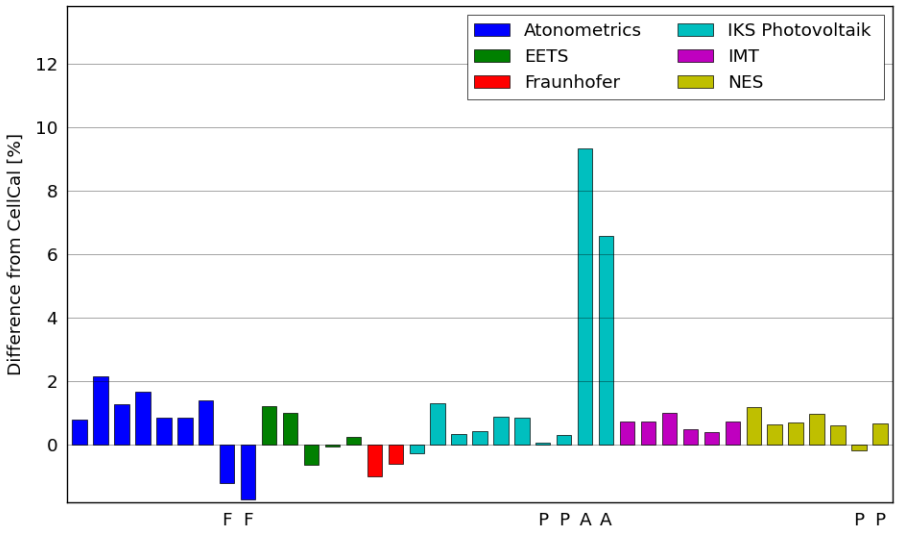

Figure 1. Deviation of factory calibrations from NREL's Cell Lab calibrations

(F: filtered, P: polycrystalline, A: amorphous)

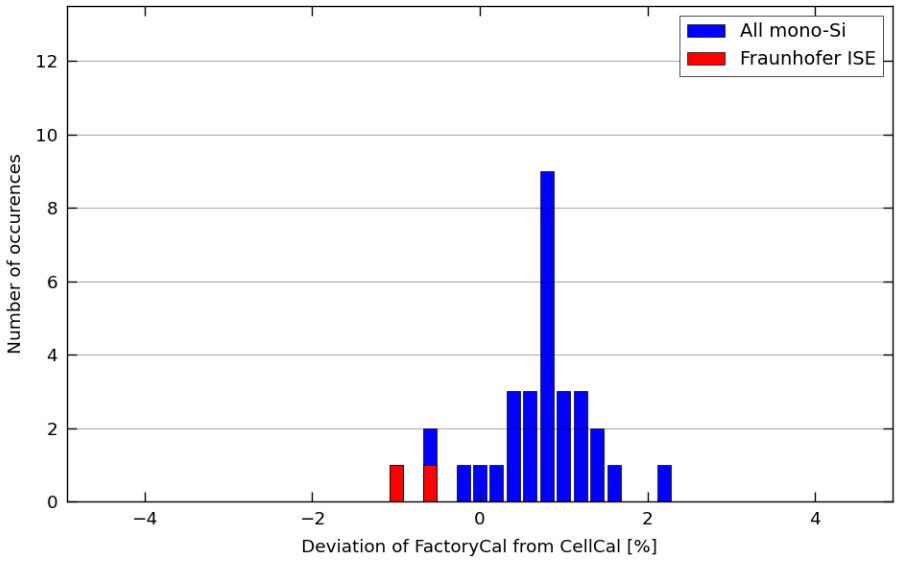

Figure 2. Distribution of the difference between the factory and NREL's Cell Lab calibrations for monocrystalline cells, showing a small positive bias of 0.8%

The overall positive bias of the factory calibrations is clearly shown in the histogram in Figure 2, which includes only the monocrystalline cells. The median value is approximately 0.8%. Even with the apparent bias, however, all these differences fall within the range of expectations, given that the NREL calibrations have an uncertainty of approximately 0.9% (k=2) and the other parties quote uncertainties ranging from 1.4%–3.0%. (Full details are provided in Appendix A.)

5 BORCAL Procedure and Reference Cell Corrections

In BORCAL, pyranometers are calibrated in a horizontal position, which means that beam radiation never strikes the receiving surface at normal incidence (in Colorado). Both the reference irradiance and the pyranometers have a nominally Lambertian directional response; therefore, only relatively small variations in responsivity are observed as a function of solar Zenith angle. (For some instruments, these variations can be quite significant despite being small.)

For reference cells, however, the variation of responsivity with zenith angle is very pronounced. Figure 3 shows such a curve from the BORCAL report for one of the IMT cells.

Figure 1. Responsivity vs Zenith Angle

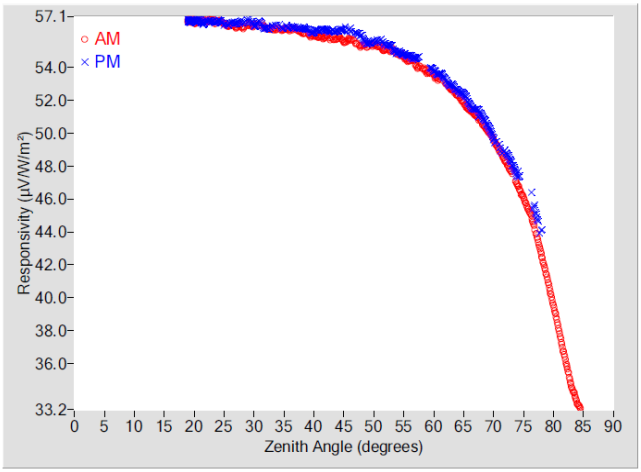

Figure 3. Responsivity vs. solar zenith angle for a sample IMT cell

It is clear from this graph and others like it that the value at zenith angle 45° lies well below the extrapolated value at normal incidence (zenith=0°), which would be required for calibration at standard test conditions. It is hardly surprising, therefore, that the reported R@45 values from BORCAL are systematically lower than the responsivities reported by NREL's CellLab. (See Figure 9.)

At this point, it might be tempting to extrapolate the responsivity curve to a zenith value of 0°, but the observed zenith response is actually the combined influence of multiple external variables that evolve over the course of each day:

- Incidence angle of beam radiation
- Diffuse fraction of global irradiance
- Hemispheric distribution of diffuse irradiance
- Spectral irradiance of beam and diffuse irradiance
- Temperature of the cell.

Thus, the zenith response curve represents multiple phenomena that will not necessarily be the same during each BORCAL event, and a simple extrapolation could not guarantee a consistent responsivity value.

A more analytical approach would be to calculate the expected influence of each external variable and adjust the measured signal, similar to the way thermopile readings are adjusted in BORCAL-SW using

a calculated thermal offset. This approach requires additional measurements of diffuse and spectral irradiance and cell temperature as well as information about the response of the cells to those variables. Essentially, the directional response, spectral response, and temperature response need to be determined in advance. Fortunately, most of this information is available at NREL.

The following three sections describe the corrections that were calculated and applied to the PV reference cell readings.

5.1 Temperature Response

For most purposes, the short-circuit current (I_{sc}) of PV cells—and hence the output signal of reference cells—is considered to vary linearly with temperature, and the temperature coefficient, dI_{sc}/dT (also referred to as α), is assumed to be constant. The primary reason for this temperature dependency is the decrease in bandgap energy with increasing temperature, which broadens the spectral response toward the infrared (Osterwald et al. 2015). Thus, the temperature coefficient is not constant but varies with both temperature and spectral distribution of incident irradiance. Figure 4 shows the partly modeled change in temperature coefficient with temperature for a silicon PV cell using several different standard spectra (Driesse 2018).

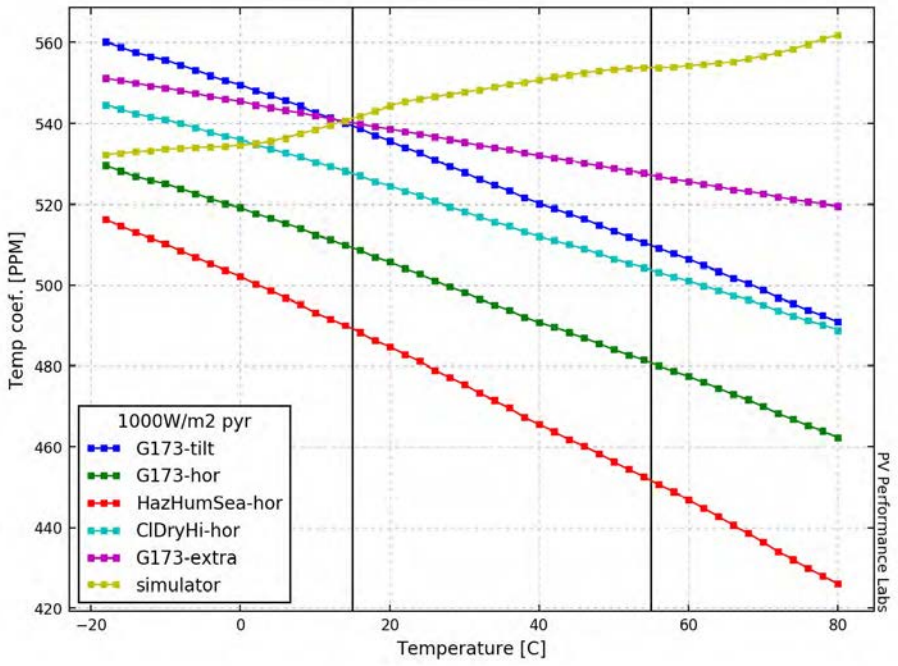

Figure 4. Variation of the temperature coefficient of Isc (TC) with temperature for a silicon PV cell under various spectra

These modeled characteristics are based on spectral response measurements at 15°C, 25°C, 35°C, and 55°C and are extrapolated outside this range. Figure reproduced from Driesse (2018).

The range of operating temperatures and variations in spectral irradiance during BORCAL are smaller than for field operations; therefore, the assumption of a constant value for dI_{sc}/dT (referred to as TC from here on) is reasonable. This behavior will be further investigated in the long-term field measurements.

The uncertainty associated with the I_{sc} temperature coefficient measurements is quite large. In a recent round-robin report (Salis et al. 2019), top laboratories provided uncertainty estimates ranging from 100–200 ppm (k=2) for their measurements on a variety of test objects. For our cells, the uncertainty would be larger because the variety of enclosure styles and materials make it difficult to control the cell temperature, and it is more difficult to measure the short-circuit current across a built-in shunt resistor with high accuracy. Thus, the variations in measured TC shown in Figure 5 by up to 100 ppm for reference cells of the same cell type are statistically not very significant. Nevertheless, for the purpose of adjustments to our measured signals, we chose to use the per-instrument temperature coefficient values measured at NREL when possible because they are traceable.

Figure 5 also shows a large discrepancy between the manufacturers' specifications and the measured TC for the filtered cells, marked by the F, and the polycrystalline cell, marked by the P. In fact, the measured coefficients for the filtered cells are reported by the manufacturer to be negative, but they are measured in the lab to be positive. These differences should be investigated in future work.

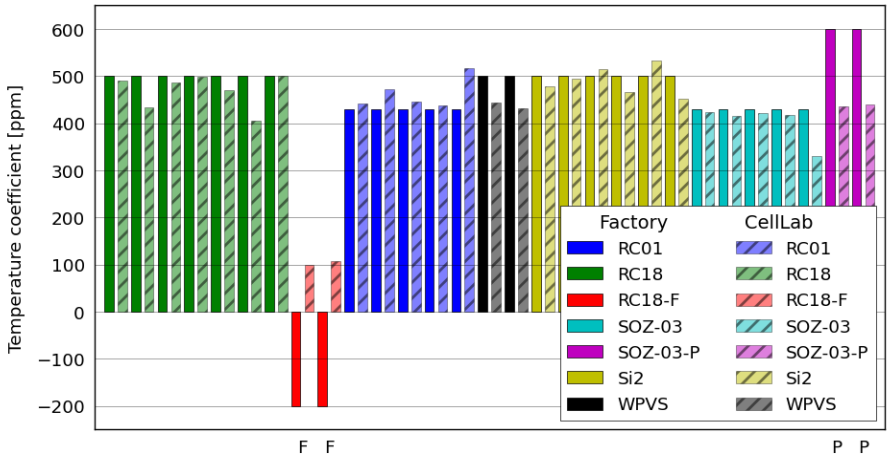

Figure 5. Comparison of temperature coefficients from manufacturers to NREL's CellLab

To compensate for the temperature dependency, the temperature correction factor is given by:

$$TCOR = 1 + (TC * (T_{cell} - 25))$$

where T_{cell} is the measured temperature of each device (or an adjacent unit of the same type).

5.2 Spectral Response

Differences in the spectral response between PV devices and/or broadband radiometers are generally accounted for by *spectral mismatch* factors (SMMs). These are described in multiple standards, such as ASTM (2016). The SMM calculation requires the spectral response of each reference cell, which was measured at NREL's Cell Lab for the indoor calibration; and also the spectral distribution of the solar irradiance during the outdoor measurements, which is recorded year-round as part of the SRRL Baseline Measurement System.

One small shortcoming of the available spectral measurements is that the wavelength range extends from 290−1650 nm, and thus it does not cover the full range of the measured broadband irradiance. To estimate the spectral distribution in the unmeasured range, we simulated the clear-sky spectra ranging

from 280−4000 nm using the Simple Model of the Atmospheric Radiative Transfer for Sunshine (SMARTS), taking into account the local observed aerosol optical depth, surface pressure, surface albedo, and solar zenith angle. Other values, such as precipitable water vapor and ozone, were estimated. The magnitudes of the simulated spectra were then scaled to match the measured spectra in the overlapping wavelength region, and finally the simulated values ranging from 1650−4000 were appended to the measured spectra. The measured energy ranging from 280–290 and exceeding 4000 nm was taken to be zero.

With this additional information, an SMM factor was calculated for each reference cell for each time step of the BORCAL data.

5.3 Directional Response

Reference cells have a flat receiver (the PV cell) and a flat window covering this receiver. For all the products in our tests, this window is made of glass—usually smooth, but sometimes textured, as many PV modules are. Because of differences in refractive index, some light is reflected when passing through the air-glass interface (and at other material interfaces as well), and more light is reflected at higher angles of incidence, as predicted by the well-known Fresnel equations (Duffie and Beckman 2006, chap. 5). Although the overall directional response or incidence angle modifier (IAM) can be quite complex, the dominant factor is the first reflection at the air-glass interface.

Unlike the temperature and spectral response, NREL was not able to measure the individual directional response of each reference cell. We therefore calculated theoretical IAM factors for beam irradiance based on the single air-glass interface and used an effective incidence angle of 60 for the diffuse irradiance. The pvlib-python implementation (Holmgren, Hansen, and Mikofski 2018) of the equations from Duffie and Beckman (2006) was used to perform these calculations using a value of 1.526 for the refractive index of glass.

5.4 Responsivity After Corrections

Figure 6 demonstrates how the three correction factors evolve over the course of a BORCAL day. For zenith angles less than 30°, the three correction factors evolve very gradually and even partially cancel each other out. Beyond 40°, however, the IAM clearly becomes the dominant factor.

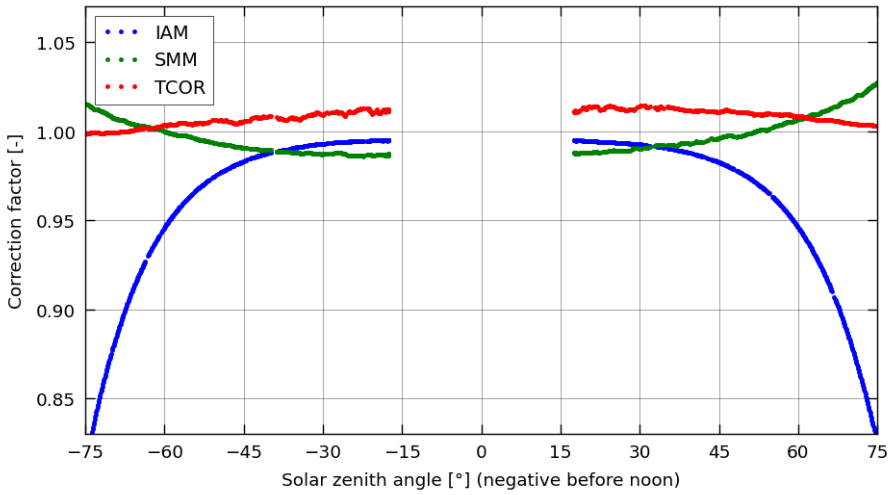

Figure 6. Example of the three correction factors over the course of a day

Dividing the device's output signal by the three factors IAM, SMM, and temperature correction (TCOR) translates the measured signal to standard conditions: normal incidence, AM1.5G spectrum and 25°C, and further dividing by the reference irradiance gives the corrected responsivity R_{corr}. The two examples in Figure 7 clearly show that the correction procedure succeeds in transforming the uncorrected responsivity, R (blue scatter points), into values with much greater consistency over the course of the day, R_{corr} (green scatter points).

Nevertheless, some diurnal variation remains, so the question arises how to determine the most appropriate single representative responsivity value from these data. The following aspects are considered:

- It is preferable to take this at a small zenith angle to avoid large IAM correction factors.
- The angle must be large enough that it can be reached during the entire BORCAL season.
- Because there is some variability in the individual readings, is it better to combine multiple values over a range of angles.

On the basis of these considerations, the following procedure was chosen:

- Fit a straight line to the *morning* data in the zenith angle ranging from 25°–35°.
- Fit a straight line to the *afternoon* data in the zenith angle ranging from 25°–35°.
- Interpolate the value for R_{corr} at 30° on each line.
- Take the average of the two interpolated values as *R'@30*.

Figure 7 shows the original BORCAL R@45 and new R'@30 as the dashed lines in the same color as the scatter points on which they are based (blue and green, respectively). In addition, the factory and Cell Lab calibration factors are shown as solid lines for comparison and the scale on the right side shows the percentage deviation from the CellCal responsivity to facilitate a visual comparison. The upper example shows one of the better results where corrections produced a nearly constant responsivity (green points) that is quite close to both the factory and Cell Lab calibrations. The lower example shows a case where the corrections did not remove systematic effects quite as well, but R'@30 nevertheless comes very close to the CellCal value.

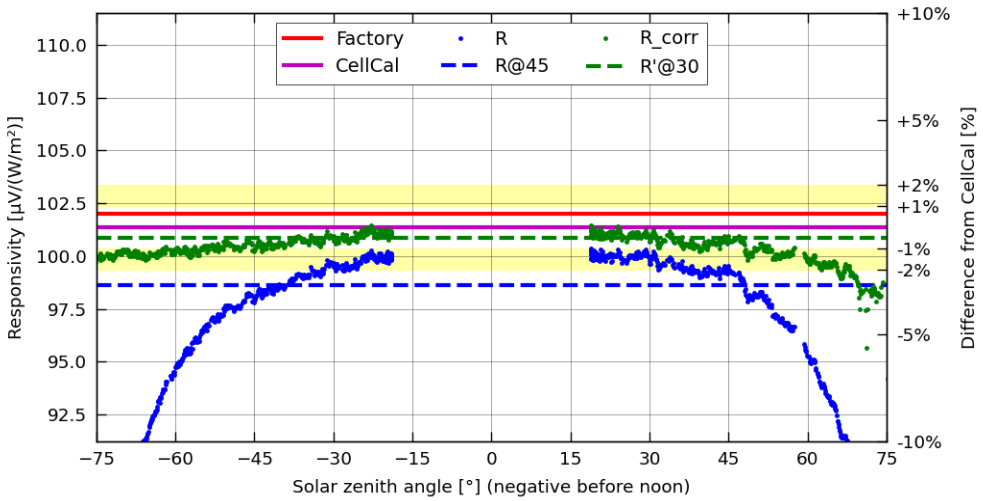

(a) Detailed results for NES SOZ-03 s/n 14313 obtained during Borcal session 2019-04

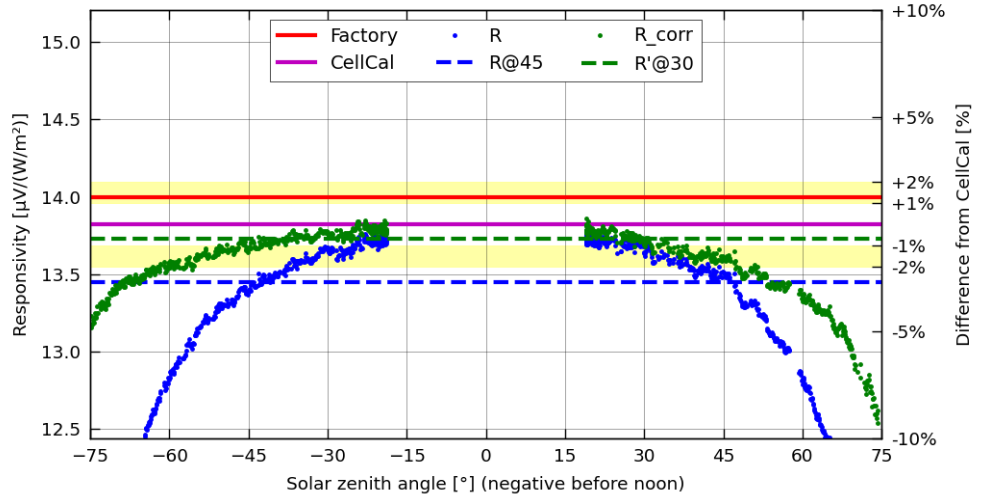

(b) Detailed results for Atonometrics 810226-02 s/n 10621 obtained during Borcal session 2019-04

Figure 7. Examples of the original BORCAL and corrected responsivity factors over the course of a day

Each graph is centered on the CellCal value. The yellow shaded regions represent deviations of 1.0%–2.0% from CellCal.

Appendix B provides 65 graphs such as these for each reference cell and for each BORCAL event. They demonstrate that the remaining systematic variations with Zenith angle vary substantially by product type. The probable reason for the differences is the physical design of the products, such as the dimensions of a raised edge (if any) and the size of the glass window in relation to the size of the cell. Variations in a.m./p.m. symmetry are at least in part caused by the imperfect instrument leveling, but asymmetry can be observed in the positioning of the cells of some units as well.

6 BORCAL Results and Comparisons

The reference cells were mounted outside horizontally for an extended period in order to participate in multiple BORCAL events in 2019 (BC03, BC04, and BC05). For logistical reasons, this deployment occurred in phases, so there are between one and three BORCAL results for each unit.

6.1 Repeatability Between Events

Repeatability is an important requirement for any calibration procedure. By comparing calibration factors found during two BORCAL events, we get a first look at this aspect. The difference is generally less than 0.5% for the uncorrected R@45 values (upper plot in Figure 8), but there is an obvious bias of approximately 0.3% between the two events. The repeatability of R'@30—after corrections—is much better and virtually without systematic bias (lower plot in Figure 8). Note also that the difference between BORCAL events for the two Fraunhofer ISE WPVS cells was extremely small in both cases.

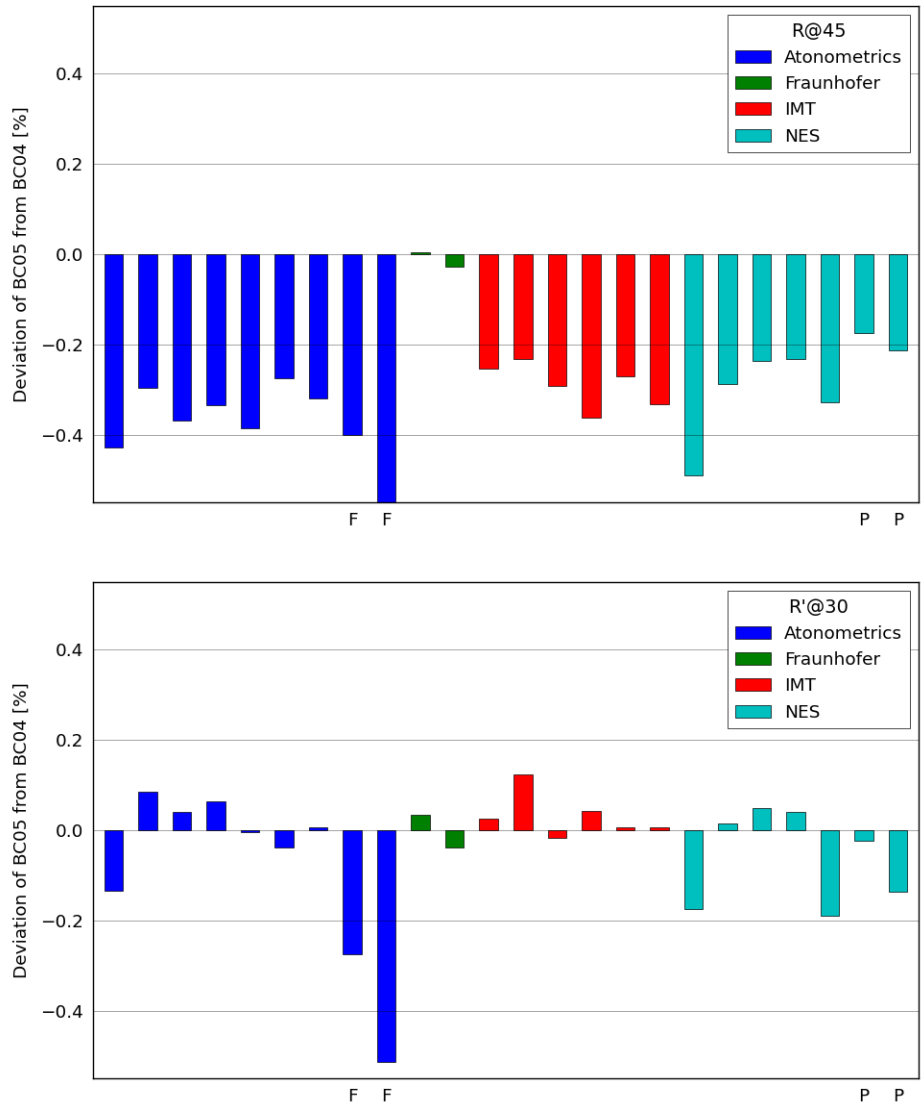

Figure 8. Differences in calibration factors between BORCAL events 4 and 5

The upper figure is based on BORCAL R@45, and the lower figure is based on BORCAL R'@30. The repeatability of R'@30 is much better than that of R@45.

6.2 Comparison to NREL's Cell Lab Calibrations

The discussion in the previous chapter and the example shown in Figure 7 lead us to expect that R@45 will systematically underestimate the true responsivity. The comparison between the BORCAL and CellCal values in the upper plot of Figure 9 confirms that this underestimation ranges from −1% to −4%. The lower plot shows that the distribution of the deviations for the new calibration factor R'@30 is both narrower and much closer to zero. The mean deviation is only −0.4% with respect to the CellCal, and there is also a much lower standard deviation of 0.5%.

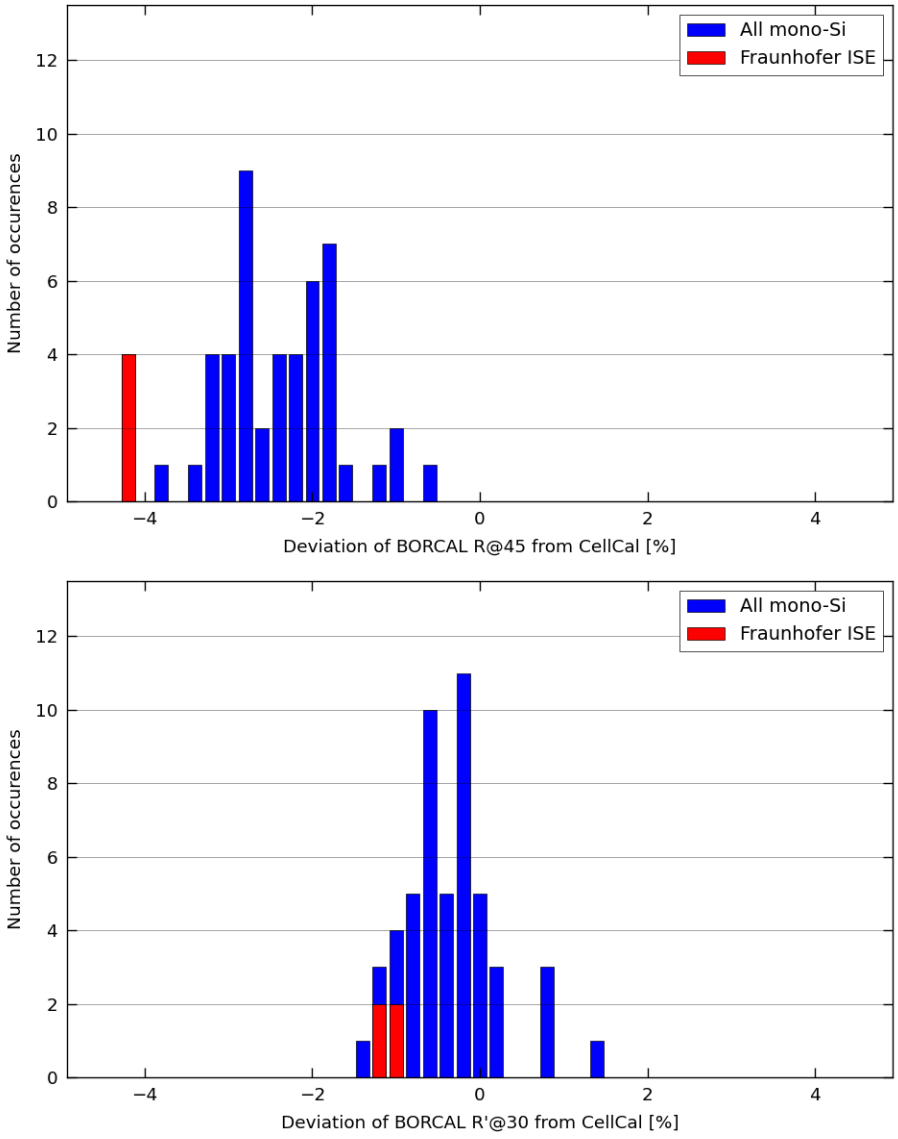

Figure 9. Differences between the BORCAL and NREL's Cell Lab calibrations for monocrystalline cells

The upper figure is based on BORCAL R@45 and shows a negative bias >2%. The lower figure is based on the BORCAL R'@30 responsivities and shows a negative bias of <1% as well as a smaller spread.
The Fraunhofer ISE cells, which were outliers in the upper graph, are much closer to the median now.

6.3 Comparison of BORCAL and Factory Values to NREL's Cell Lab

Figure 10 through Figure 15 shows all the calibration results for all the manufacturers.

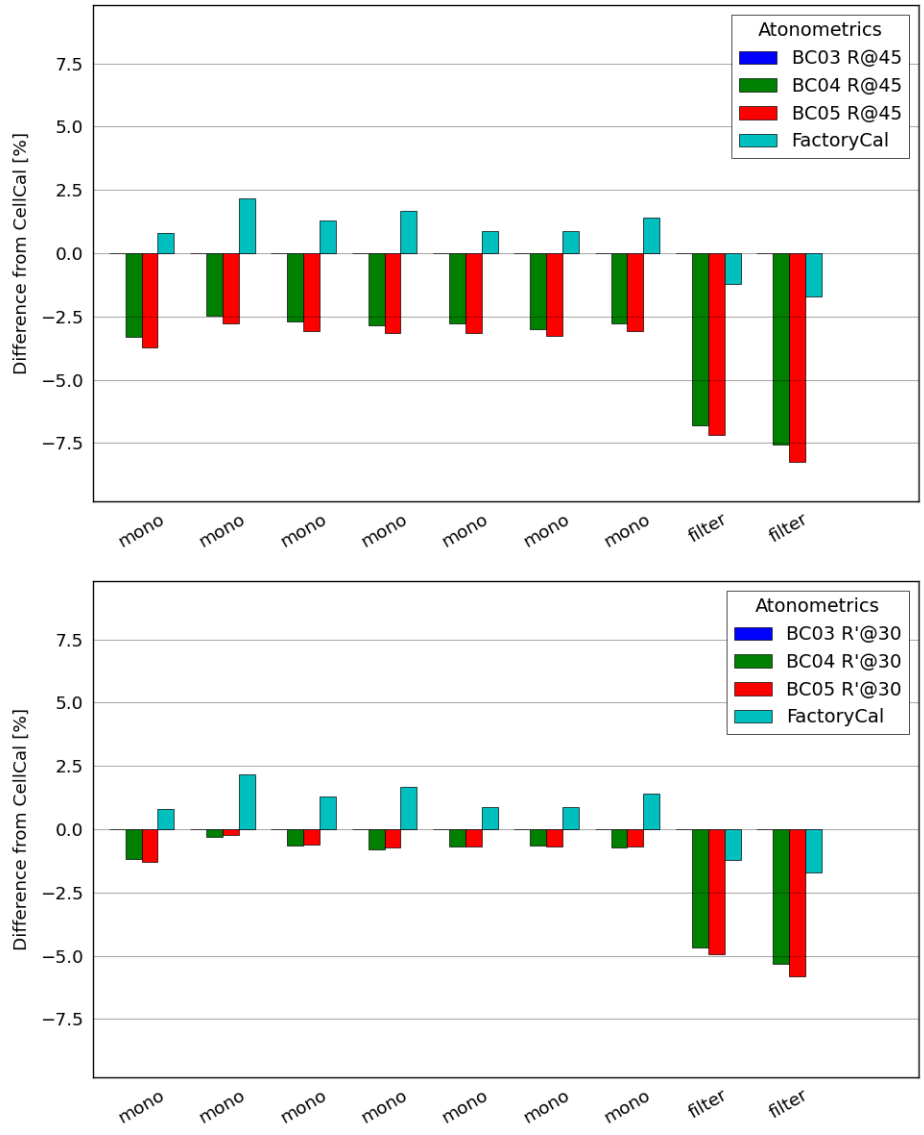

Figure 10. Comparison of all calibrations for cells supplied by Atonometrics

The upper figure is based on BORCAL R@45, and the lower figure is based on BORCAL R'@30.

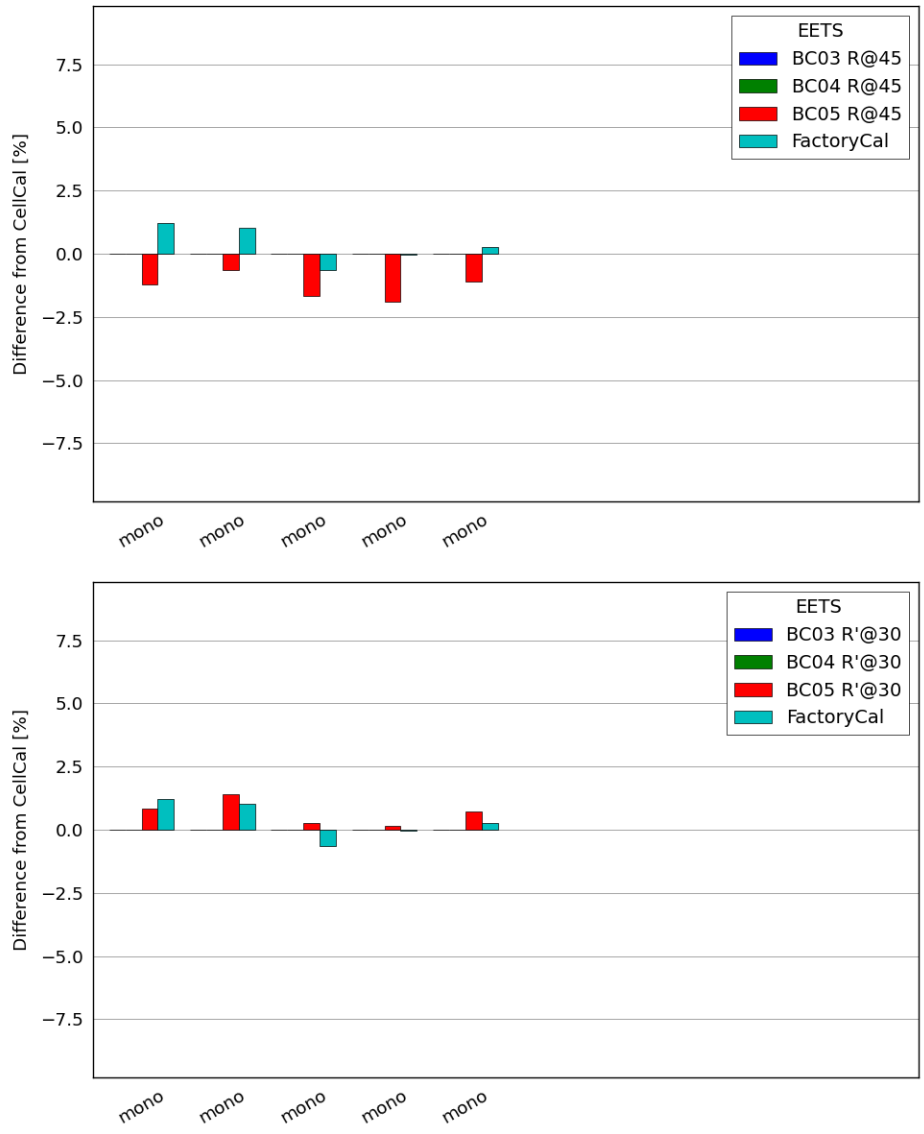

Figure 11. Comparison of all calibrations for cells supplied by EETS

The upper figure is based on BORCAL R@45, and the lower figure is based on BORCAL R'@30.

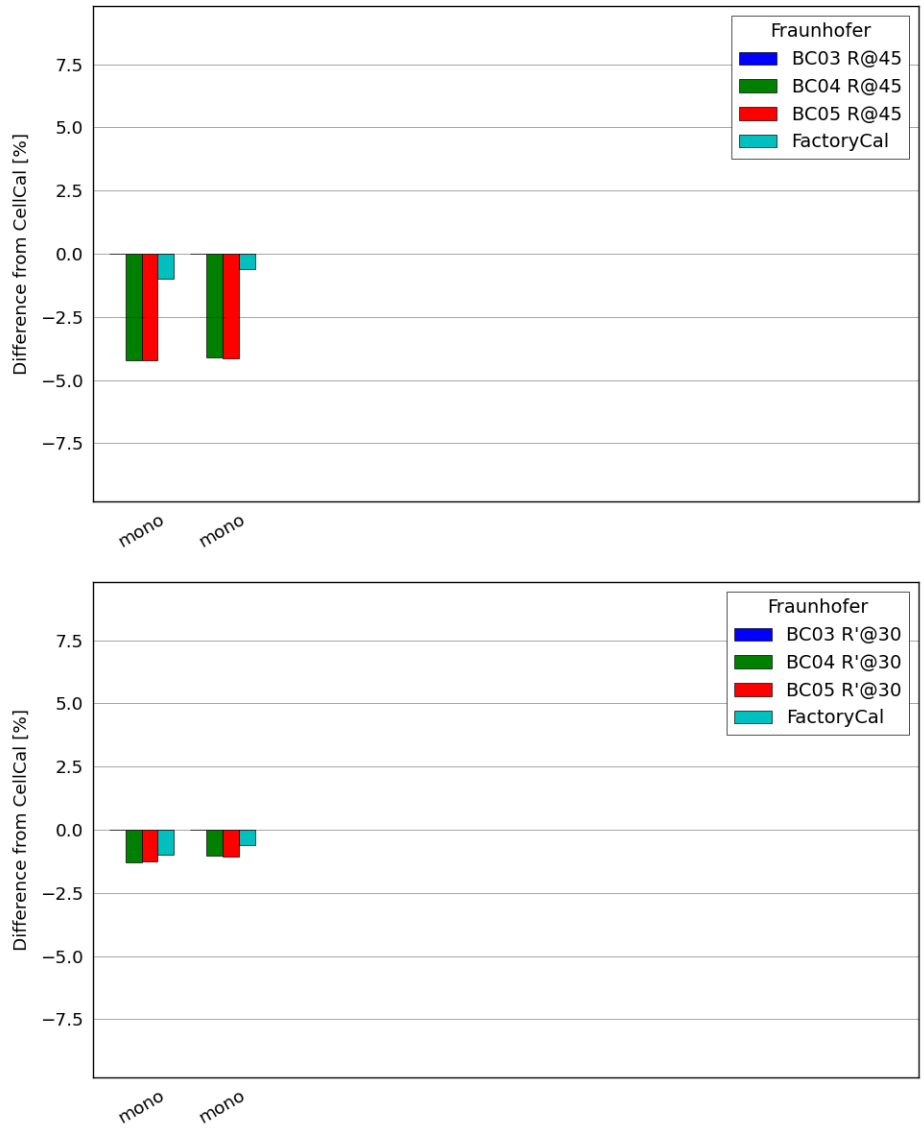

Figure 12. Comparison of all calibrations for cells supplied by Fraunhofer ISE

The upper figure is based on BORCAL R@45, and the lower figure is based on BORCAL R'@30.

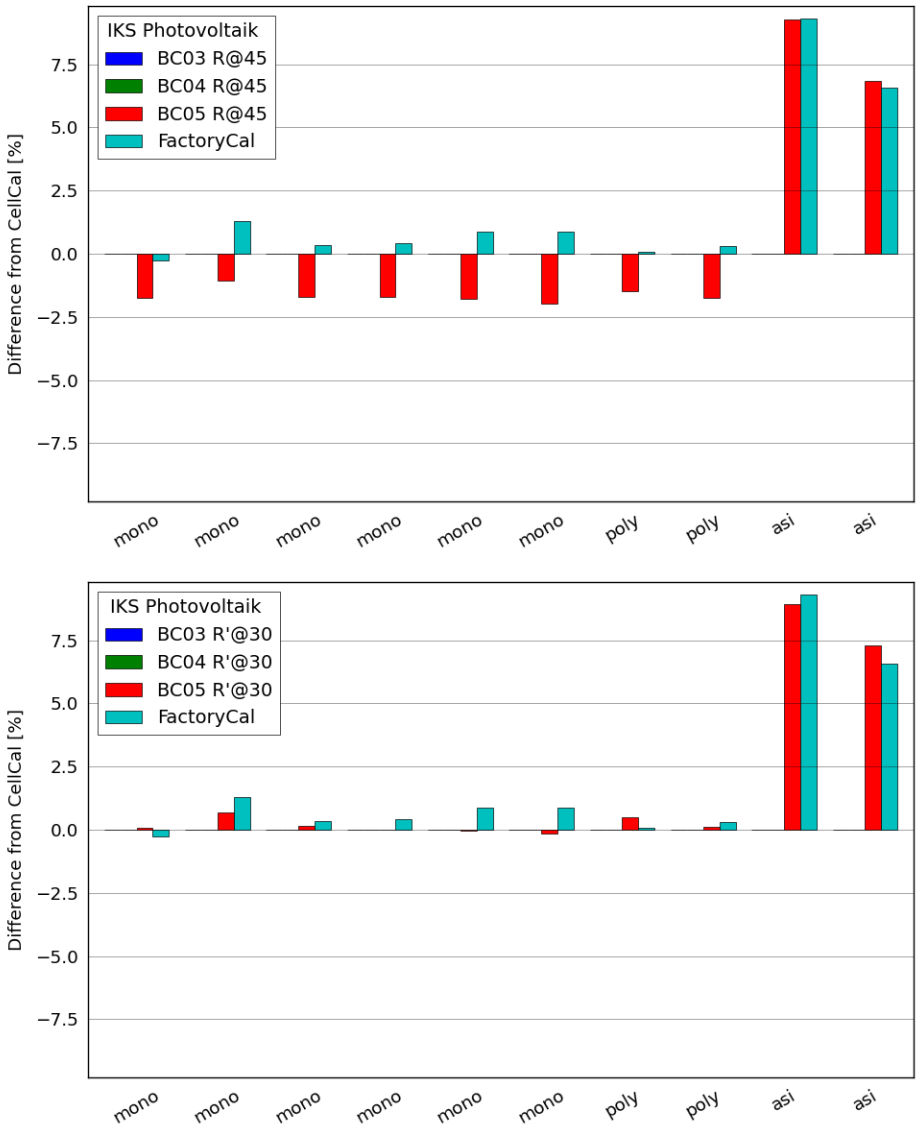

Figure 13. Comparison of all calibrations for cells supplied by IKS Photovoltaik

The upper figure is based on BORCAL R@45, and the lower figure is based on BORCAL R'@30.

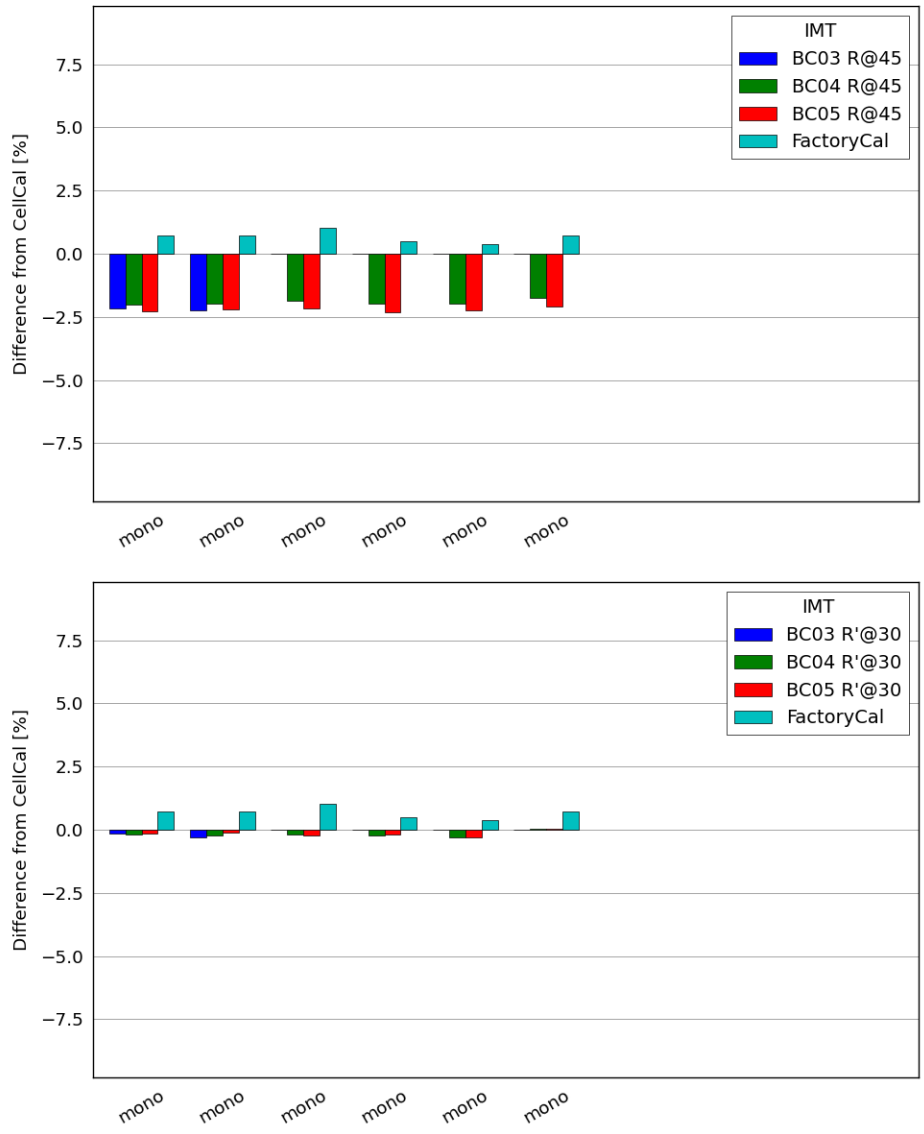

Figure 14. Comparison of all calibrations for cells supplied by IMT

The upper figure is based on BORCAL R@45, and the lower figure is based on BORCAL R'@30.

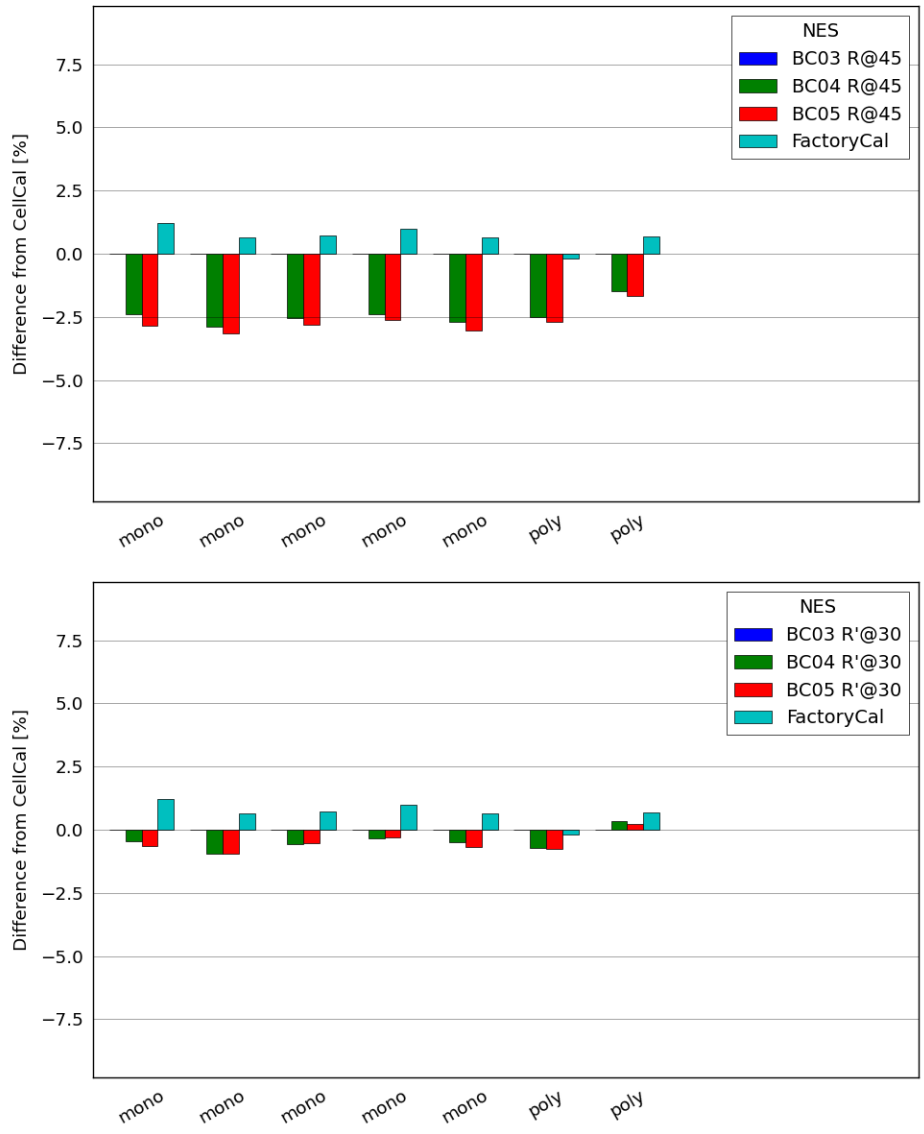

Figure 15. Comparison of all calibrations for cells supplied by NES

The upper figure is based on BORCAL R@45, and the lower figure is based on BORCAL R'@30.

7 Summary and Conclusions

Accurate sensor calibrations and traceability to the WRR are essential for reliable solar resource measurements. In this study, we compared calibration factors of many commercial PV reference cells from different sources and obtained by different methods. Four main cell types are represented: monocrystalline, polycrystalline, amorphous, and monocrystalline with a spectral filter for CdTe. The latter two are for special applications and are not further discussed in the conclusions. The former two are different in principle, but they did not reveal any systematic differences during calibration; hence, the conclusions apply equally to both.

Factory calibrations had a mean difference of approximately +0.7% with respect to NREL's Cell Lab calibrations. This excludes the two WPVS cells from Fraunhofer ISE, which together had a mean bias of −0.8%. The standard deviations for the two groups are less than 0.7%, and all individual differences are well within the overlapping range of the uncertainties of the two values, suggesting that some manufacturer's uncertainty claims might be overly conservative. In any case, this is a positive result.

Standard BORCAL R@45 calibration factors proved to be consistently lower than NREL's Cell Lab values by 2.4% on average (excluding WPVS cells, which were 4.2% lower). The differences between the calibration factors for BORCAL events 4 and 5 was small but systematic, at approximately 0.3%. Again, the WPVS cells became an exception by having virtually the same result in both BORCAL events. These differences confirm that the broadband procedure cannot be used in its current form to calibrate reference cells; however, the good repeatability strengthens the perception that the observed differences are systematic.

A new BORCAL calibration factor, R'@30, was defined that incorporates corrections for temperature, spectrum, and solar incidence angle. This factor nearly replicated the Cell Lab calibrations, with a mean deviation of only −0.4% and a standard deviation of 0.5%. Further, the two WPVS cells no longer appeared as outliers. The differences between BORCAL events 4 and 5 also reduced to ±0.2% using the corrections. These results demonstrate that the factor R'@30 might open the door to using the BORCAL infrastructure for calibrating PV reference cells; however, this is likely useful only for exploiting spare capacity because other methods would be less time and/or resource intensive.

One advantage of the BORCAL procedure is that it generates a full daily profile of the instrument responsivity. From the daily profiles, it is apparent that there is a residual directional response in most reference cells even after the air-glass reflection corrections are applied, and these patterns tend to be product specific. The residual variations have little or no effect on calibration factors; however, they will much more strongly affect field measurements, where irradiance must be measured accurately over the full range of sun positions.

For field measurements, the usual working assumption is that reference cells have a directional response that is "similar" to PV modules. It is accepted that not all PV modules have the same directional response, and in this work we have demonstrated that not all PV reference cells have the same directional either. Thus, the assumption of similarity constitutes a source of uncertainty.

In future work, we will examine the field measurement errors and uncertainties that result from differences among reference cells—caused by not only directional response but also spectral and temperature response difference. Because of the greater variation in operating conditions in field operation compared to calibration, we expect that this will further demonstrate the need for greater

uniformity in reference cells. In parallel with the measurement campaign, we will explore avenues to promote more uniformity in products, which could include the development of new guidelines and standards.

References

Andreas, A. M., and S. M. Wilcox. 2016. *Radiometer Calibration and Characterization (RCC) User's Manual: Windows Version 4.0*. Golden, CO: National Renewable Energy Laboratory. NREL/TP-3B10-65844. https://doi.org/10.2172/1240772.

ASTM International. 2016. "ASTM E973-16 Test Method for Determination of the Spectral Mismatch Parameter Between a Photovoltaic Device and a Photovoltaic Reference Cell." https://doi.org/10.1520/E0973-16.

Driesse. A. "Irradiance: What Is Your Sensor Really Telling You?" Presented at the 2018 PV Systems Symposium, Albuquerque, NM, May 1, 2018. https://pvpmc.sandia.gov/download/6756/.

Driesse, A., and W. Zaaiman. 2015. "Characterization of Global Irradiance Sensors for Use with PV Systems." Presented at the 2015 IEEE 42nd Photovoltaic Specialist Conference (PVSC), New Orleans, Louisiana, June 2015, pp. 1–5. https://doi.org/10.1109/PVSC.2015.7356004.

Duffie, J. A., and W. A. Beckman. 2006. *Solar Engineering of Thermal Processes*. Hoboken, N.J: Wiley. Third edition.

Habte, A. M., et al. 2018. *Developing a Framework for Reference Cell Standards for PV Resource Applications*. Golden, CO: National Renewable Energy Laboratory. NREL/TP-5D00-72599. https://doi.org/10.2172/1487333.

Holmgren, W. F., C. W. Hansen, and M. A. Mikofski. 2018. "pvlib python: A python Package for Modeling Solar Energy Systems." *Journal of Open Source Software* 3 (29): 884, Sep. https://doi.org/10.21105/joss.00884.

International Electrotechnical Commission (IEC). 2015. "IEC 60904-2: Photovoltaic devices – Part 2: Requirements for photovoltaic reference devices." Geneva, Switzerland. Third edition.

International Electrotechnical Commission (IEC). 2019. "IEC 60904-4: Photovoltaic devices – Part 4: Reference solar devices – Procedures for establishing calibration traceability." Geneva, Switzerland. Second edition.

Emery, K. A. 2009. "Uncertainty Analysis of Certified Photovoltaic Measurements at the National Renewable Energy Laboratory." NREL/TP-520-45299. https://www.nrel.gov/docs/fy09osti/45299.pdf.

Osterwald, C. R., M. Campanelli, T. Moriarty, K. A. Emery, and R. Williams. 2015. "Temperature-Dependent Spectral Mismatch Corrections." *IEEE Journal of Photovoltaics* 5 (6): 1692–97, Nov. https://doi.org/10.1109/JPHOTOV.2015.2459914.

Salis, E., et al. 2019. "Results of Four European Round-Robins on Short-Circuit Current Temperature Coefficient Measurements of Photovoltaic Devices of Different Size." *Solar Energy* 179: 424–36, Feb. https://doi.org/10.1016/j.solener.2018.10.051.

Appendix A. Numerical Results for Each Instrument

The following table lists all the temperature coefficients and responsivities calculated, discussed, and depicted graphically in this report. Temperature coefficients are given in parts per million (ppm), and responsivities are in $\mu V/(W/m^2)$.

Company	Model	Subtype	SerialNo	FactoryTC	CellTC	FactoryCal	CellCal	BC03 R@45	BC04 R@45	BC05 R@45	BC03 R`@30	BC04 R`@30	BC05 R`@30
Atonometrics	810226-02	mono	10603	500	490	13.77	13.66		13.207	13.15		13.5	13.482
Atonometrics	810226-02	mono	10611	500	434	13.78	13.487		13.151	13.113		13.444	13.455
Atonometrics	810226-02	mono	10621	500	486	14	13.823		13.449	13.4		13.732	13.738
Atonometrics	810226-02	mono	10623	500	498	14.29	14.054		13.655	13.609		13.942	13.951
Atonometrics	810226-02	mono	10632	500	470	14	13.879		13.493	13.441		13.782	13.782
Atonometrics	810226-02	mono	10635	500	405	14.14	14.02		13.598	13.56		13.931	13.926
Atonometrics	810226-02	mono	10650	500	500	14.15	13.952		13.564	13.52		13.853	13.854
Atonometrics	810226-03	filter	10720	-200	99	7.98	8.077		7.5285	7.4983		7.7007	7.6795
Atonometrics	810226-03	filter	10722	-200	107	8.12	8.261		7.6379	7.5791		7.8218	7.7815
EETS	RC01	mono	1360	430	441	57.4	56.71			56.02			57.183
EETS	RC01	mono	1361	430	472	57.3	56.72			56.346			57.517
EETS	RC01	mono	1362	430	446	56.4	56.76			55.805			56.906
EETS	RC01	mono	1365	430	437	56.9	56.93			55.858			57.019
EETS	RC01	mono	1366	430	517	54.3	54.16			53.569			54.558
Fraunhofer	511311102	mono	028-2019	500	443	47.72	48.2		46.167	46.169		47.581	47.597
Fraunhofer	511311102	mono	029-2019	500	431	47.83	48.115		46.135	46.122		47.625	47.606
IKS Photovoltaik	ISET	mono	01665	500		27.543	27.614			27.135			27.634
IKS Photovoltaik	ISET	mono	01715	500		27.616	27.261			26.968			27.452
IKS Photovoltaik	ISET	mono	01808	500		27.584	27.486			27.015			27.531
IKS Photovoltaik	ISET	mono	01820	500		27.722	27.602			27.128			27.6
IKS Photovoltaik	ISET	mono	02471	500		27.627	27.383			26.895			27.376
IKS Photovoltaik	ISET	mono	02501	500		27.62	27.383			26.847			27.345
IKS Photovoltaik	ISET-poly	poly	03227	500		28.909	28.887			28.461			29.026
IKS Photovoltaik	ISET-poly	poly	03238	500		29.213	29.125			28.618			29.161

Company	Model	Subtype	SerialNo	FactoryTC	CellTC	FactoryCal	CellCal	BC03 R@45	BC04 R@45	BC05 R@45	BC03 R`@30	BC04 R`@30	BC05 R`@30
IKS Photovoltaik	ISET-aSi	asi	A0229	800		114.9	105.113			114.87			114.49
IKS Photovoltaik	ISET-aSi	asi	A0244	800		115.4	108.291			115.71			116.18
IMT	Si-mV-85-PT1000	mono	17-18120001	500	479	57.53	57.115	55.874	55.959	55.817	57.031	57.01	57.024
IMT	Si-mV-85-PT1000	mono	17-18120002	500	495	58.34	57.917	56.627	56.774	56.642	57.752	57.782	57.853
IMT	Si-mV-85-PT1000	mono	17-18120003	500	515	57.97	57.391		56.321	56.156		57.276	57.266
IMT	Si-mV-85-PT1000	mono	17-18120004	500	466	59.22	58.922		57.763	57.554		58.786	58.811
IMT	Si-mV-85-PT1000	mono	17-18120005	500	534	56.85	56.627		55.506	55.356		56.449	56.453
IMT	Si-mV-85-PT1000	mono	17-18120006	500	452	58.44	58.011		56.999	56.81		58.028	58.032
NES	SOZ-03	mono	14309	430	424	101.7	100.492		98.097	97.615		100.03	99.852
NES	SOZ-03	mono	14310	430	416	103.1	102.448		99.499	99.213		101.48	101.49
NES	SOZ-03	mono	14311	430	421	103.3	102.574		99.947	99.71		101.98	102.02
NES	SOZ-03	mono	14312	430	417	103	102.01		99.571	99.34		101.67	101.71
NES	SOZ-03	mono	14313	430	330	102	101.361		98.61	98.287		100.85	100.66
NES	SOZ-03-P	poly	14422	600	435	102.2	102.381		99.812	99.637		101.63	101.61
NES	SOZ-03-P	poly	14423	600	440	100.3	99.61		98.144	97.934		99.957	99.82

Appendix B. Graphical Results for Each Instrument

The following pages provide a detailed graphic for each instrument and each BORCAL event in which it was observed. Further explanations about the design of the graphs are found in Section 5.4.

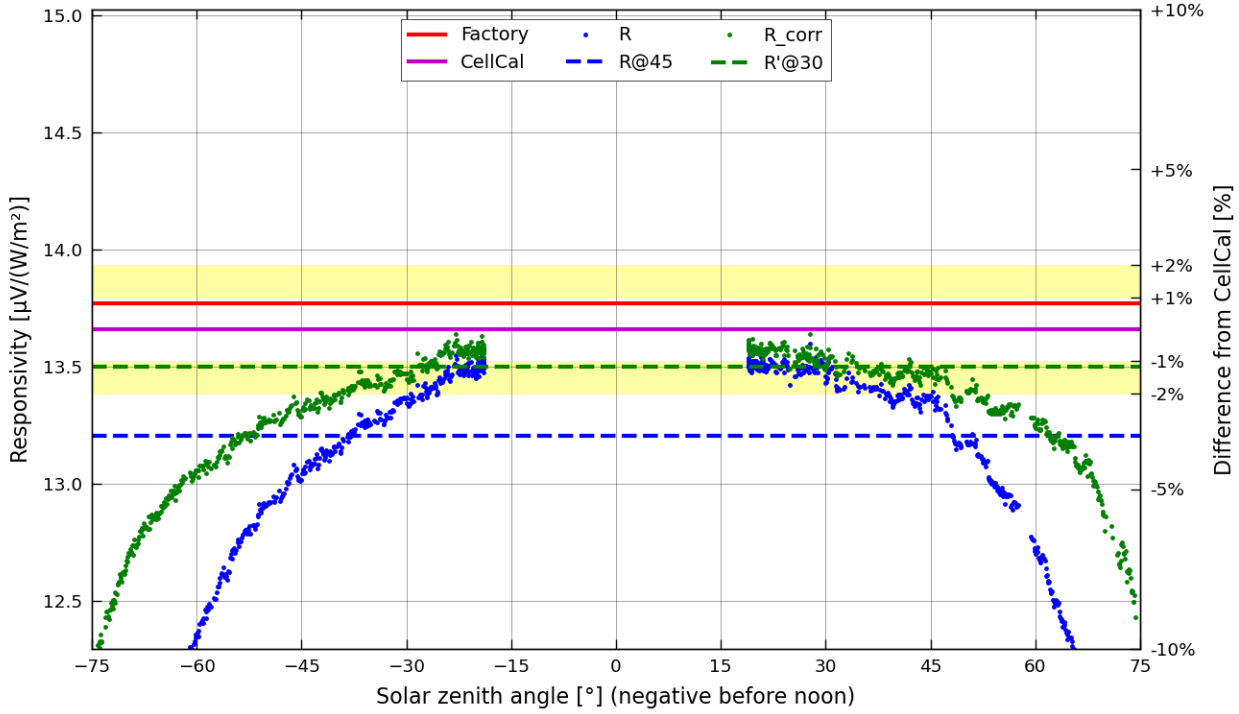

Figure B-1 Detailed results for Atonometrics 810226-02 s/n 10603
obtained during Borcal session 2019-04

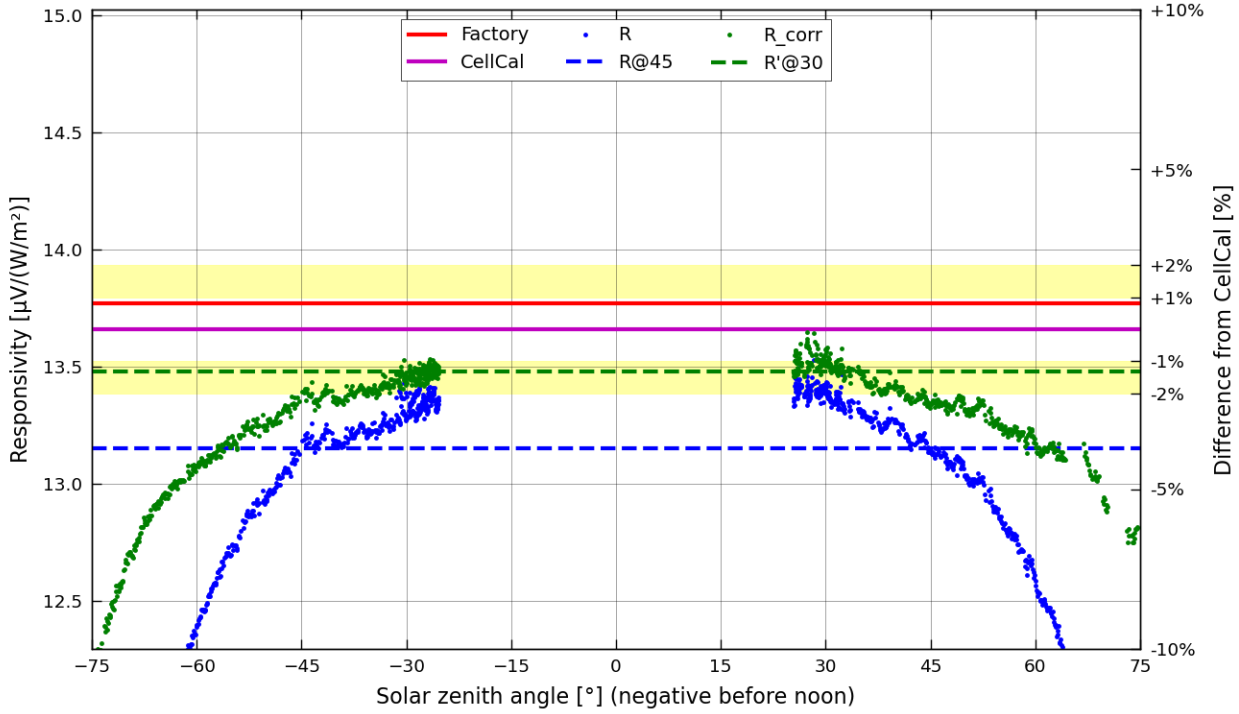

Figure B-2 Detailed results for Atonometrics 810226-02 s/n 10603
obtained during Borcal session 2019-05

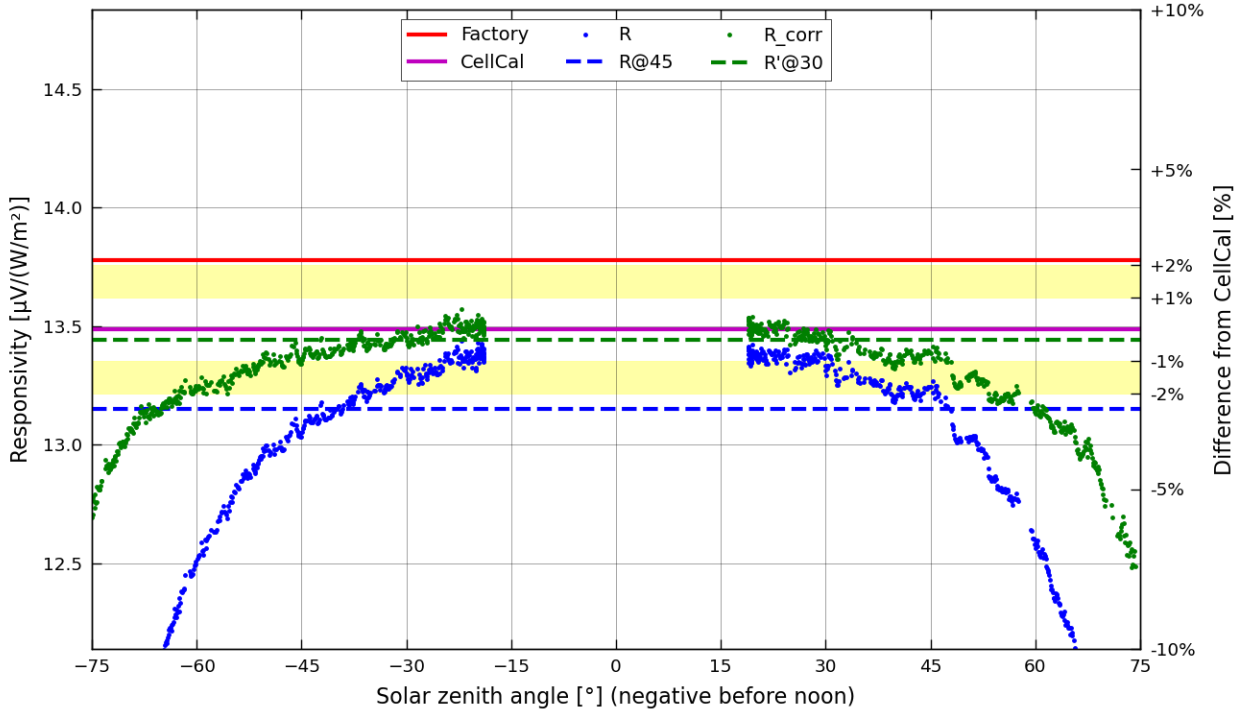

Figure B-3 Detailed results for Atonometrics 810226-02 s/n 10611
obtained during Borcal session 2019-04

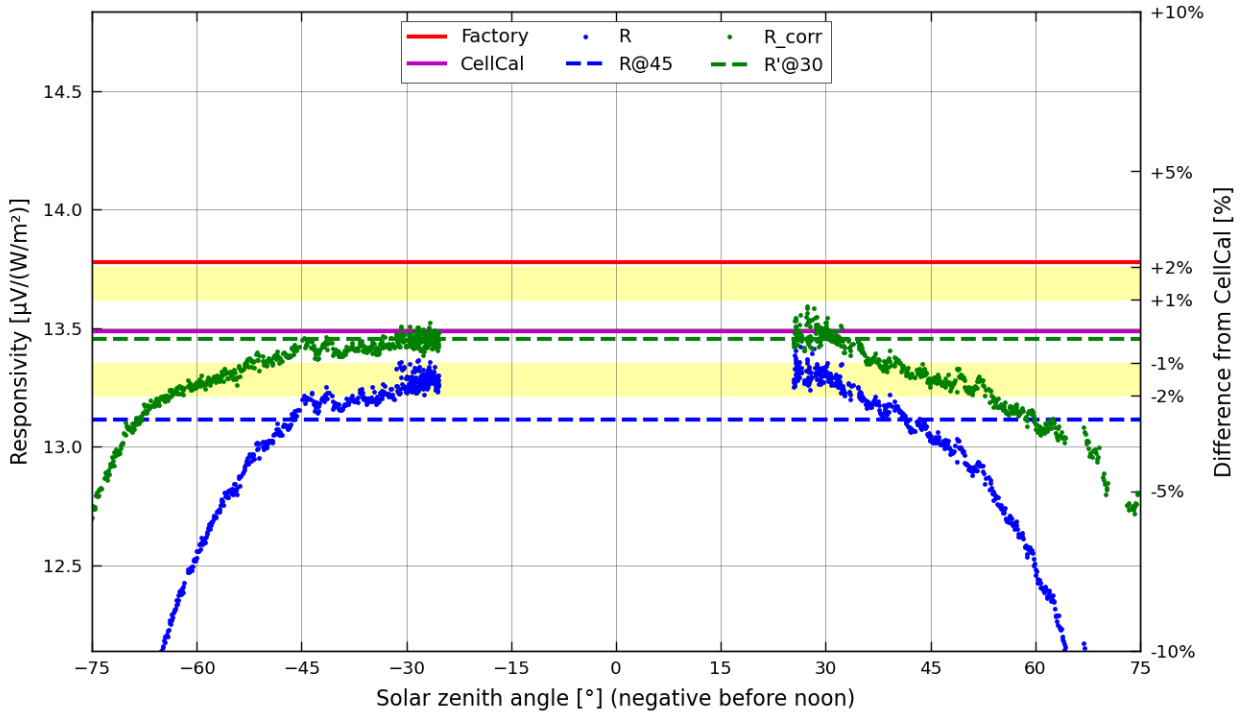

Figure B-4 Detailed results for Atonometrics 810226-02 s/n 10611
obtained during Borcal session 2019-05

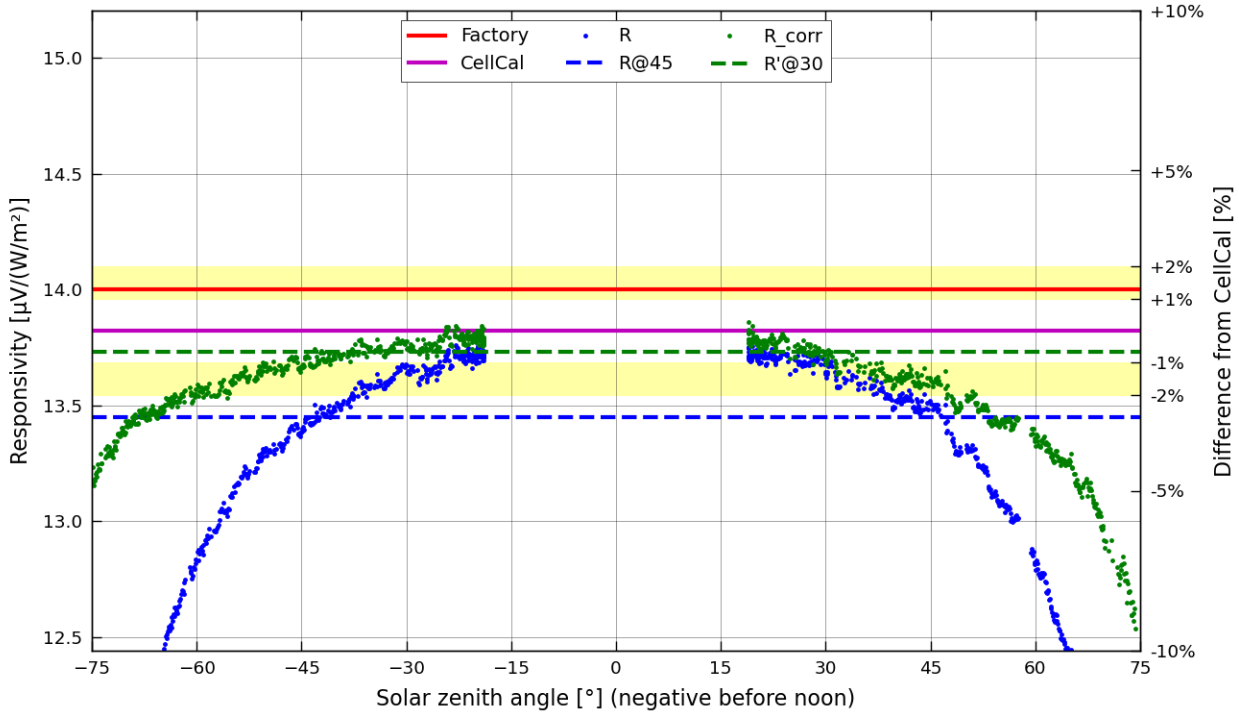

Figure B-5 Detailed results for Atonometrics 810226-02 s/n 10621
obtained during Borcal session 2019-04

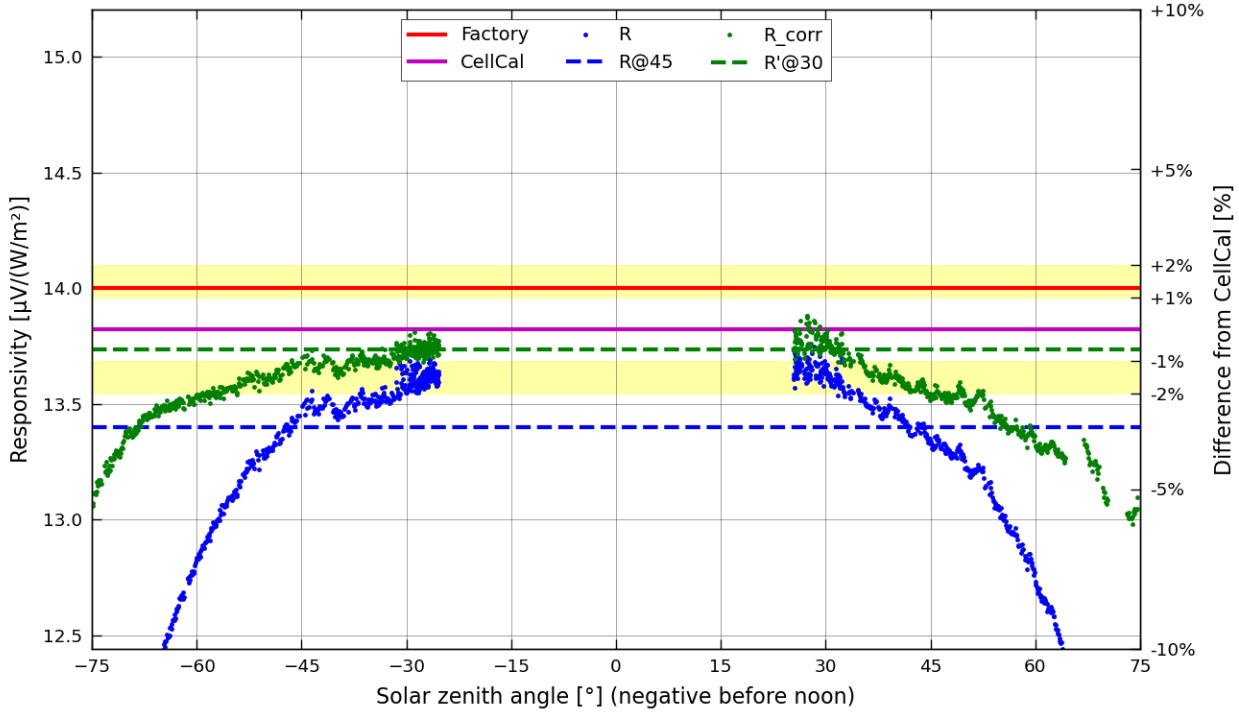

Figure B-6 Detailed results for Atonometrics 810226-02 s/n 10621
obtained during Borcal session 2019-05

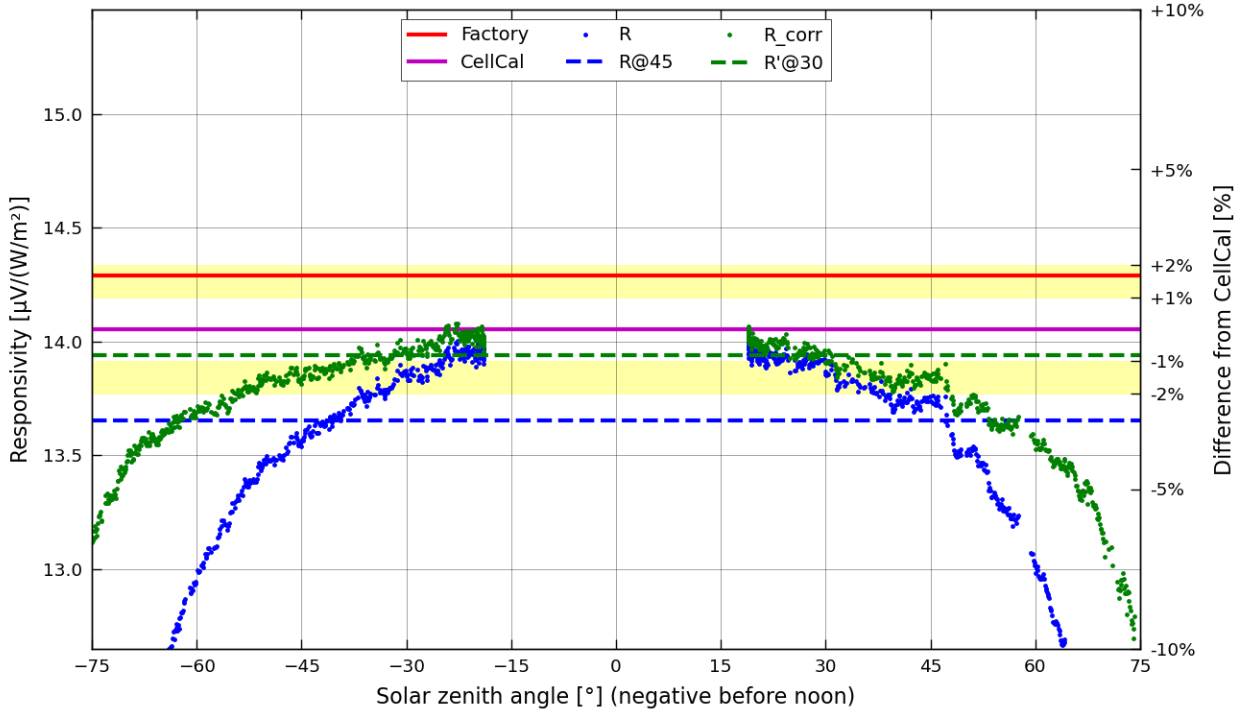

Figure B-7 Detailed results for Atonometrics 810226-02 s/n 10623
obtained during Borcal session 2019-04

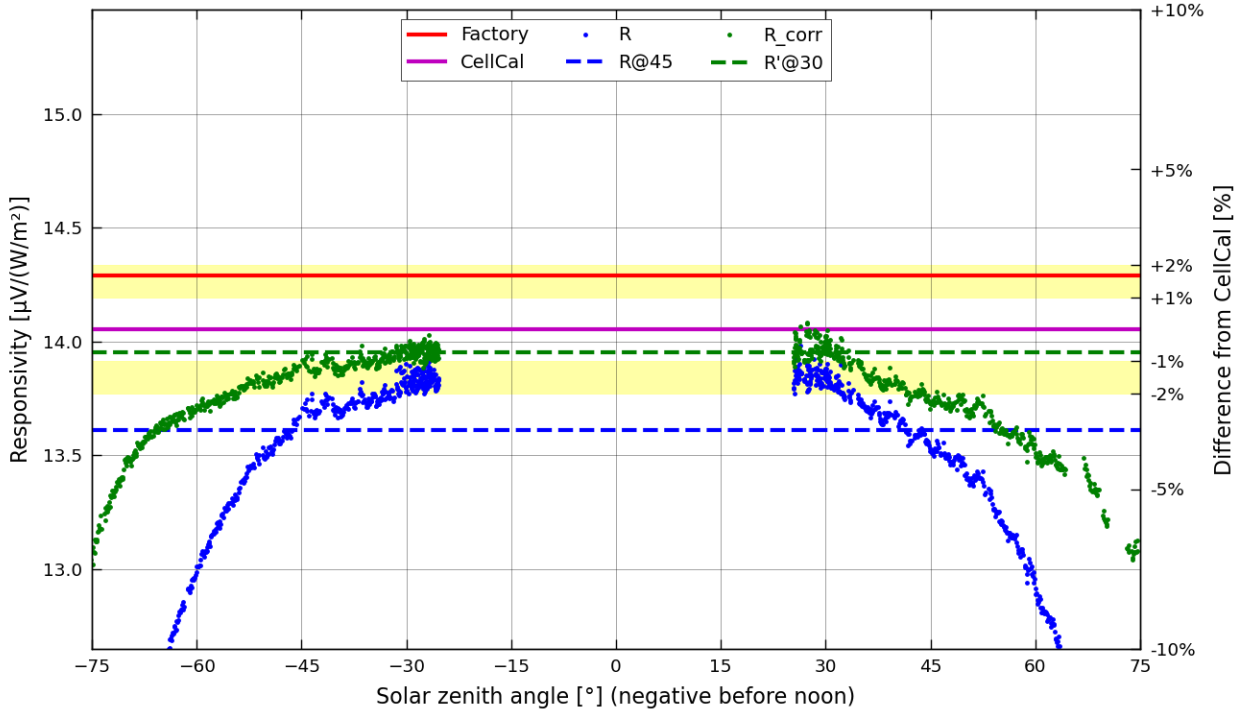

Figure B-8 Detailed results for Atonometrics 810226-02 s/n 10623
obtained during Borcal session 2019-05

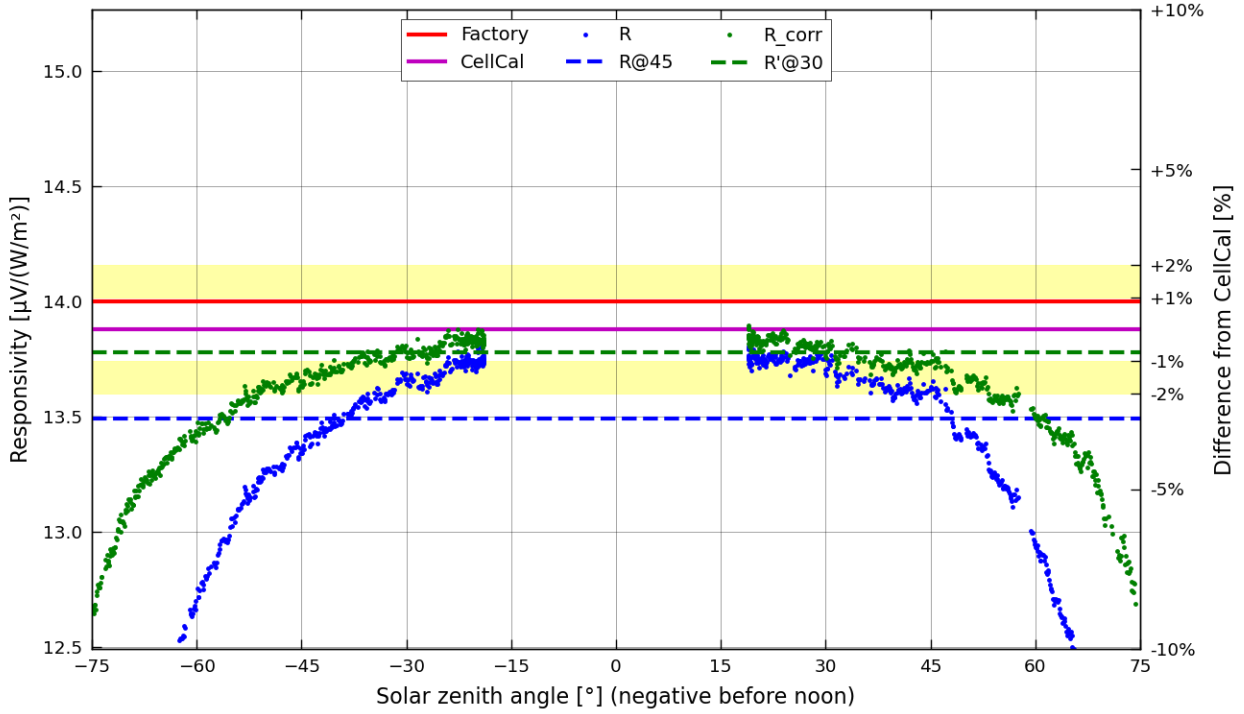

Figure B-9 Detailed results for Atonometrics 810226-02 s/n 10632
obtained during Borcal session 2019-04

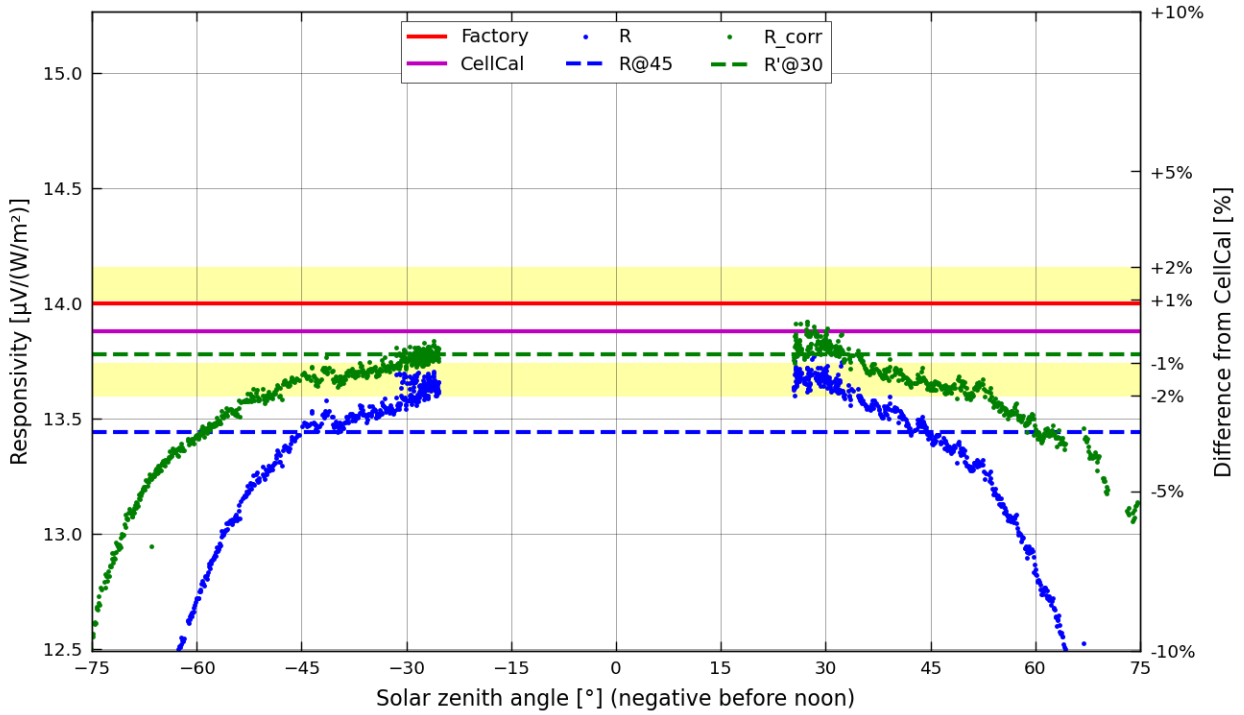

Figure B-10 Detailed results for Atonometrics 810226-02 s/n 10632
obtained during Borcal session 2019-05

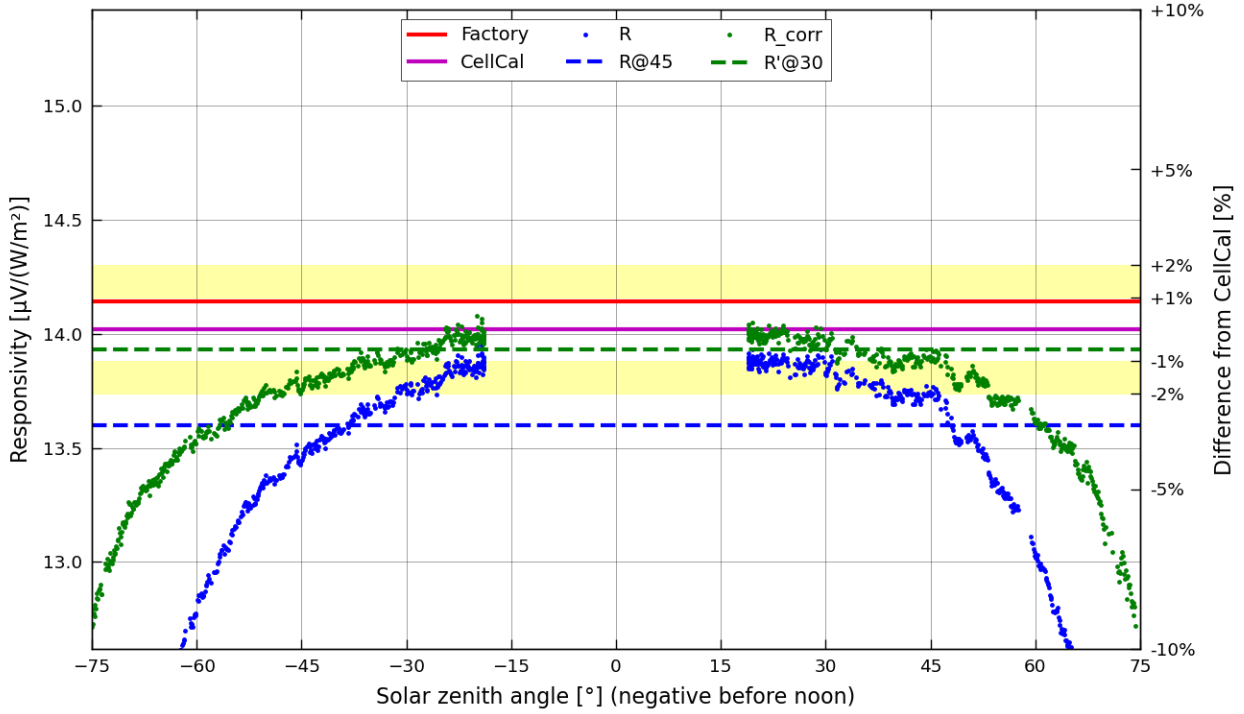

Figure B-11 Detailed results for Atonometrics 810226-02 s/n 10635
obtained during Borcal session 2019-04

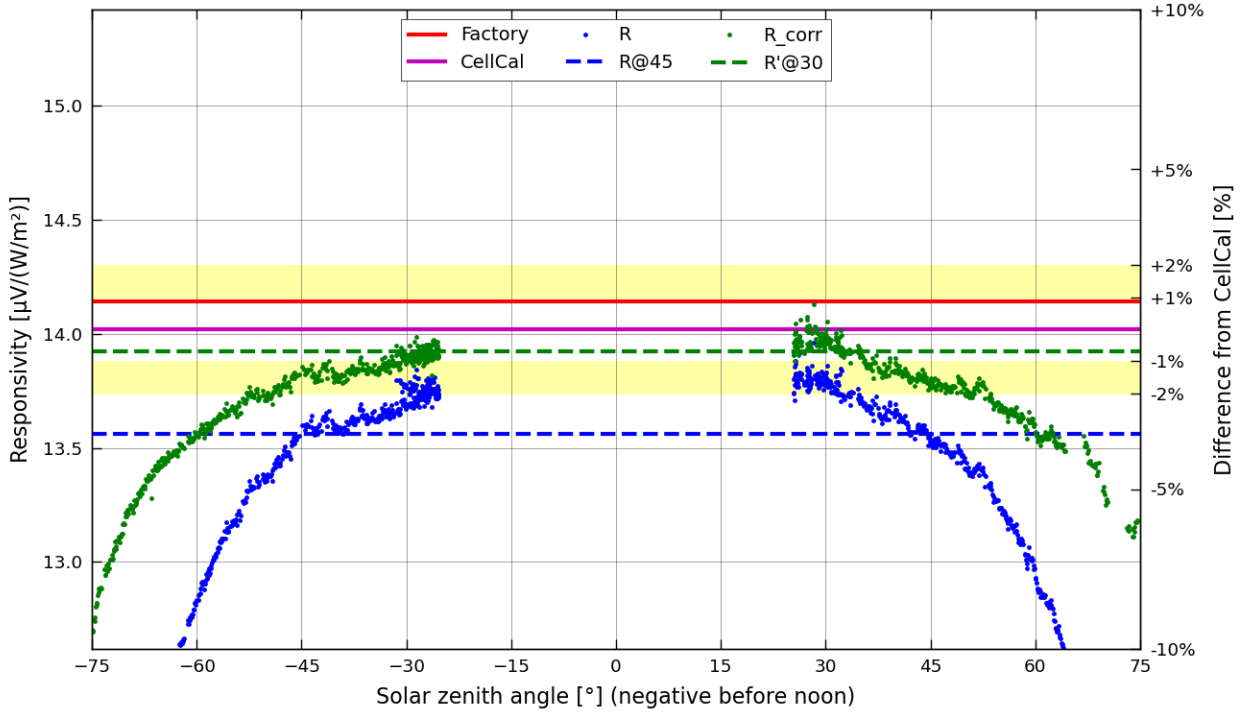

Figure B-12 Detailed results for Atonometrics 810226-02 s/n 10635
obtained during Borcal session 2019-05

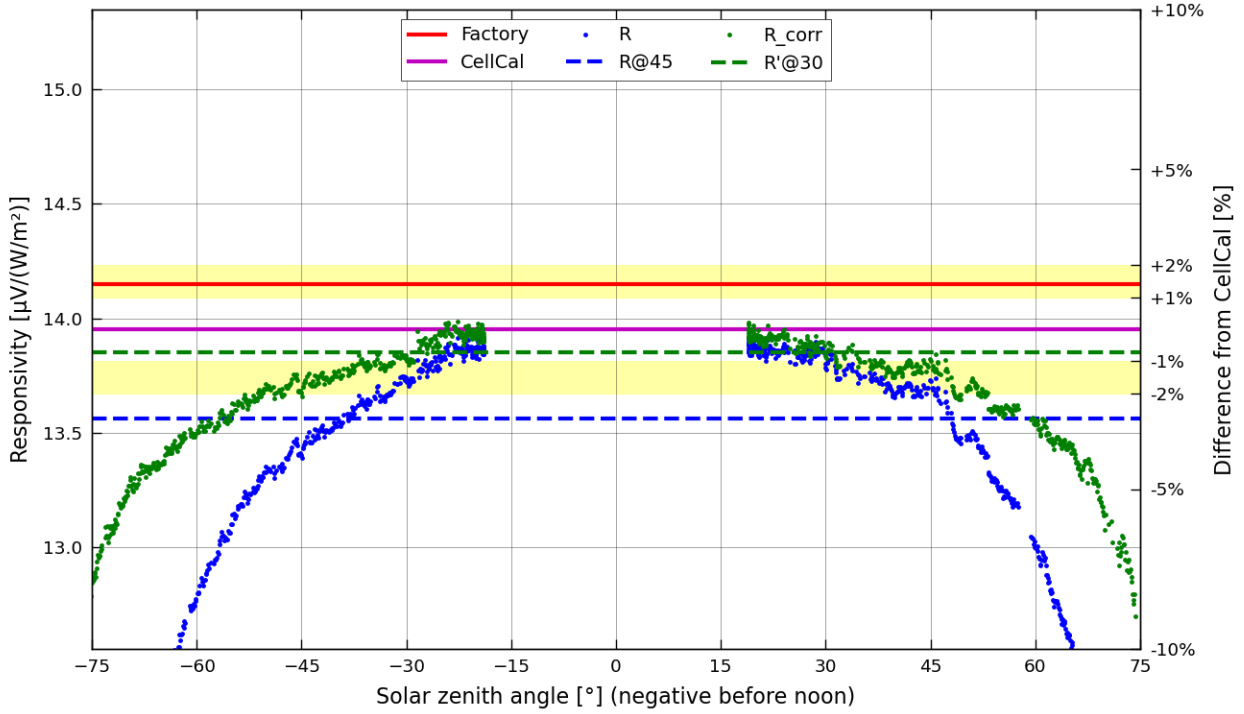

Figure B-13 Detailed results for Atonometrics 810226-02 s/n 10650
obtained during Borcal session 2019-04

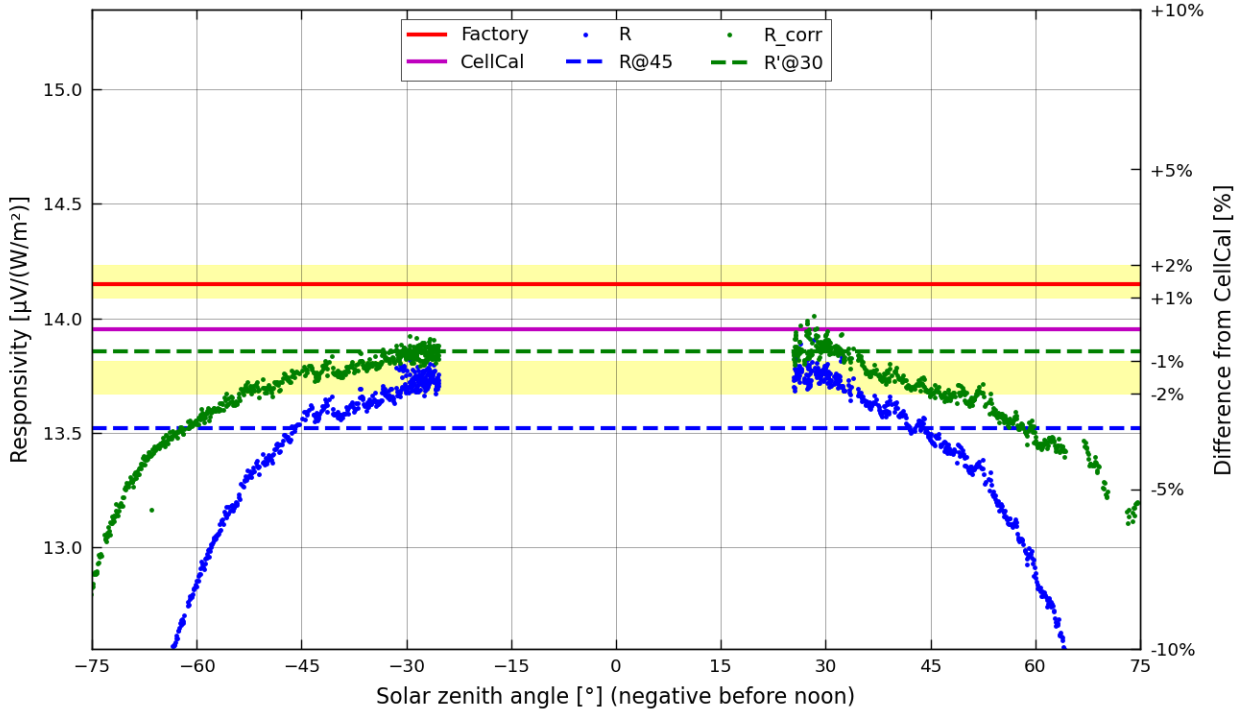

Figure B-14 Detailed results for Atonometrics 810226-02 s/n 10650
obtained during Borcal session 2019-05

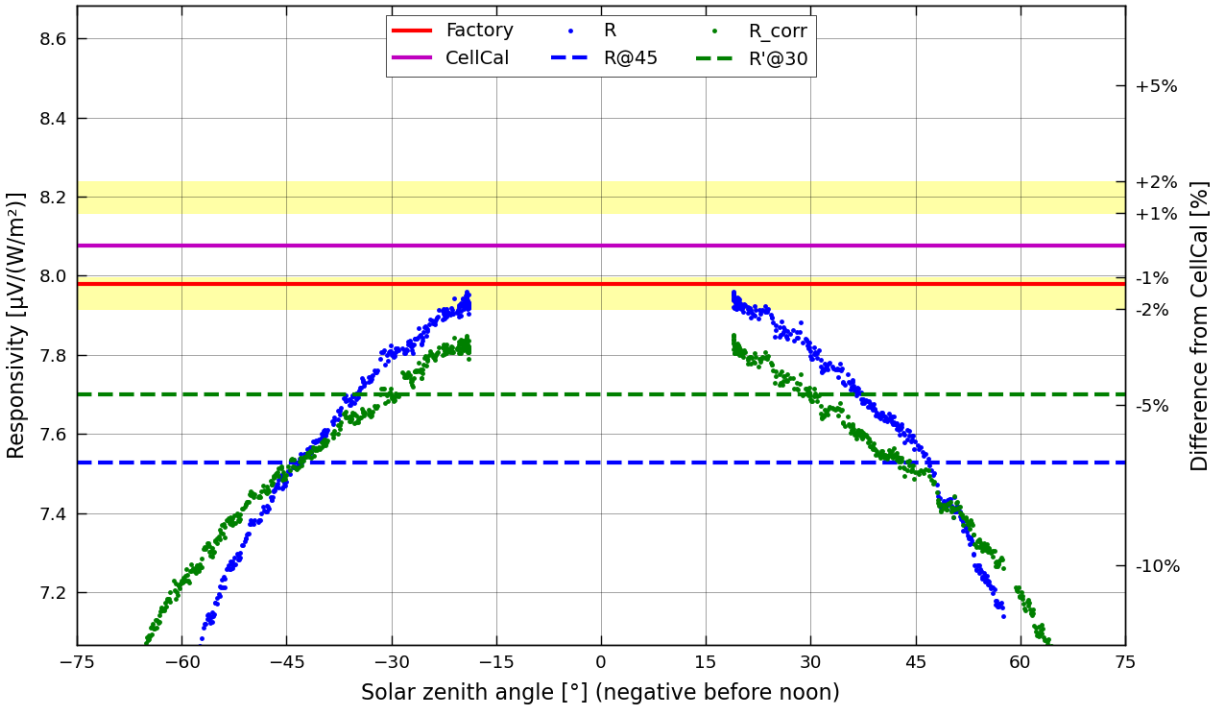

Figure B-15 Detailed results for Atonometrics 810226-03 s/n 10720
obtained during Borcal session 2019-04

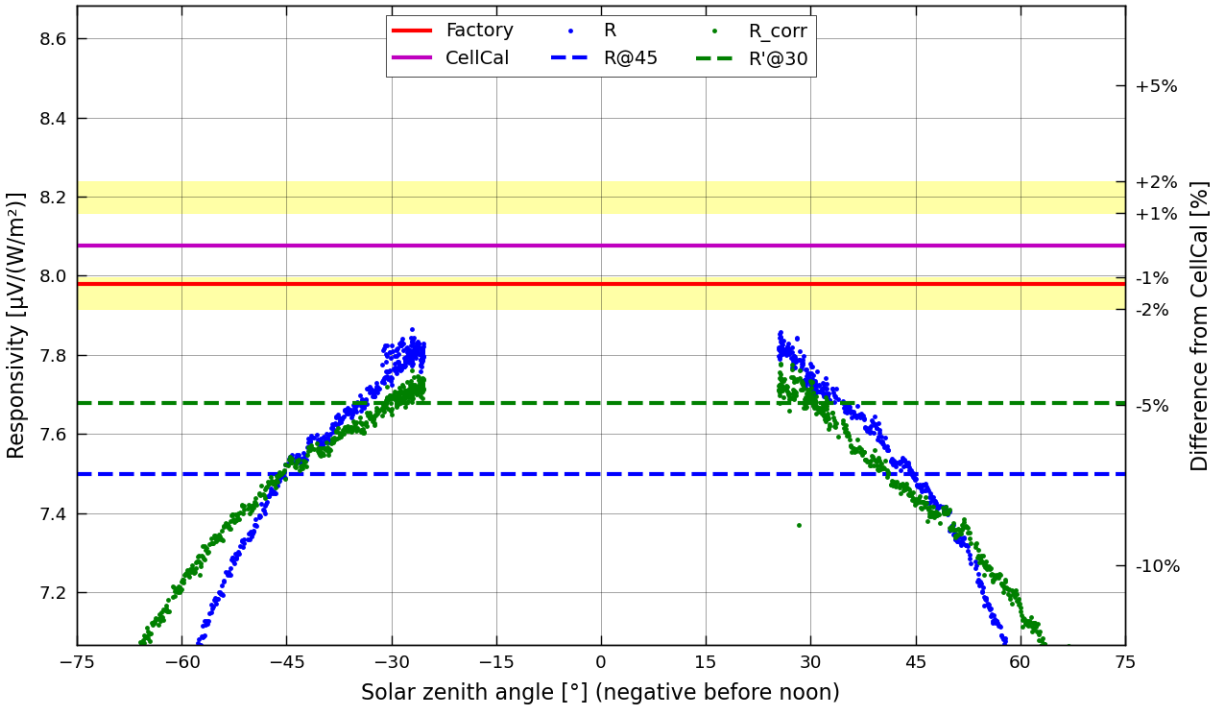

Figure B-16 Detailed results for Atonometrics 810226-03 s/n 10720
obtained during Borcal session 2019-05

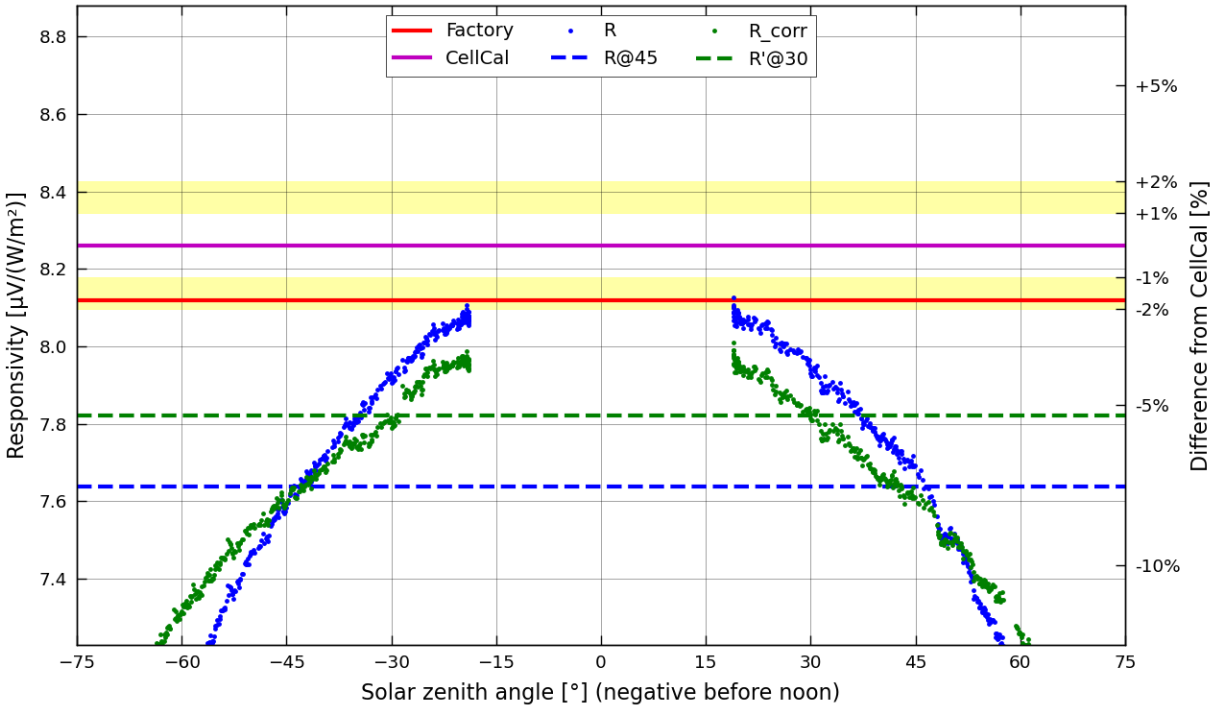

Figure B-17 Detailed results for Atonometrics 810226-03 s/n 10722
obtained during Borcal session 2019-04

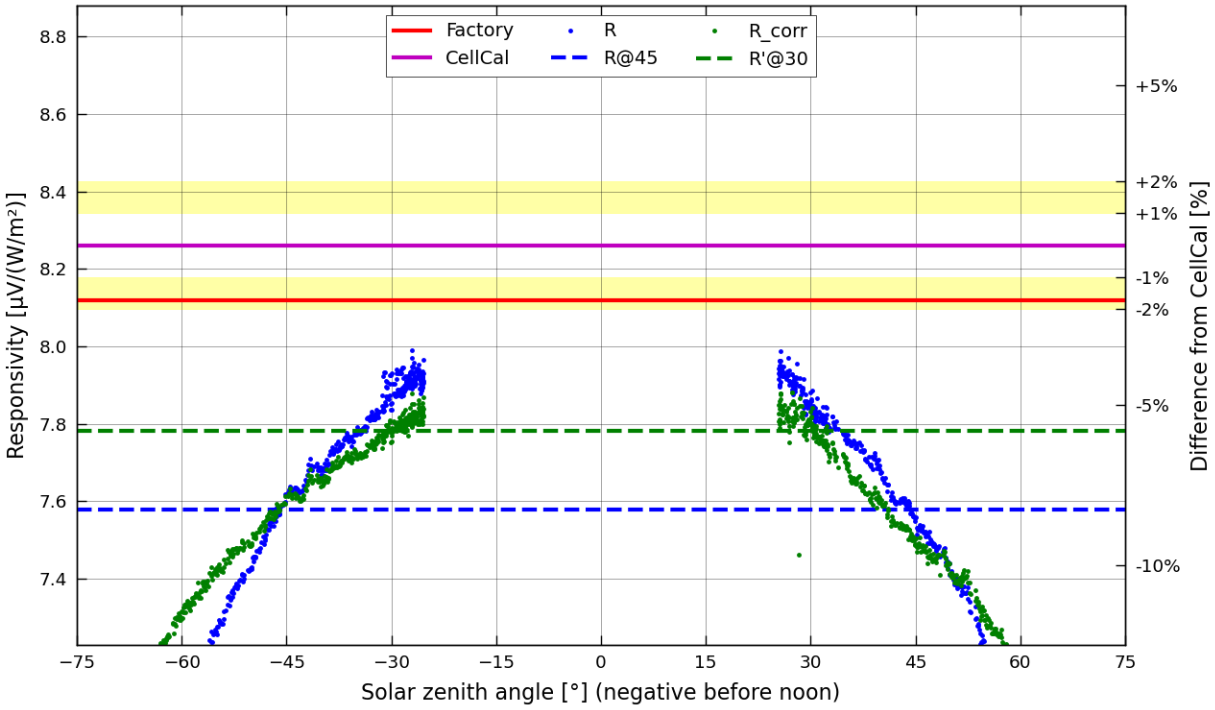

Figure B-18 Detailed results for Atonometrics 810226-03 s/n 10722
obtained during Borcal session 2019-05

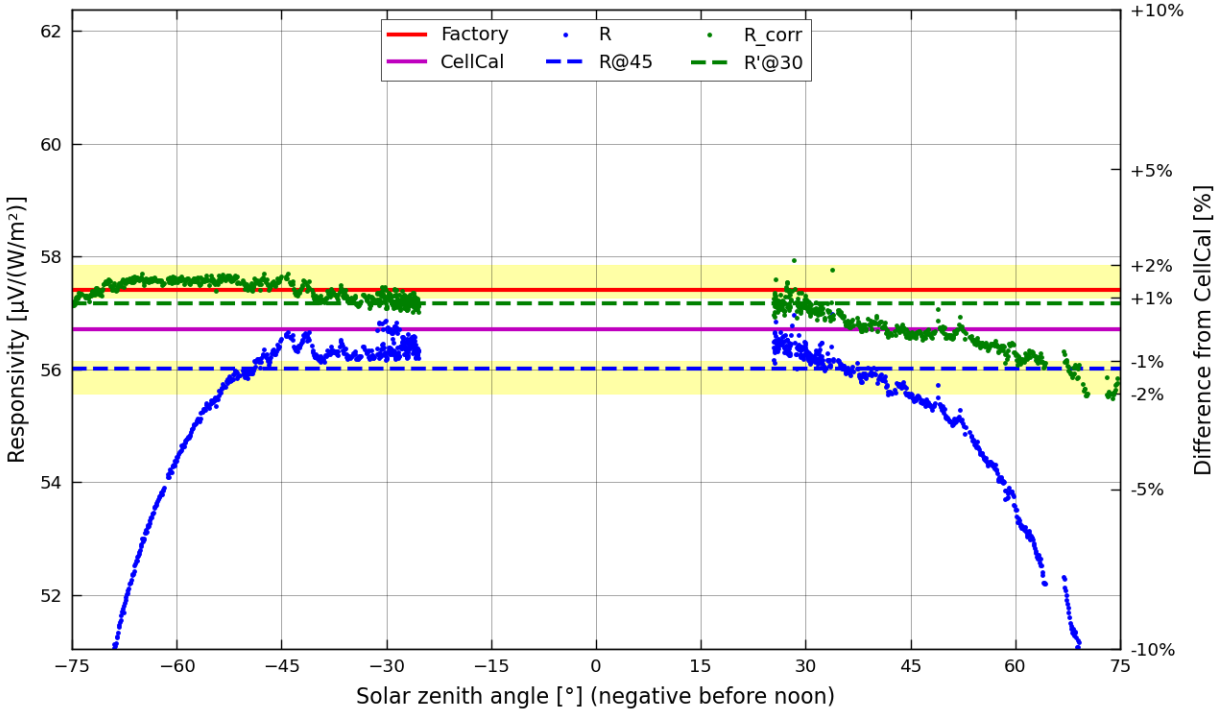

Figure B-19 Detailed results for EETS RC01 s/n 1360
obtained during Borcal session 2019-05

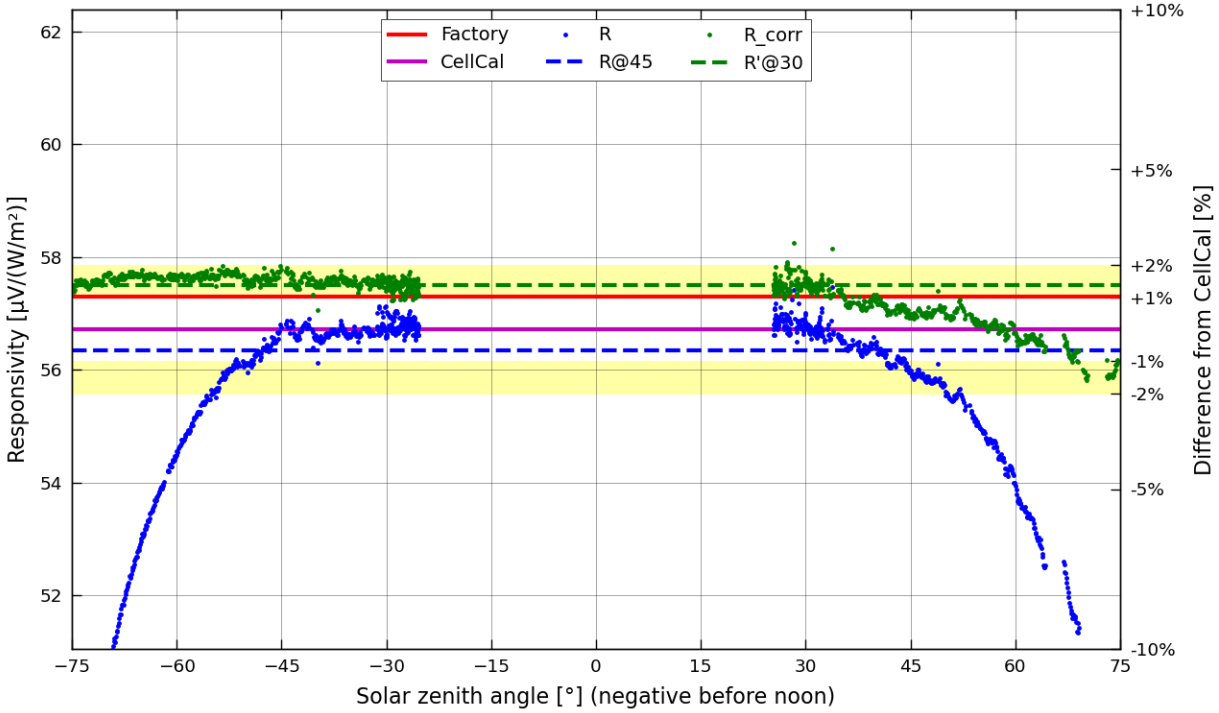

Figure B-20 Detailed results for EETS RC01 s/n 1361
obtained during Borcal session 2019-05

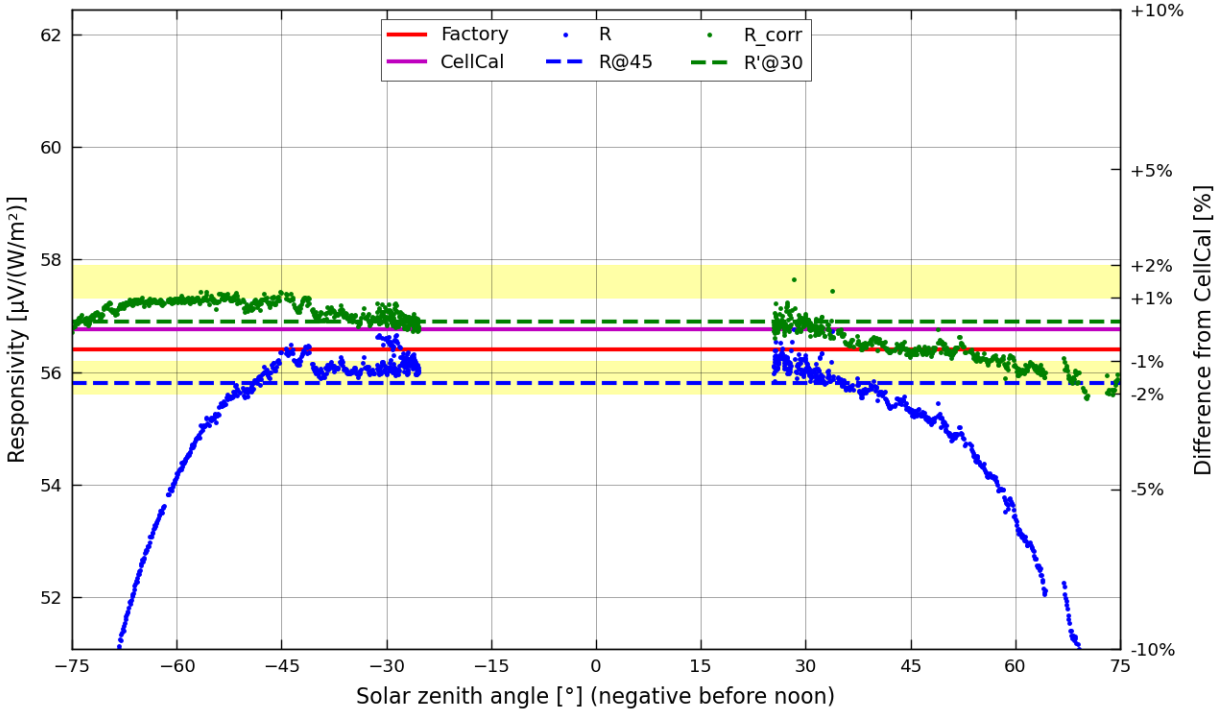

Figure B-21 Detailed results for EETS RC01 s/n 1362
obtained during Borcal session 2019-05

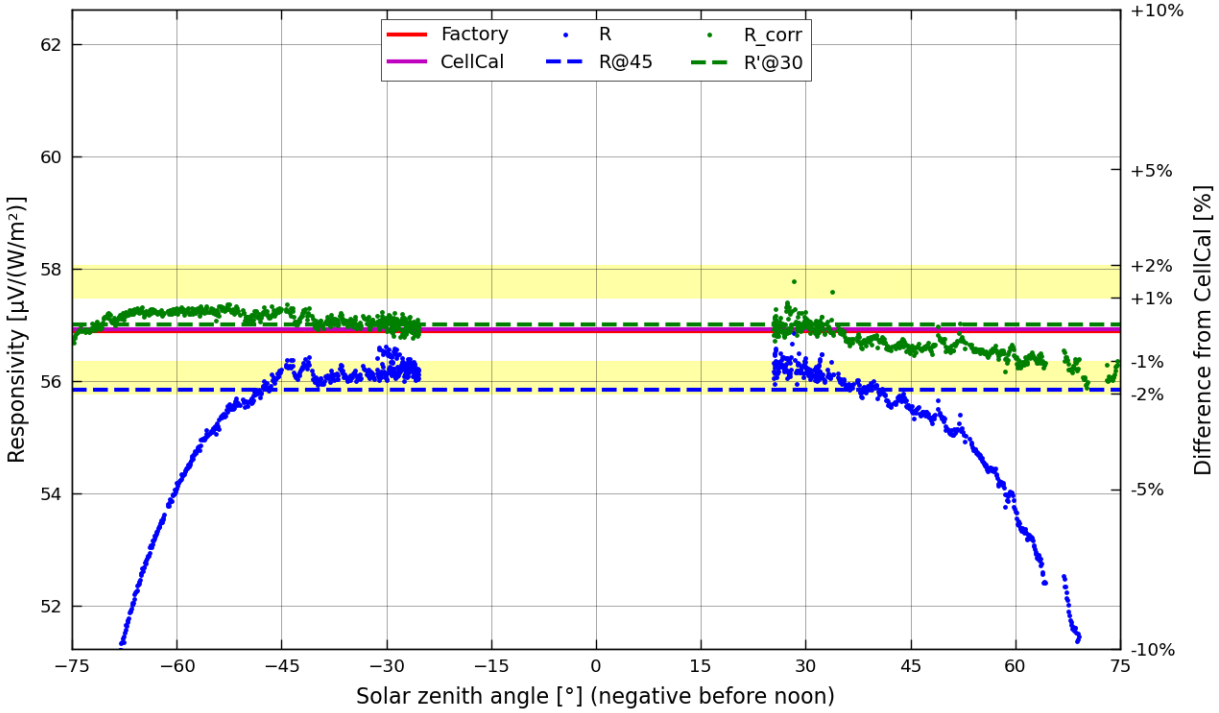

Figure B-22 Detailed results for EETS RC01 s/n 1365
obtained during Borcal session 2019-05

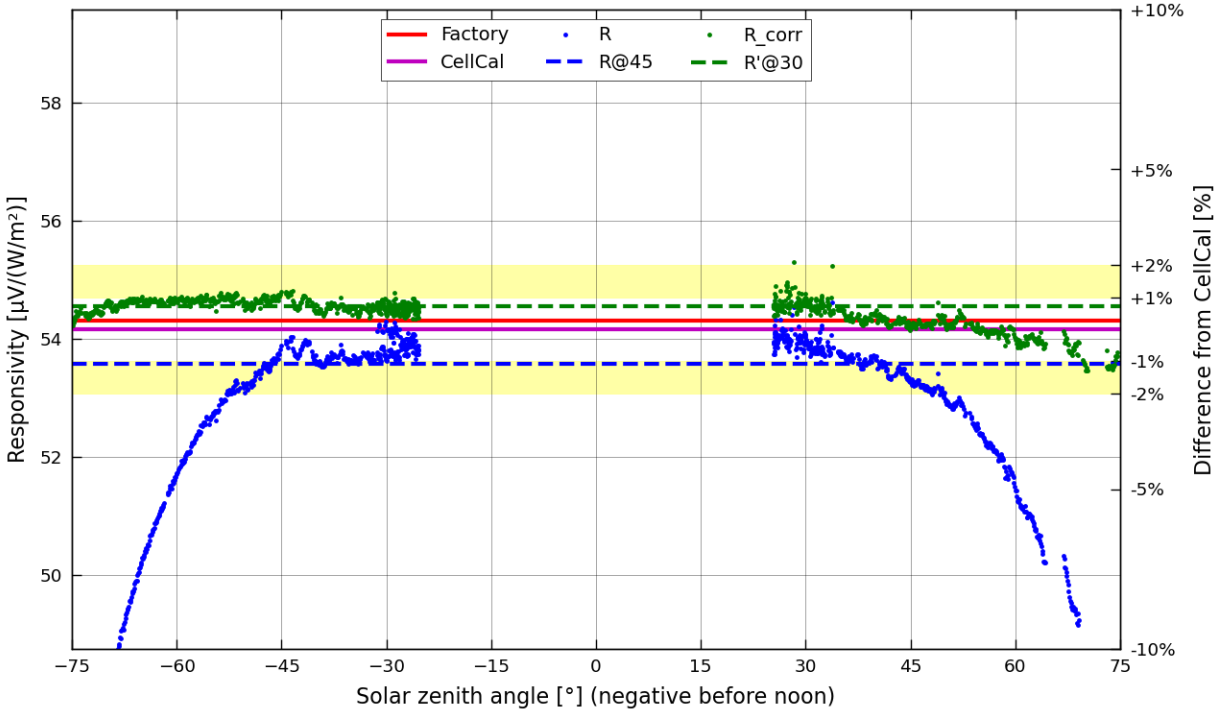

Figure B-23 Detailed results for EETS RC01 s/n 1366
obtained during Borcal session 2019-05

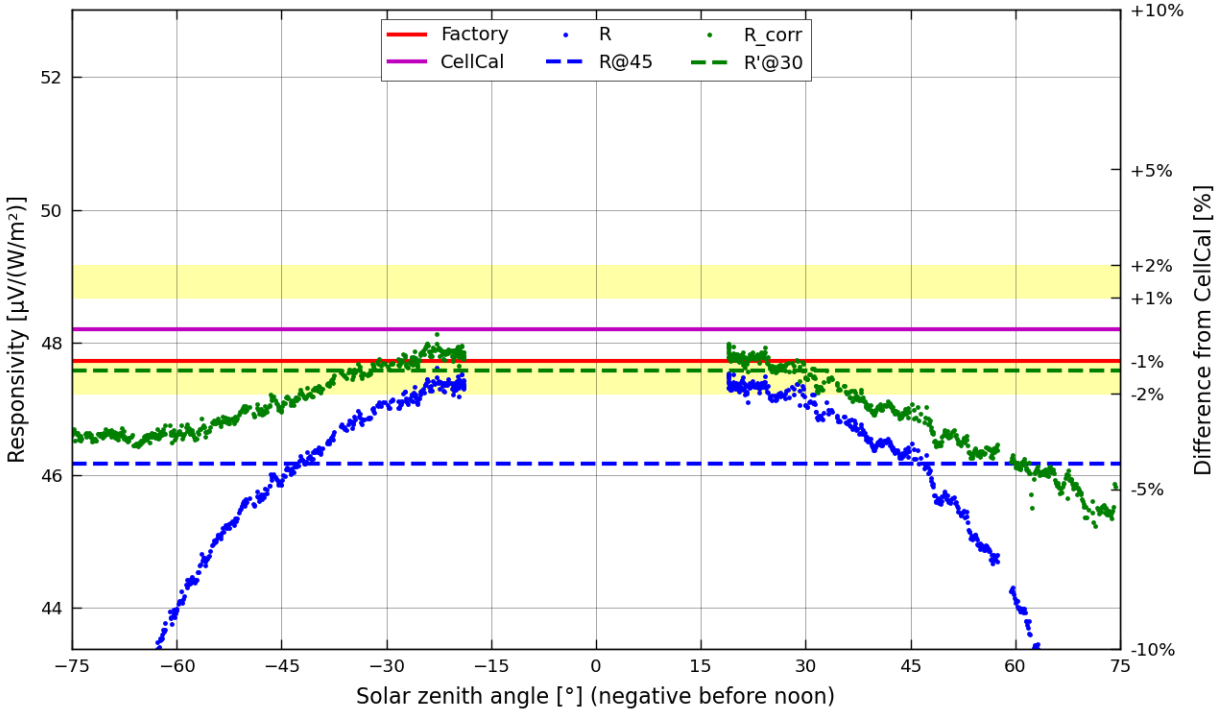

Figure B-24 Detailed results for Fraunhofer 511311102 s/n 028-2019
obtained during Borcal session 2019-04

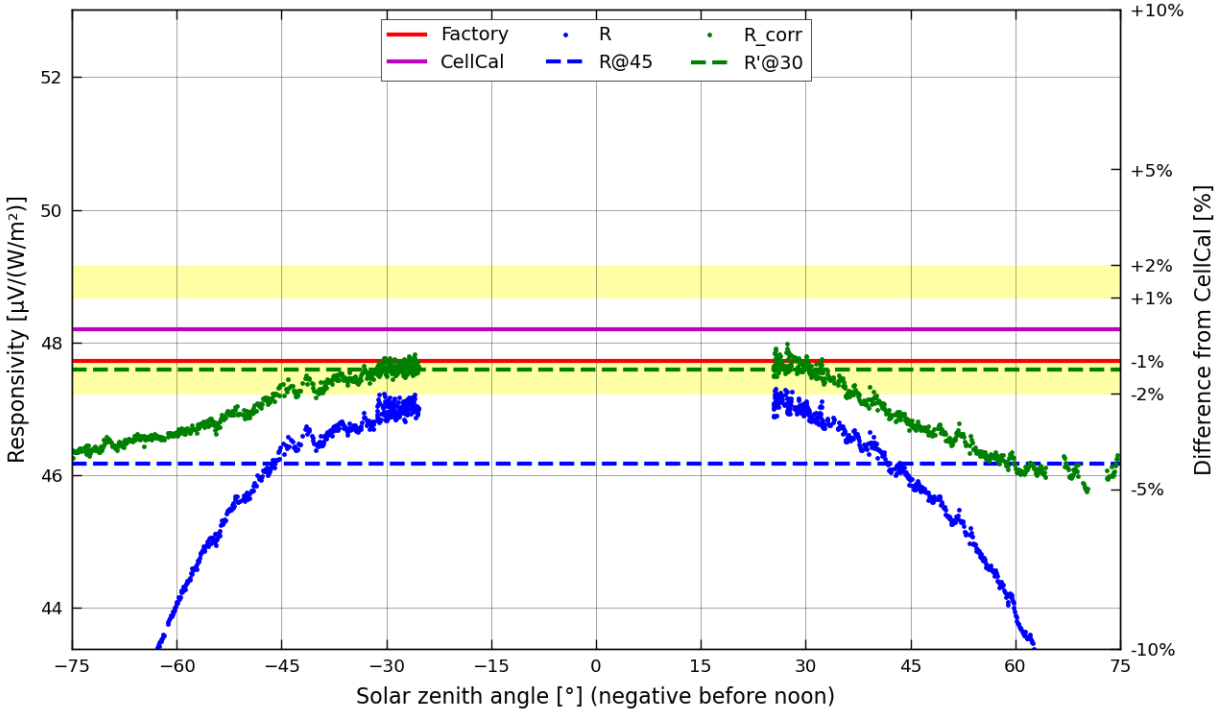

Figure B-25 Detailed results for Fraunhofer 511311102 s/n 028-2019
obtained during Borcal session 2019-05

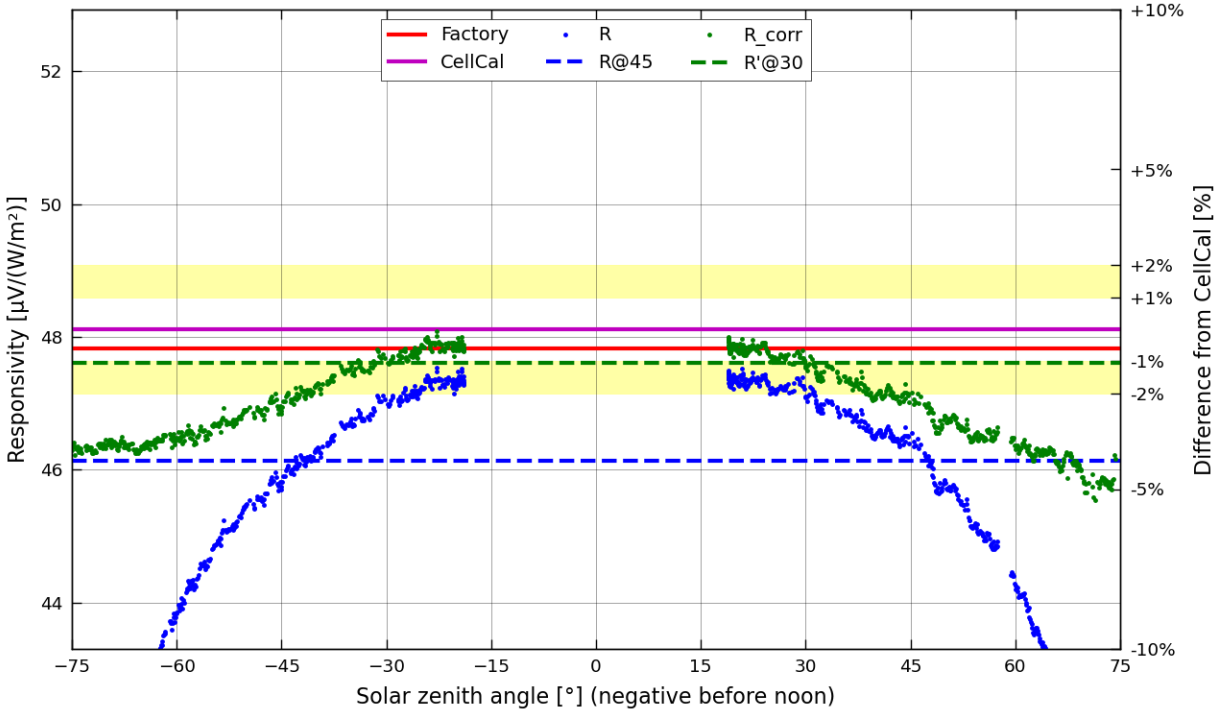

Figure B-26 Detailed results for Fraunhofer 511311102 s/n 029-2019
obtained during Borcal session 2019-04

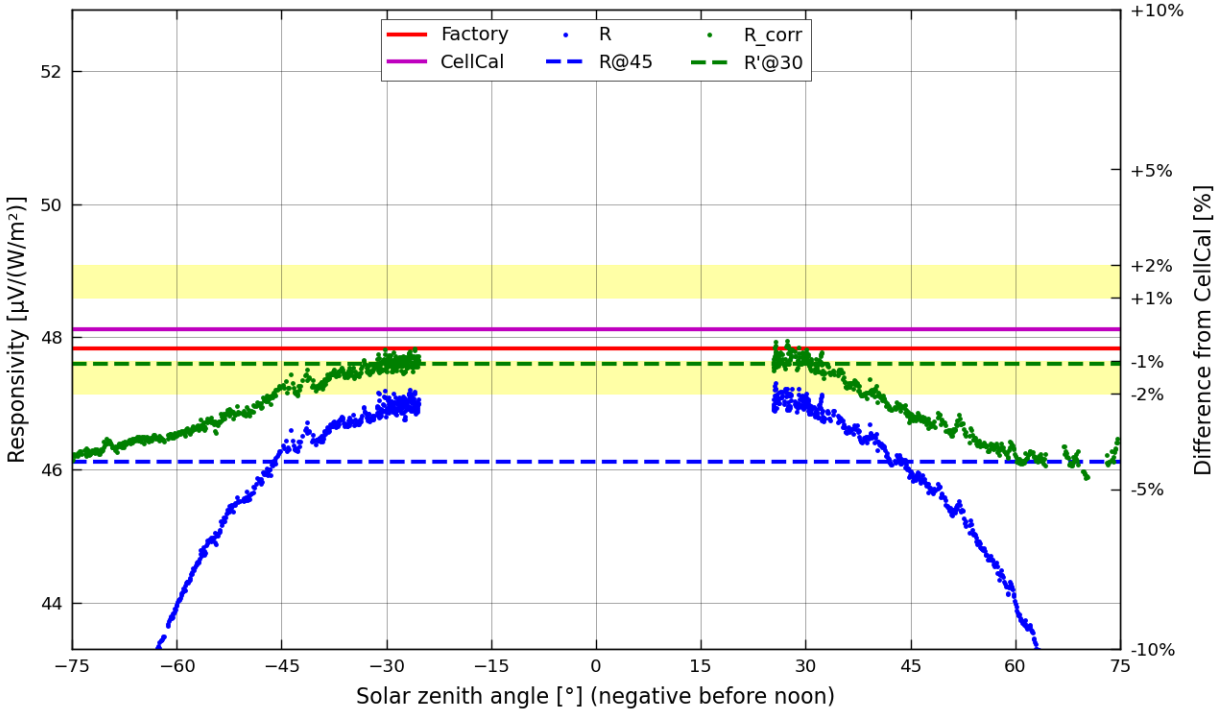

Figure B-27 Detailed results for Fraunhofer 511311102 s/n 029-2019
obtained during Borcal session 2019-05

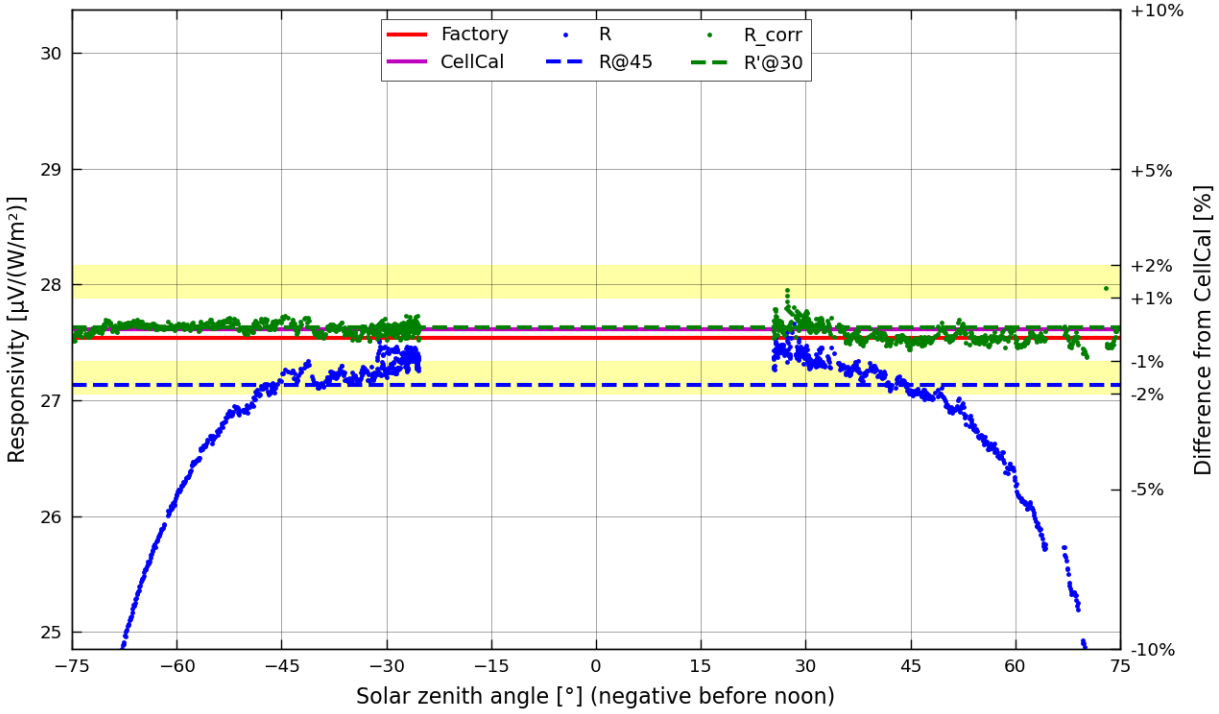

Figure B-28 Detailed results for IKS Photovoltaik ISET s/n 01665
obtained during Borcal session 2019-05

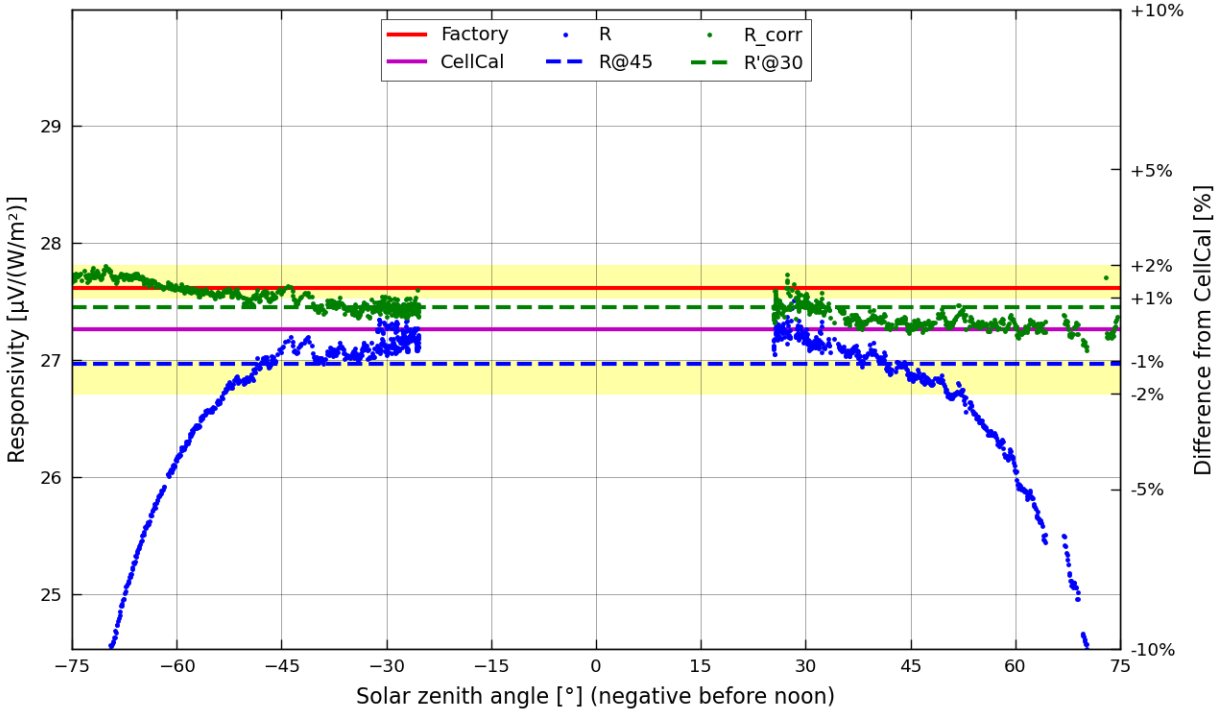

Figure B-29 Detailed results for IKS Photovoltaik ISET s/n 01715
obtained during Borcal session 2019-05

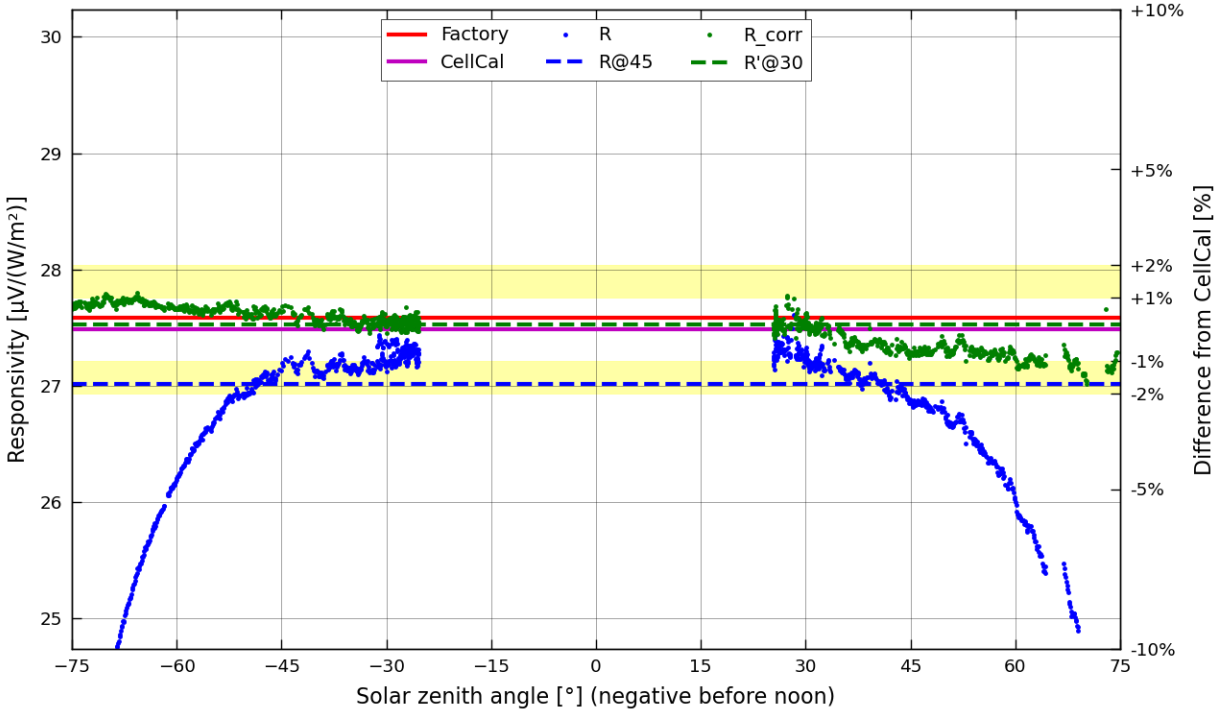

Figure B-30 Detailed results for IKS Photovoltaik ISET s/n 01808
obtained during Borcal session 2019-05

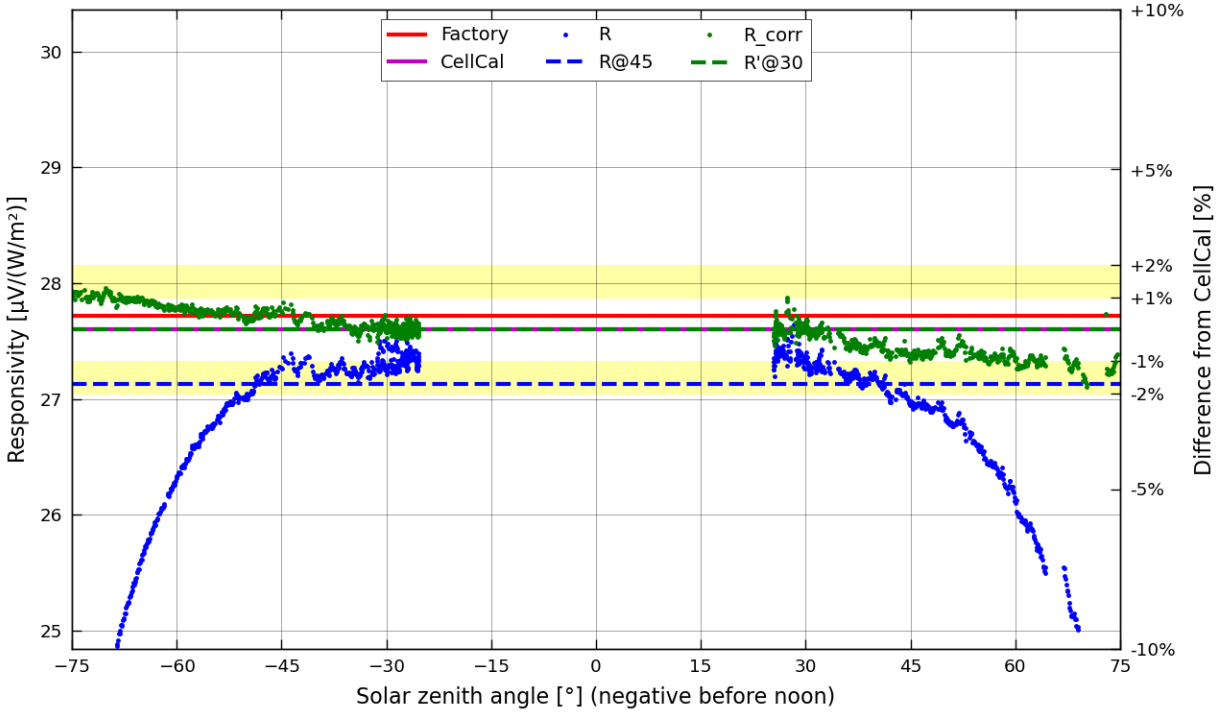

Figure B-31 Detailed results for IKS Photovoltaik ISET s/n 01820
obtained during Borcal session 2019-05

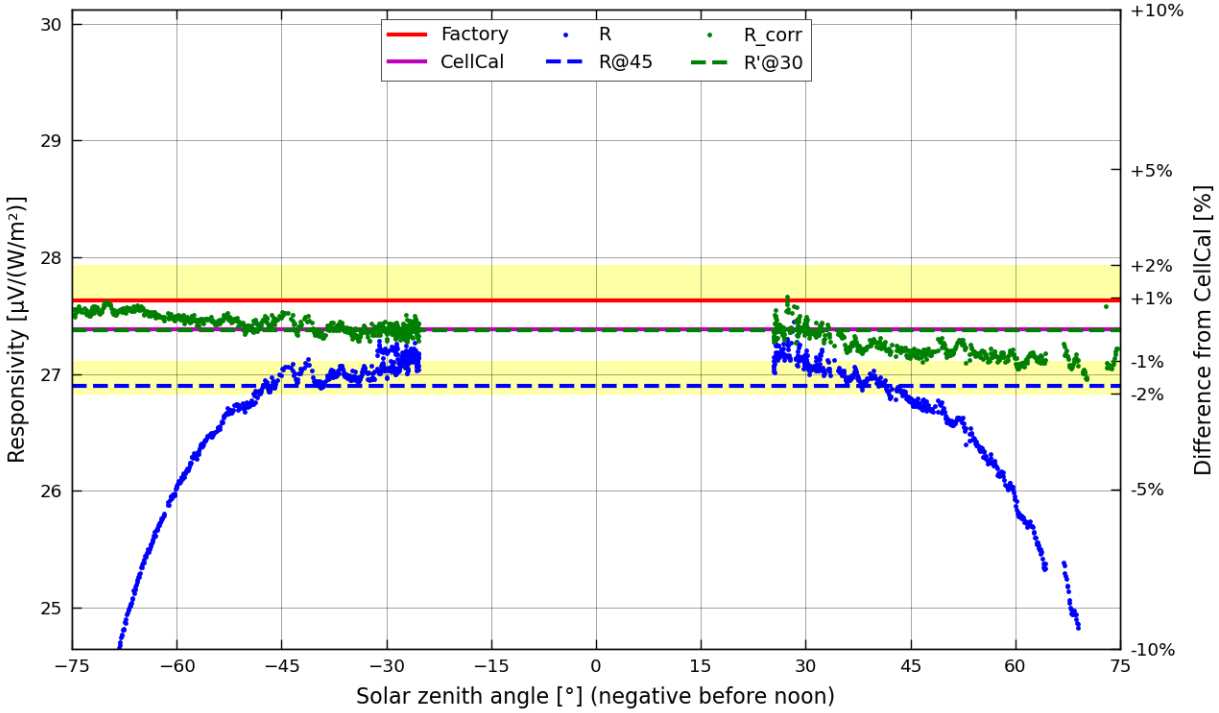

Figure B-32 Detailed results for IKS Photovoltaik ISET s/n 02471
obtained during Borcal session 2019-05

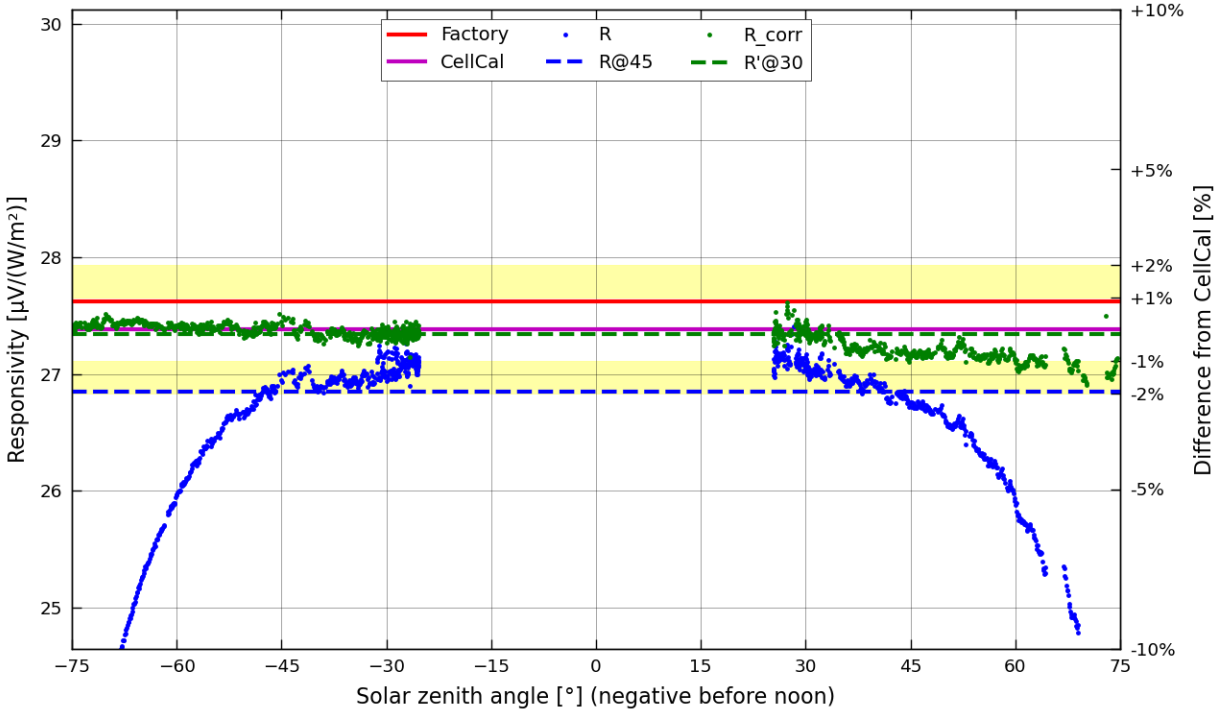

Figure B-33 Detailed results for IKS Photovoltaik ISET s/n 02501
obtained during Borcal session 2019-05

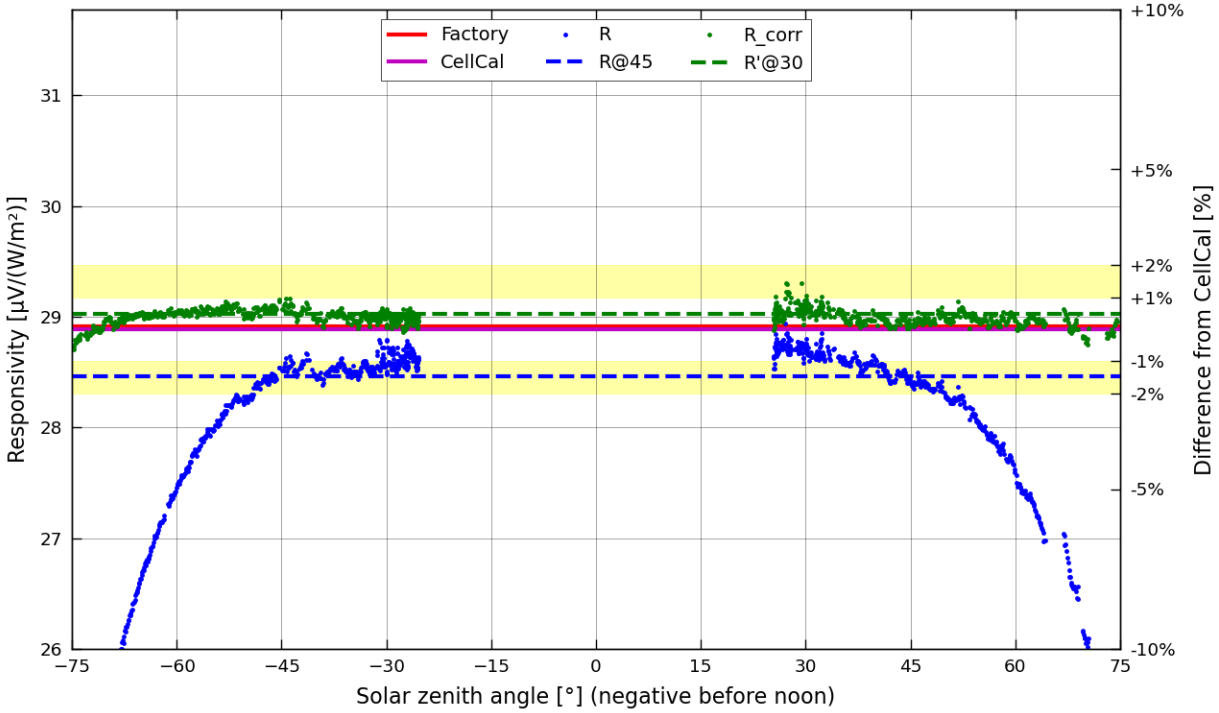

Figure B-34 Detailed results for IKS Photovoltaik ISET-poly s/n 03227
obtained during Borcal session 2019-05

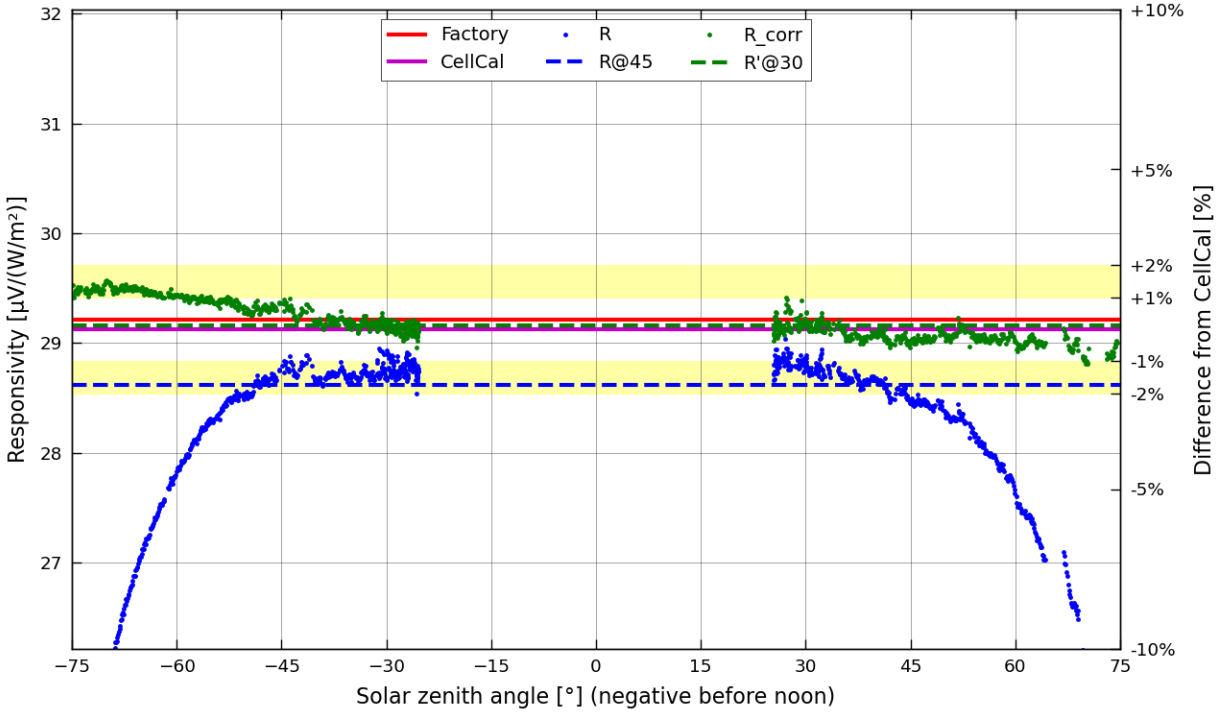

Figure B-35 Detailed results for IKS Photovoltaik ISET-poly s/n 03238
obtained during Borcal session 2019-05

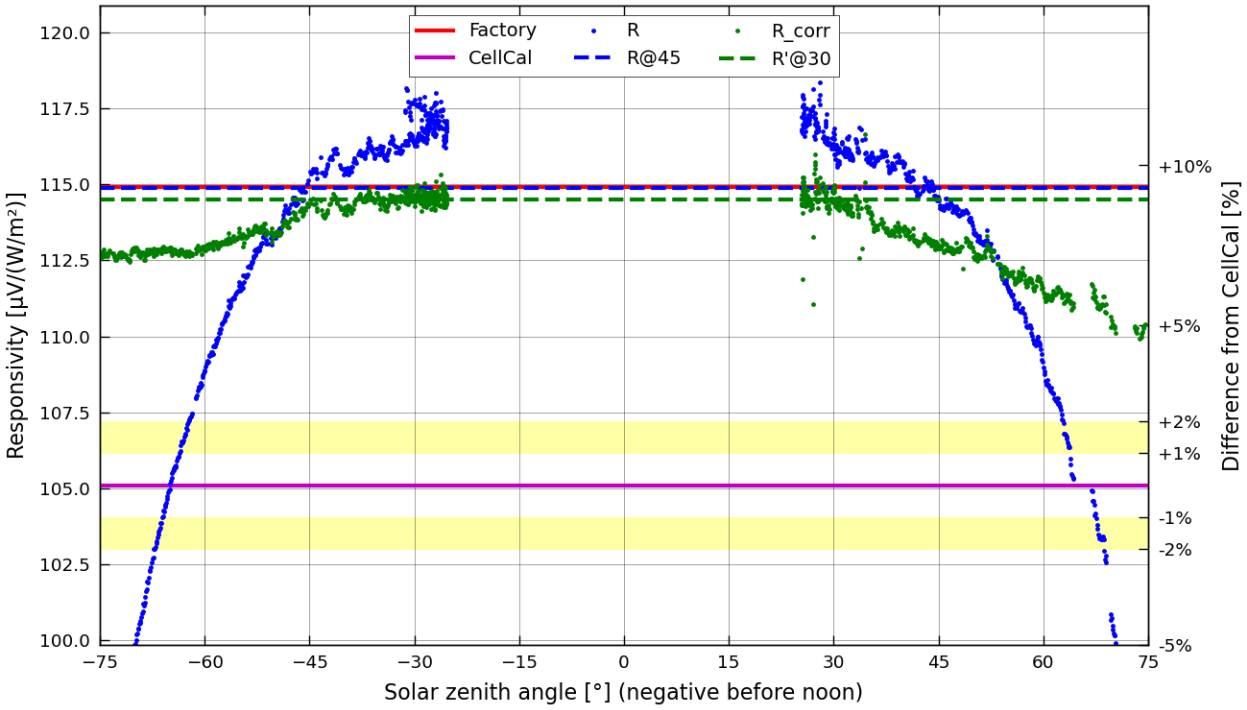

Figure B-36 Detailed results for IKS Photovoltaik ISET-aSi s/n A0229
obtained during Borcal session 2019-05

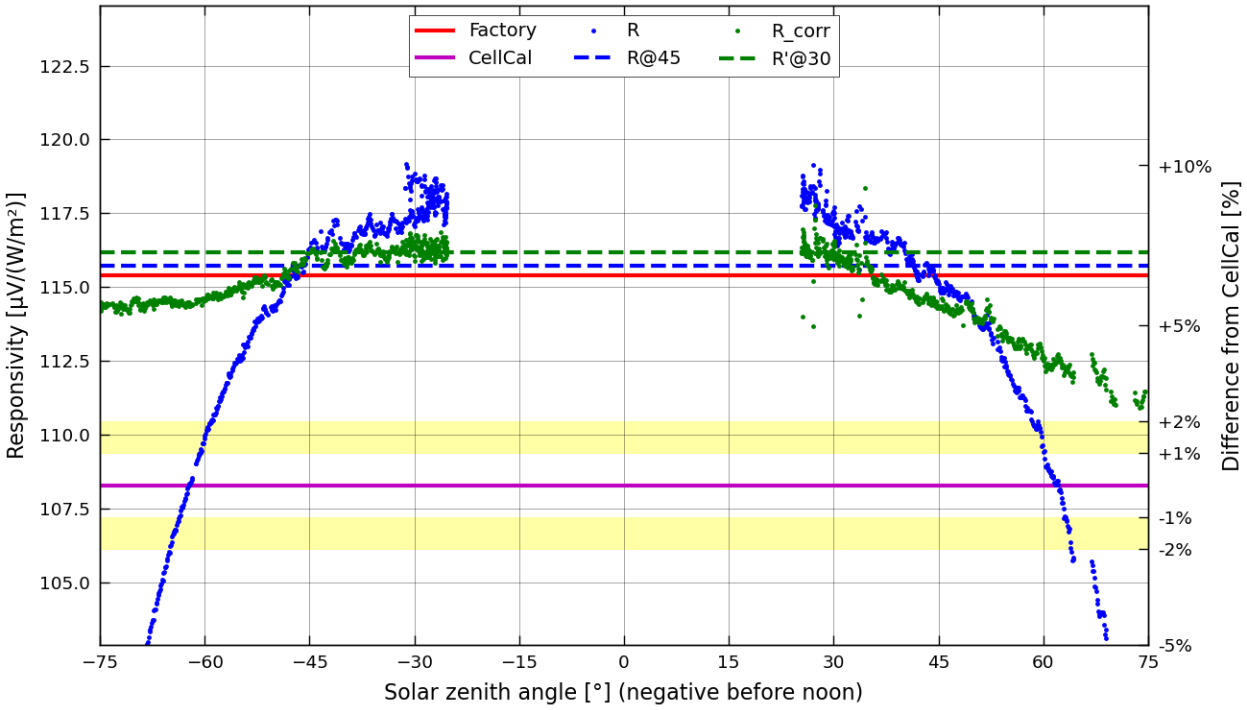

Figure B-37 Detailed results for IKS Photovoltaik ISET-aSi s/n A0244
obtained during Borcal session 2019-05

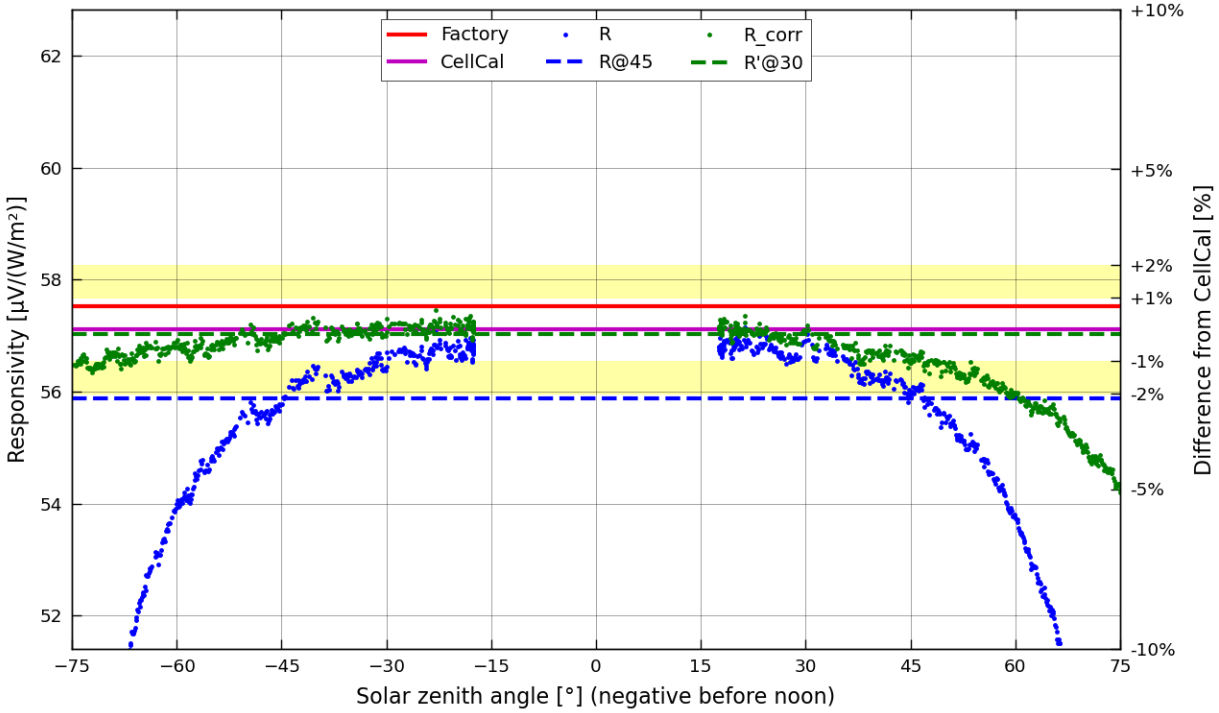

Figure B-38 Detailed results for IMT Si-mV-85-PT1000 s/n 17-18120001
obtained during Borcal session 2019-03

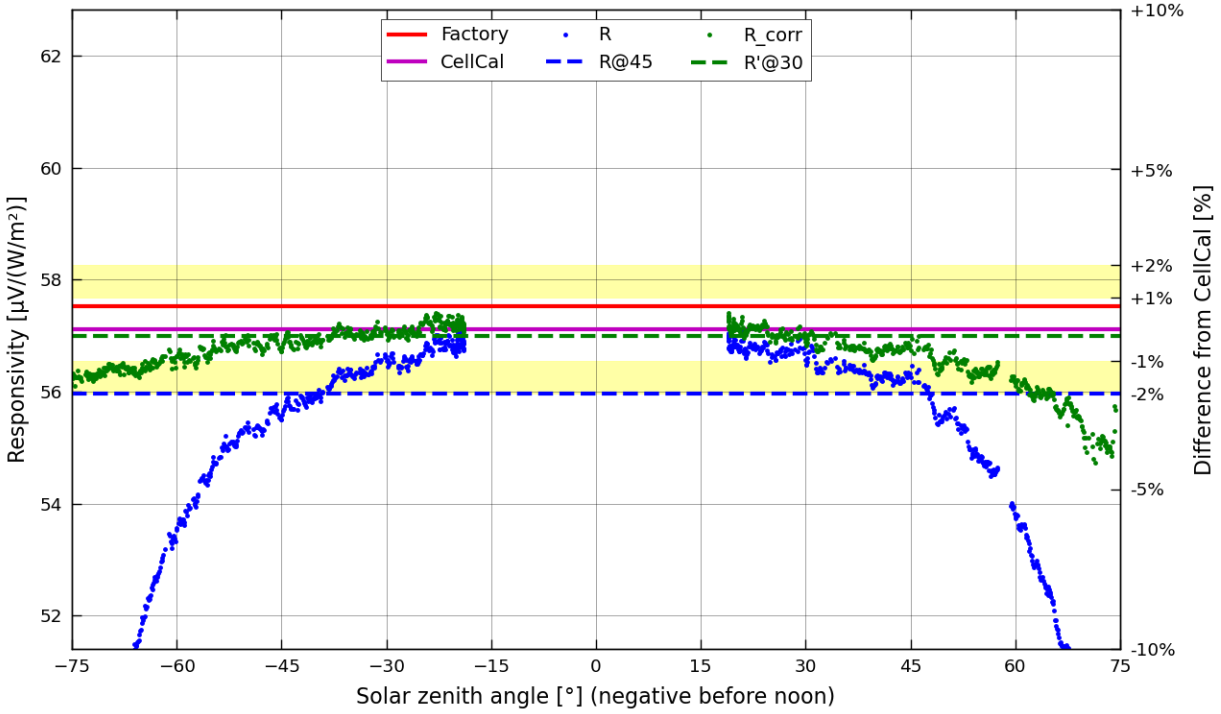

Figure B-39 Detailed results for IMT Si-mV-85-PT1000 s/n 17-18120001
obtained during Borcal session 2019-04

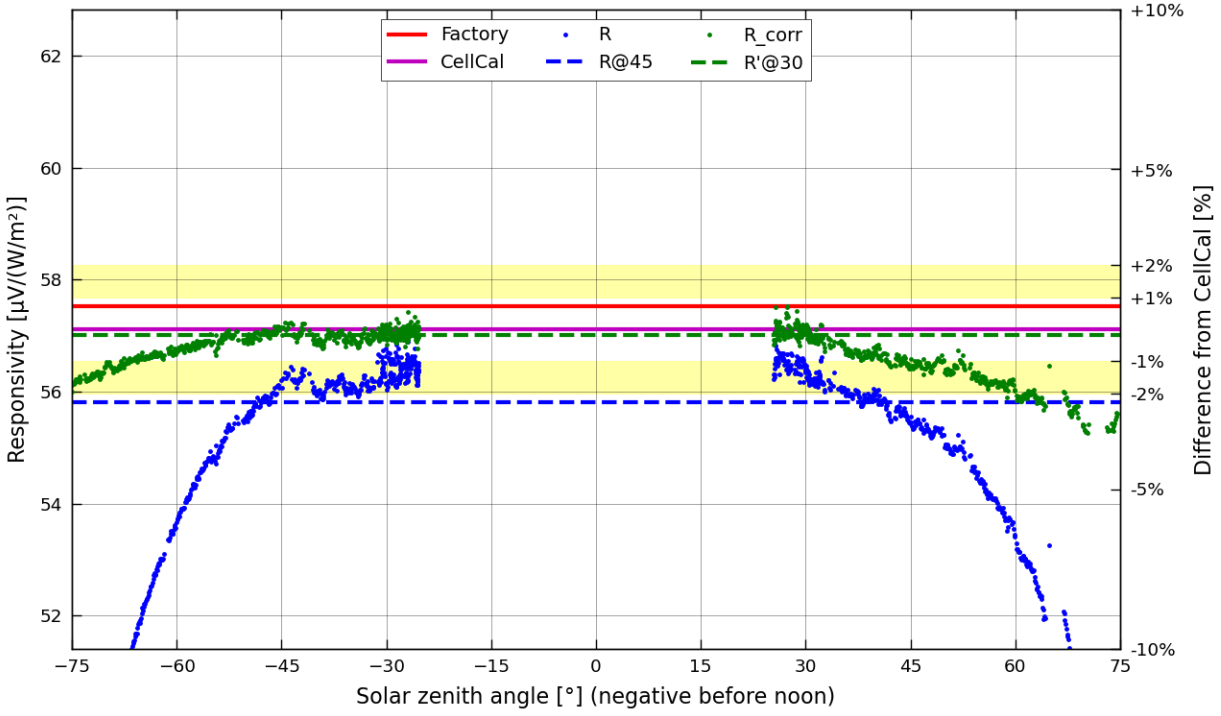

Figure B-40 Detailed results for IMT Si-mV-85-PT1000 s/n 17-18120001
obtained during Borcal session 2019-05

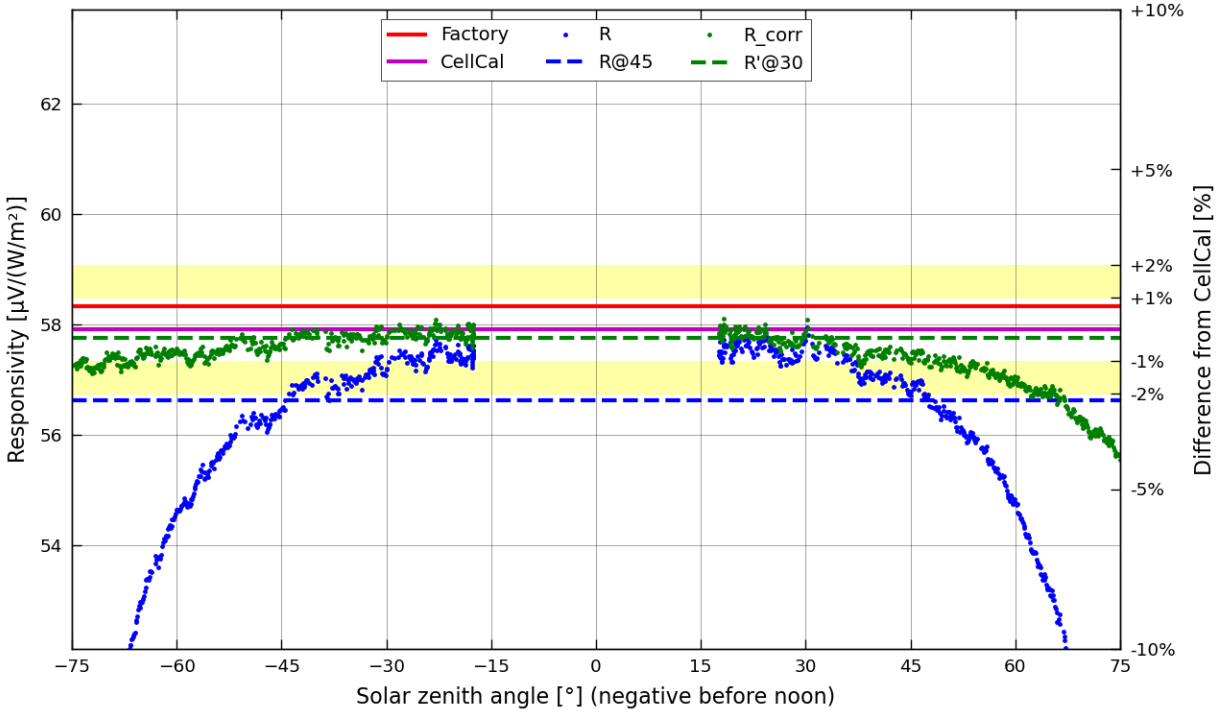

Figure B-41 Detailed results for IMT Si-mV-85-PT1000 s/n 17-18120002 obtained during Borcal session 2019-03

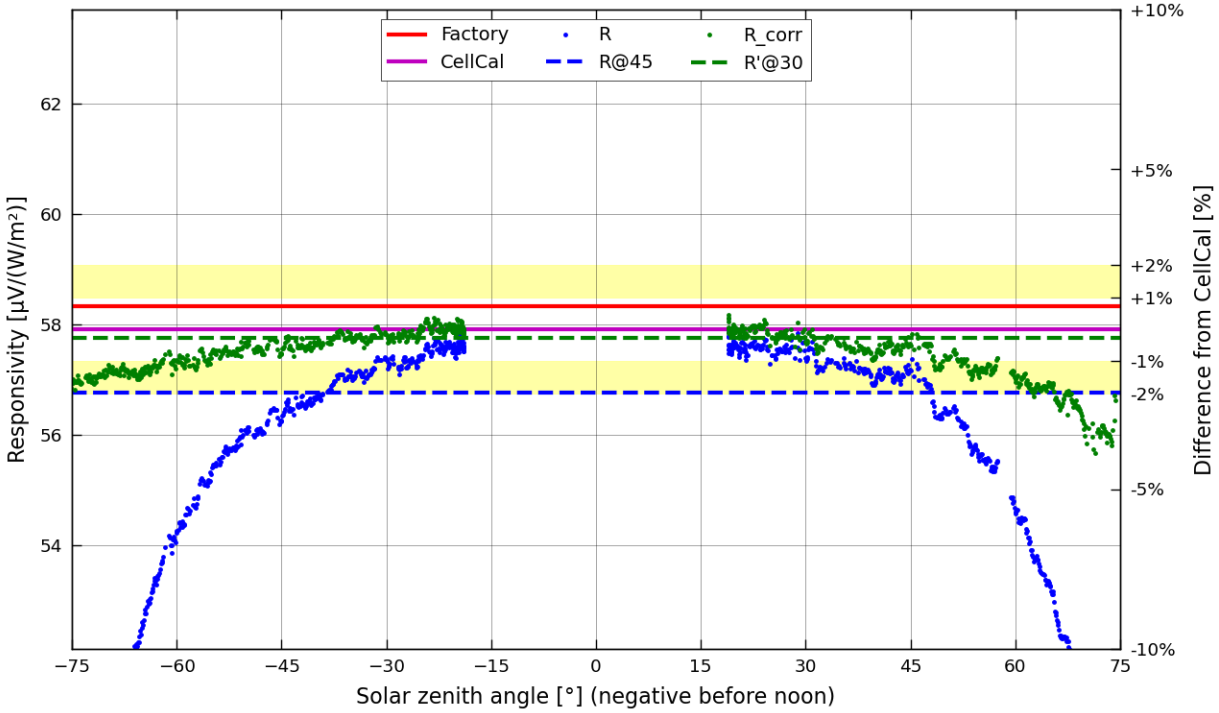

Figure B-42 Detailed results for IMT Si-mV-85-PT1000 s/n 17-18120002 obtained during Borcal session 2019-04

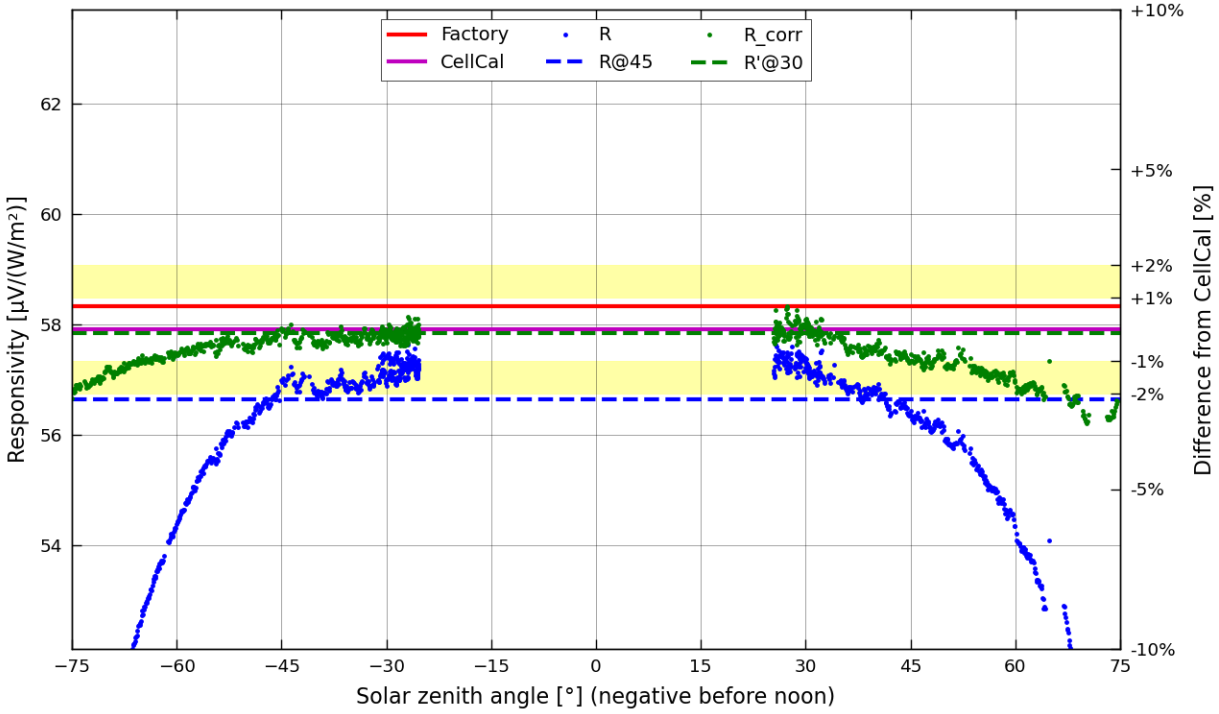

Figure B-43 Detailed results for IMT Si-mV-85-PT1000 s/n 17-18120002
obtained during Borcal session 2019-05

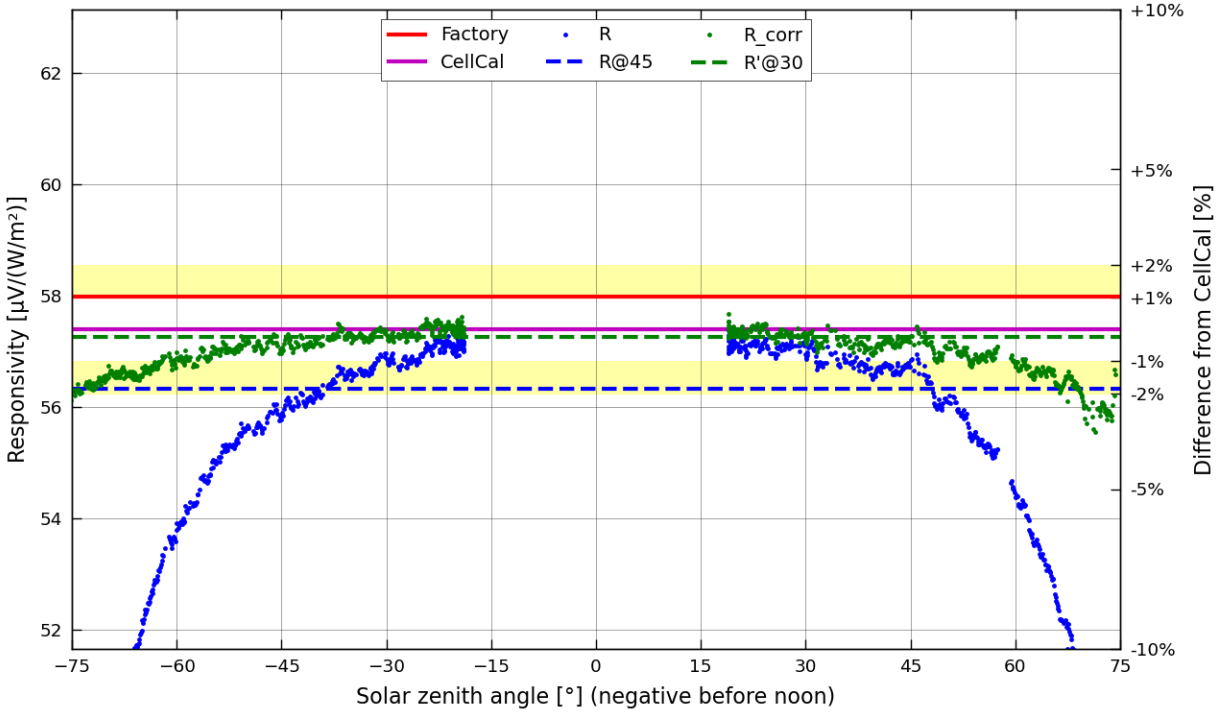

Figure B-44 Detailed results for IMT Si-mV-85-PT1000 s/n 17-18120003
obtained during Borcal session 2019-04

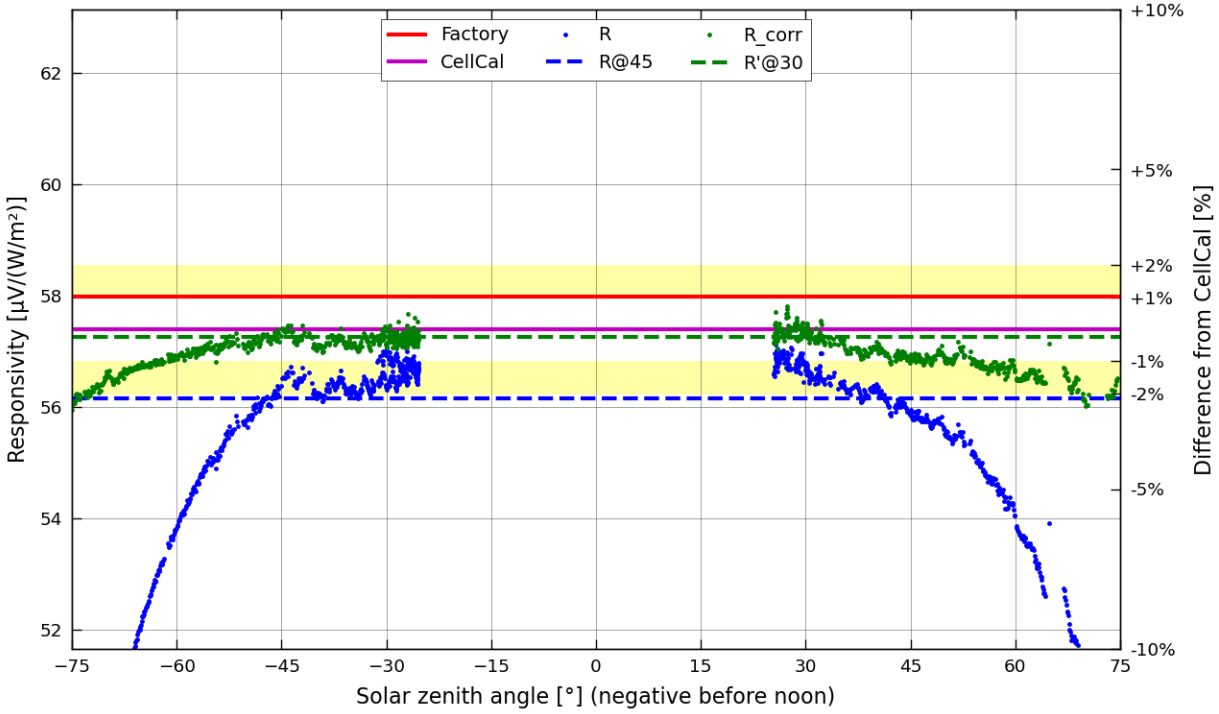

Figure B-45 Detailed results for IMT Si-mV-85-PT1000 s/n 17-18120003
obtained during Borcal session 2019-05

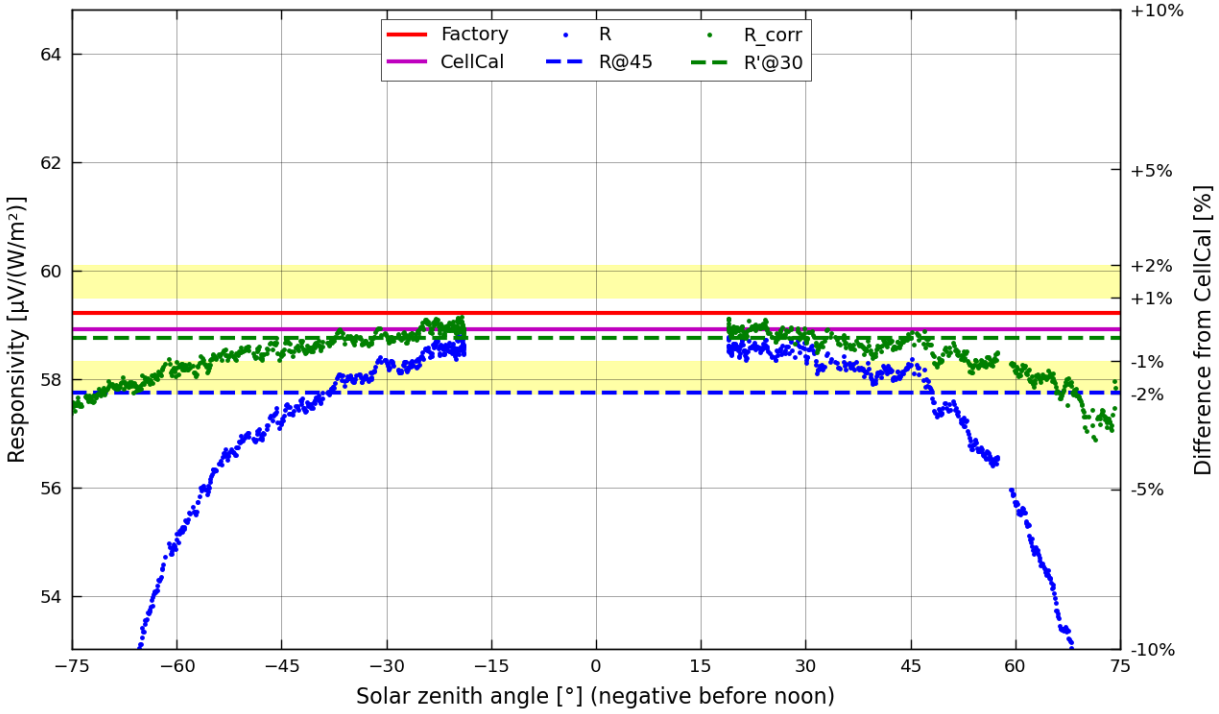

Figure B-46 Detailed results for IMT Si-mV-85-PT1000 s/n 17-18120004
obtained during Borcal session 2019-04

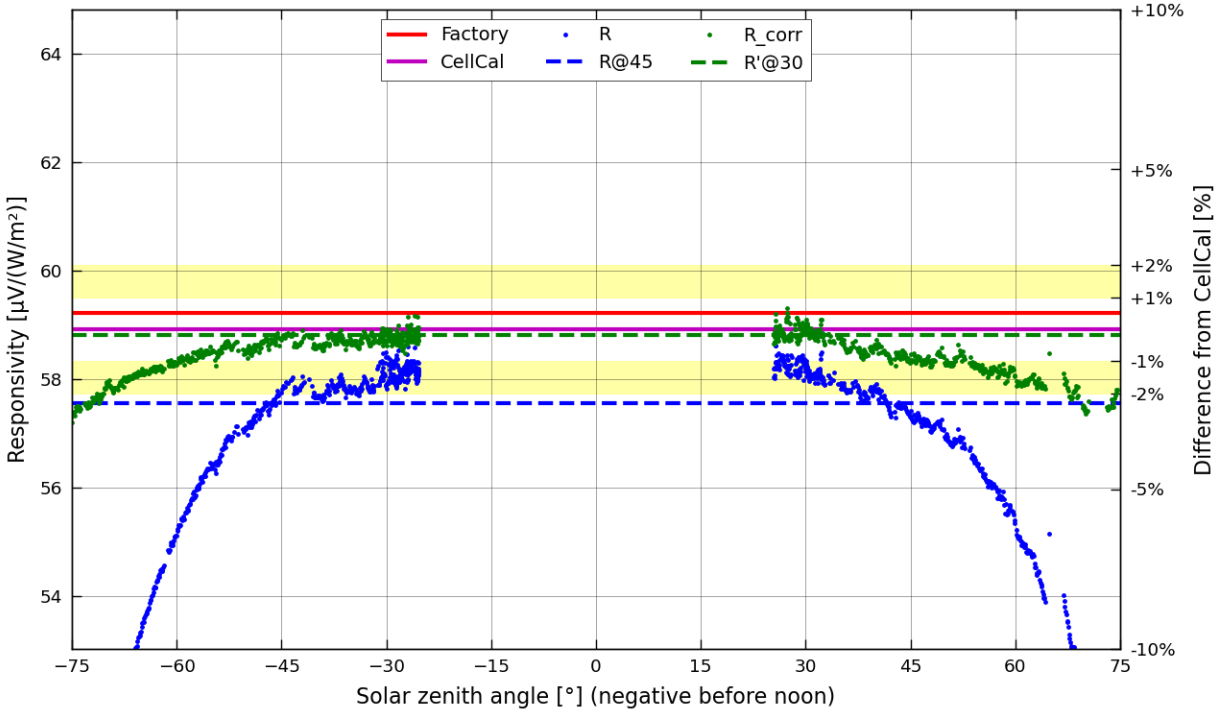

Figure B-47 Detailed results for IMT Si-mV-85-PT1000 s/n 17-18120004
obtained during Borcal session 2019-05

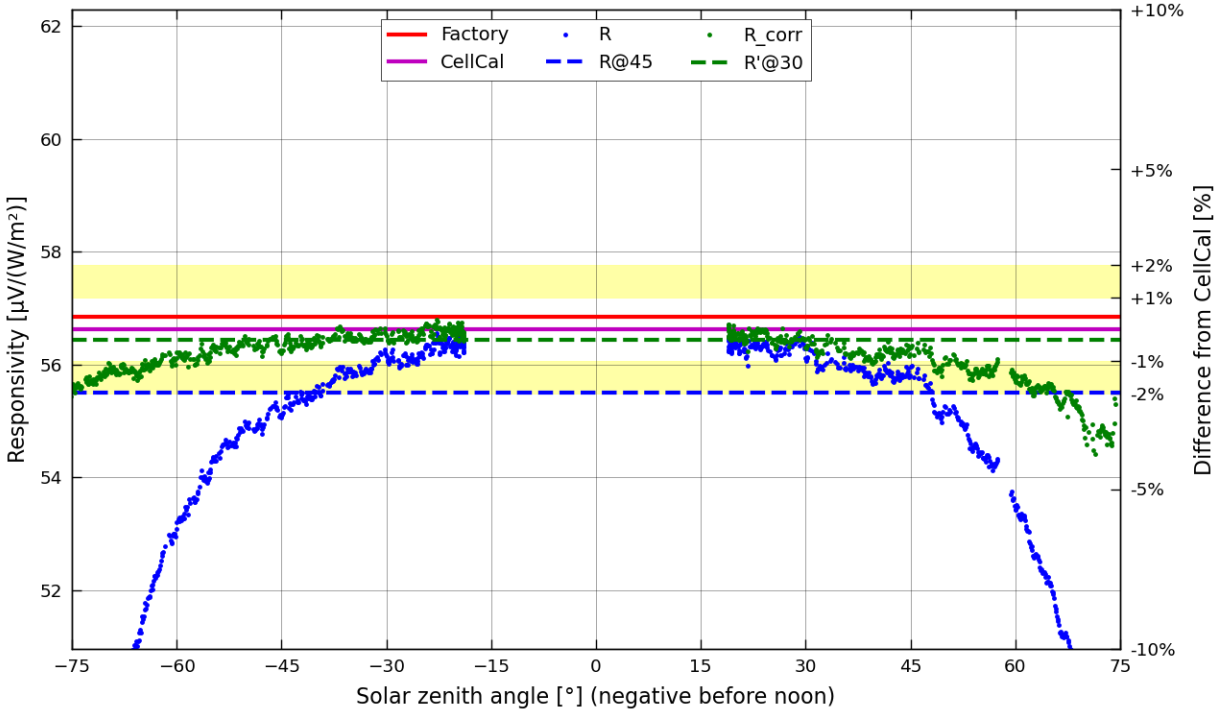

Figure B-48 Detailed results for IMT Si-mV-85-PT1000 s/n 17-18120005
obtained during Borcal session 2019-04

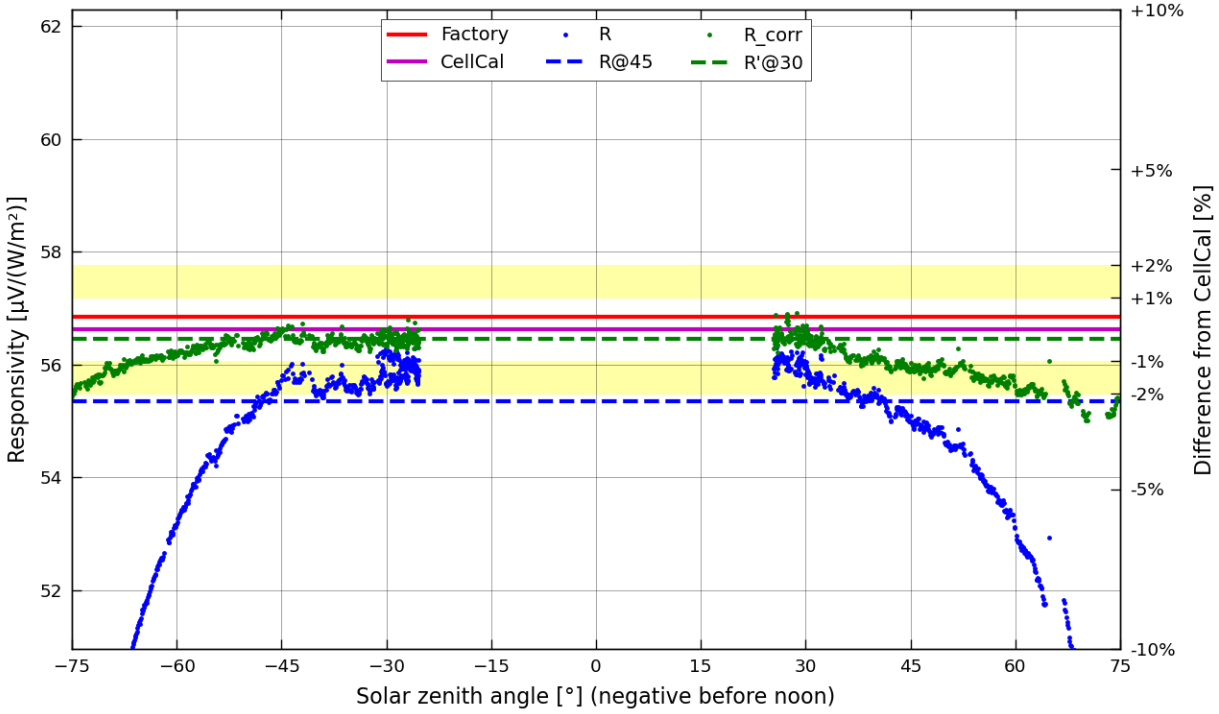

Figure B-49 Detailed results for IMT Si-mV-85-PT1000 s/n 17-18120005
obtained during Borcal session 2019-05

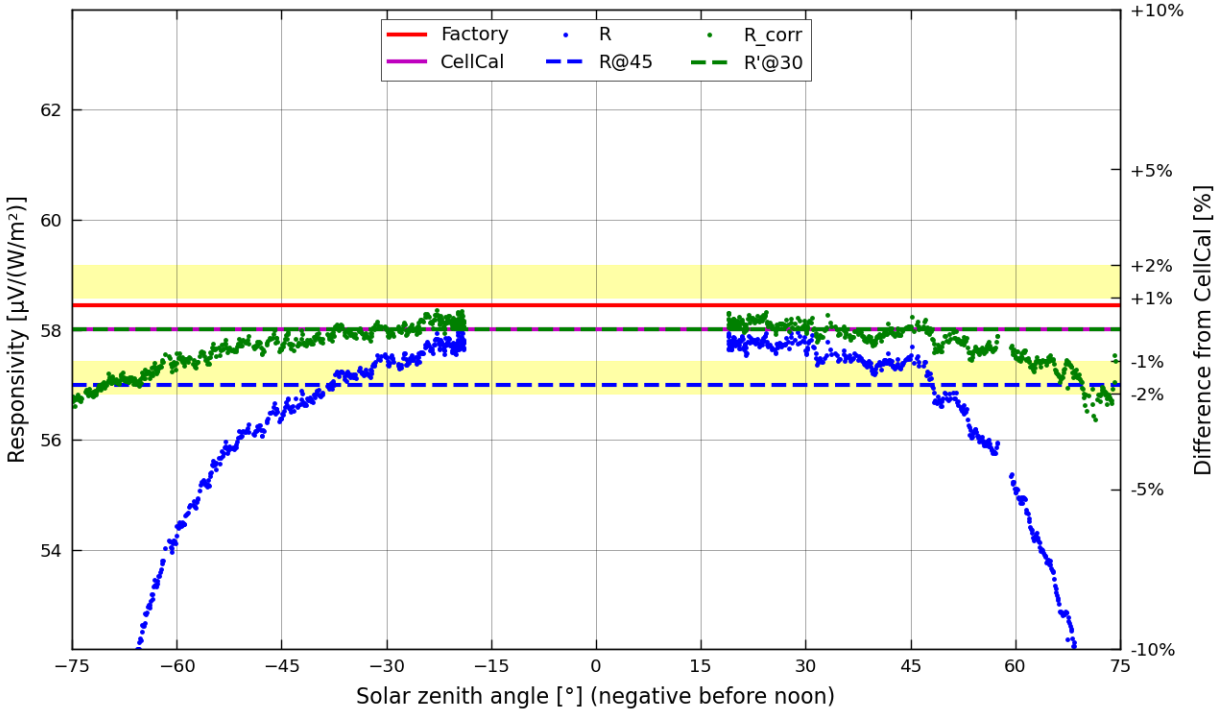

Figure B-50 Detailed results for IMT Si-mV-85-PT1000 s/n 17-18120006
obtained during Borcal session 2019-04

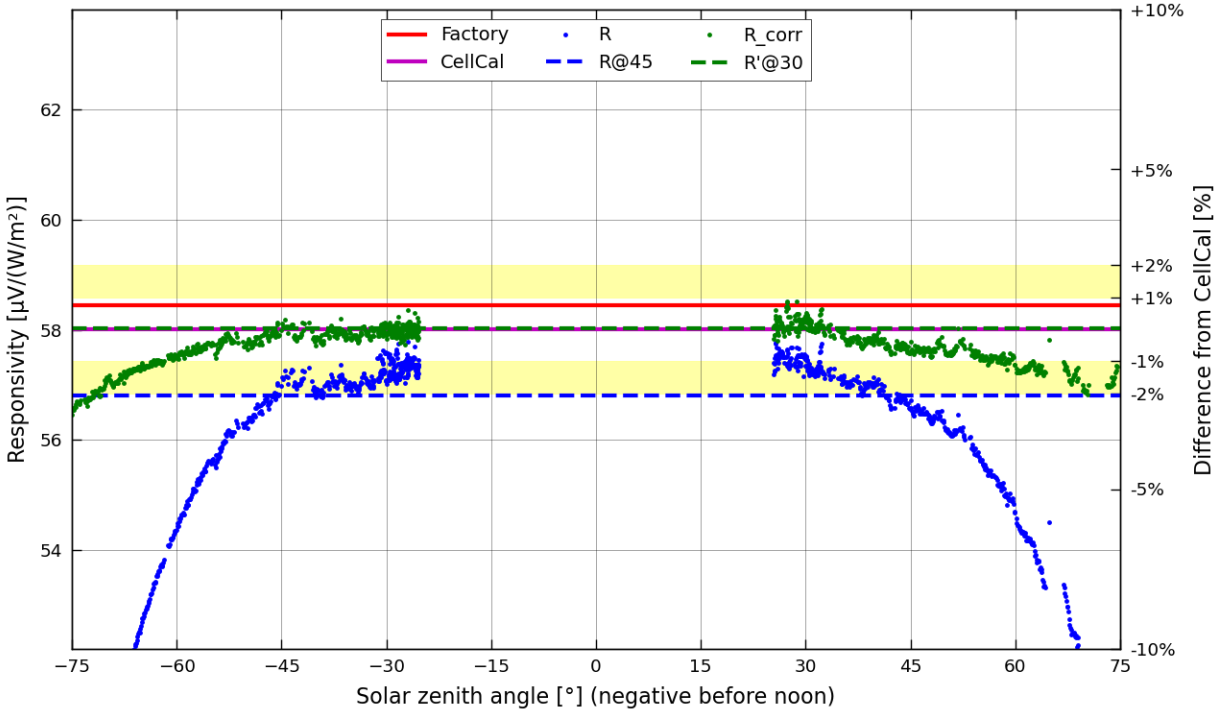

Figure B-51 Detailed results for IMT Si-mV-85-PT1000 s/n 17-18120006
obtained during Borcal session 2019-05

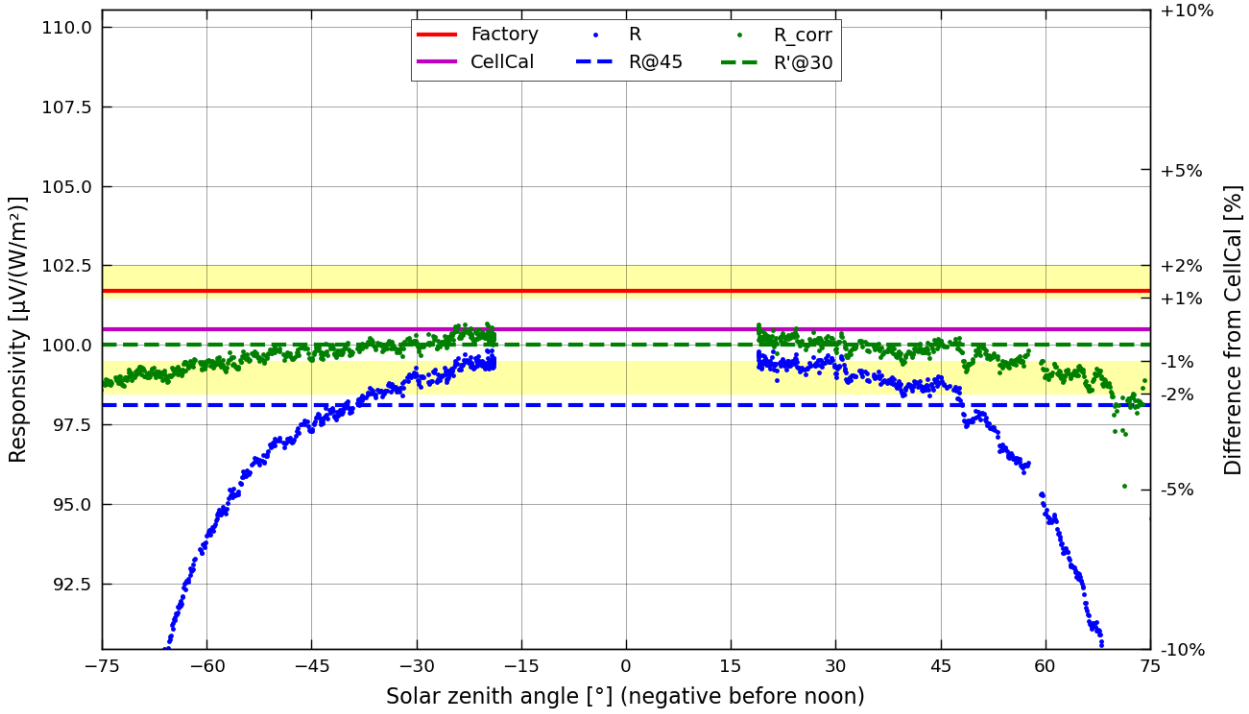

Figure B-52 Detailed results for NES SOZ-03 s/n 14309
obtained during Borcal session 2019-04

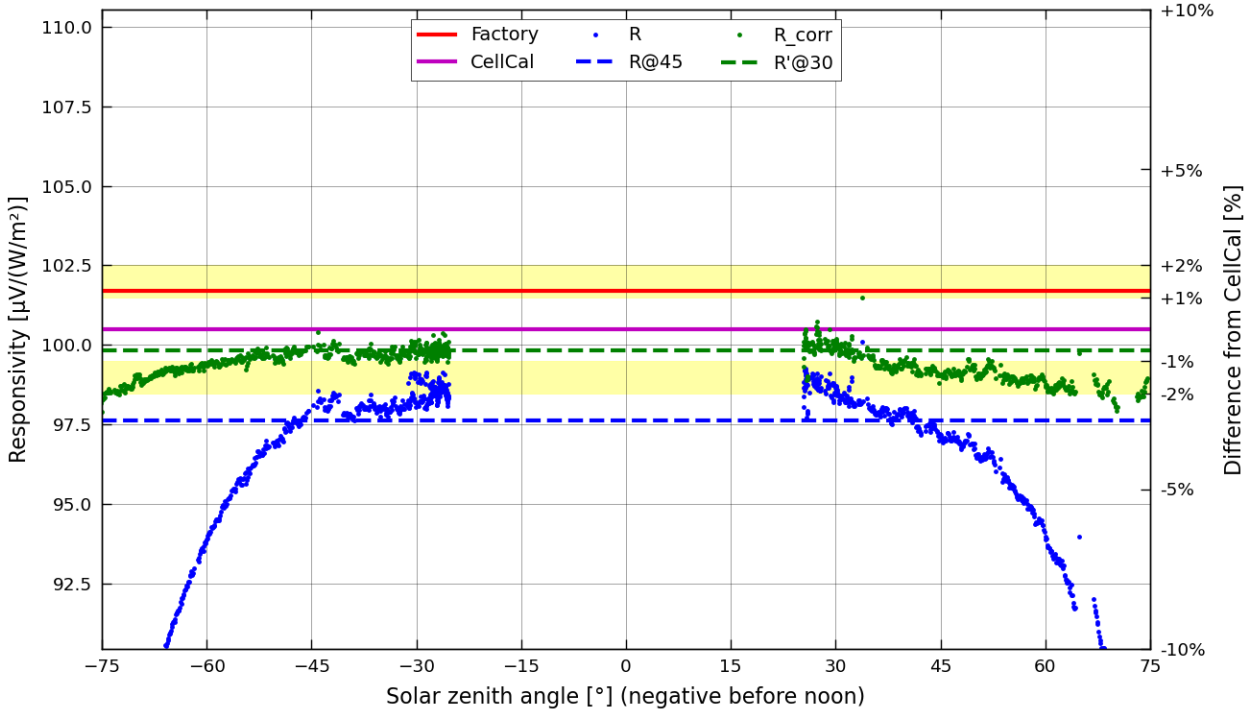

Figure B-53 Detailed results for NES SOZ-03 s/n 14309
obtained during Borcal session 2019-05

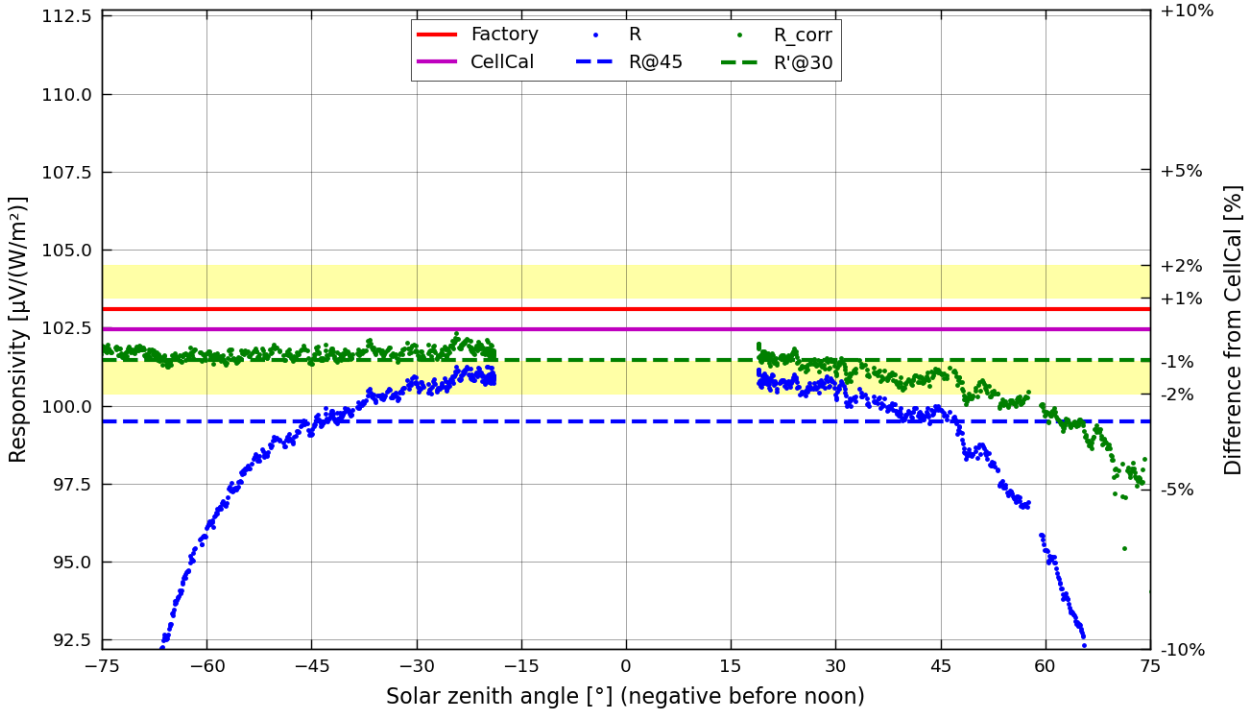

Figure B-54 Detailed results for NES SOZ-03 s/n 14310
obtained during Borcal session 2019-04

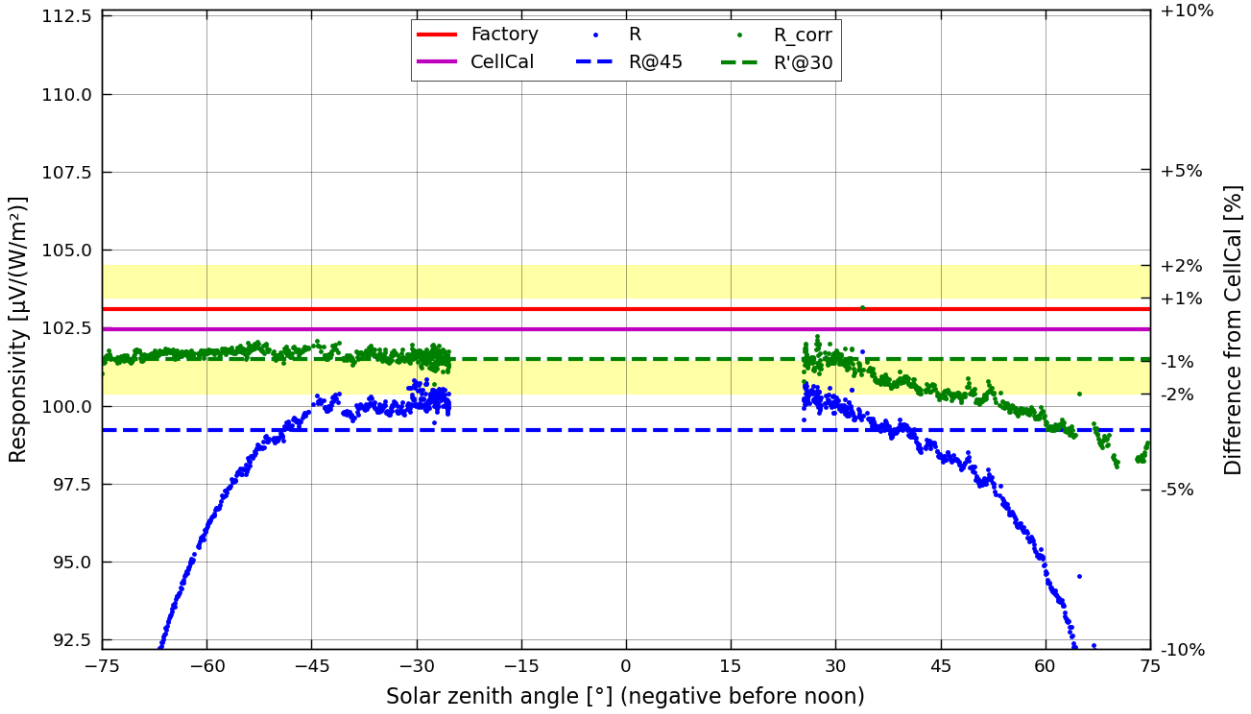

Figure B-55 Detailed results for NES SOZ-03 s/n 14310
obtained during Borcal session 2019-05

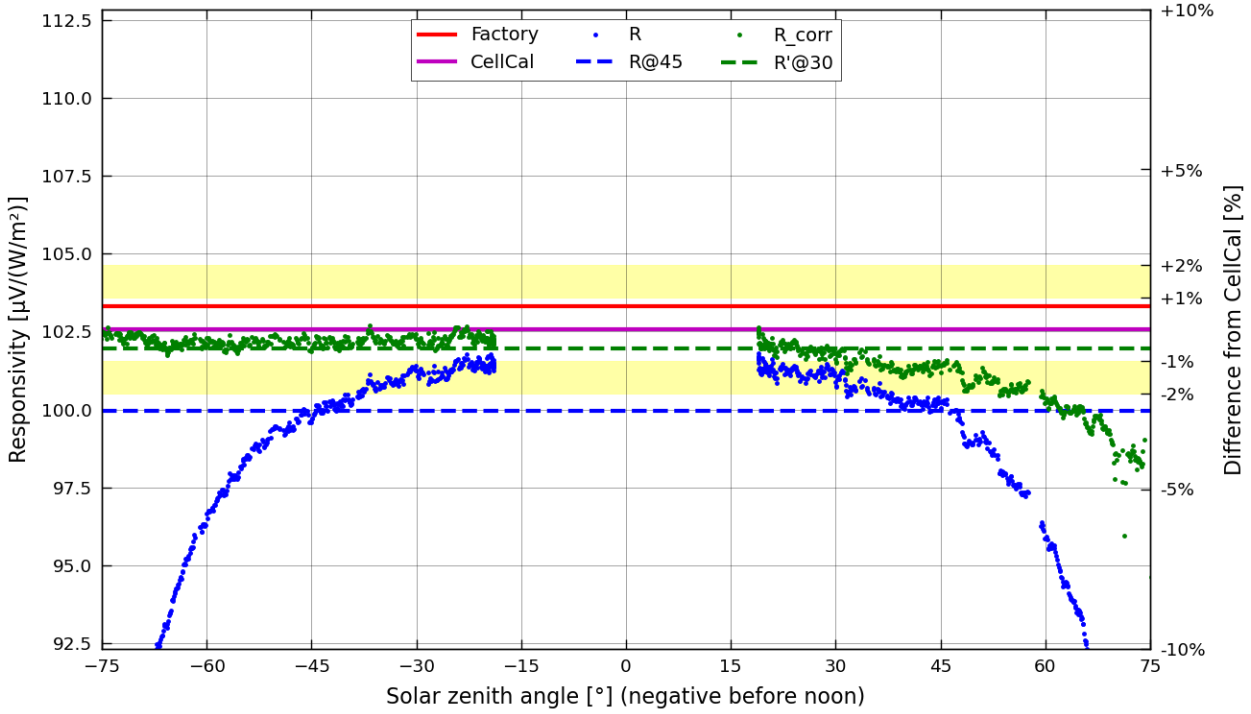

Figure B-56 Detailed results for NES SOZ-03 s/n 14311
obtained during Borcal session 2019-04

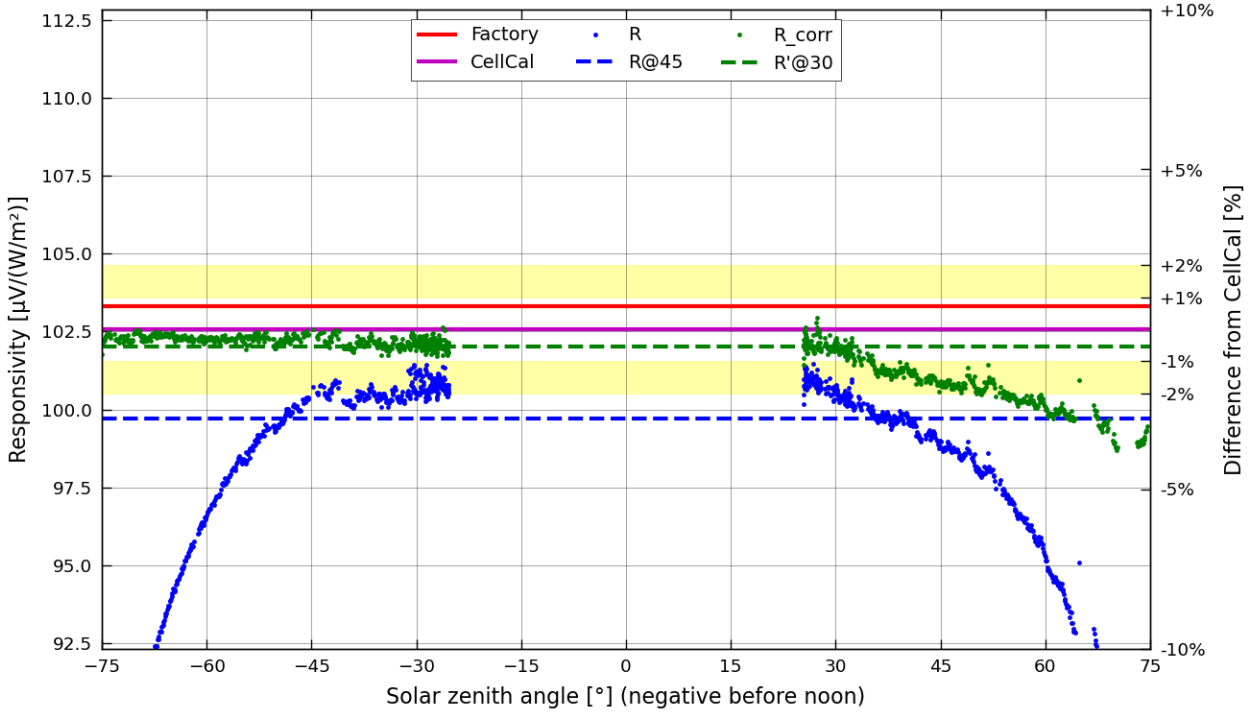

Figure B-57 Detailed results for NES SOZ-03 s/n 14311
obtained during Borcal session 2019-05

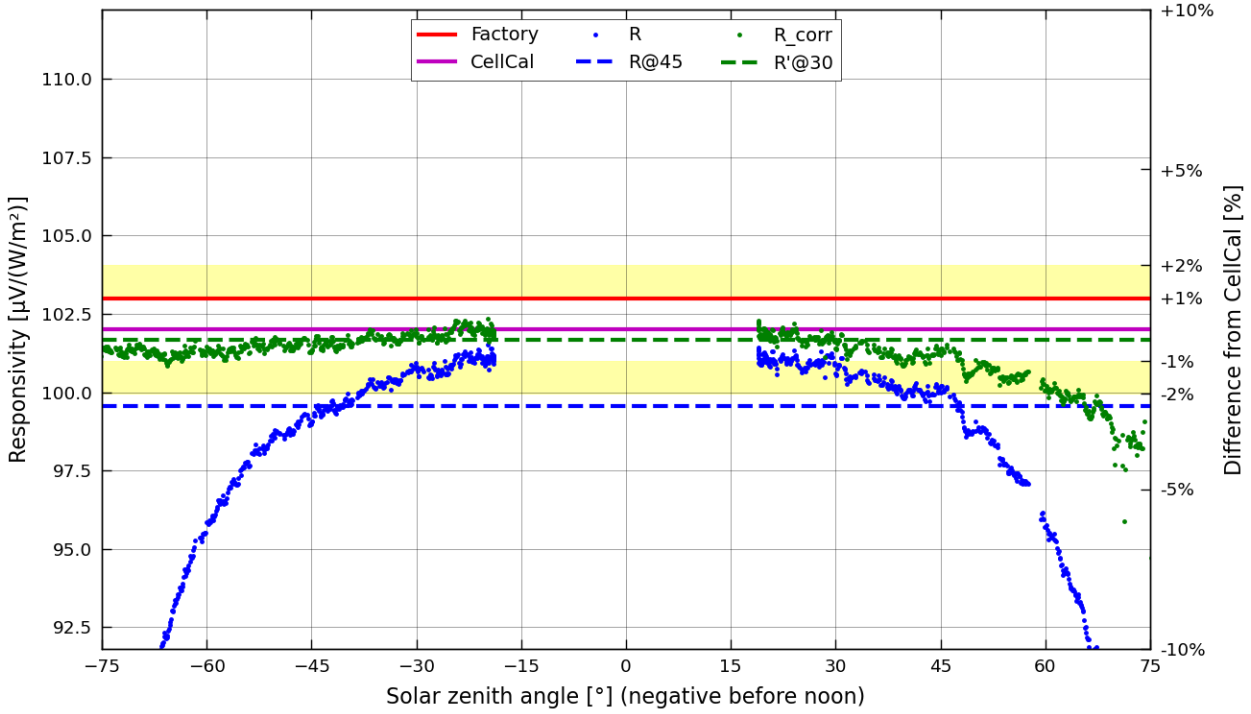

Figure B-58 Detailed results for NES SOZ-03 s/n 14312
obtained during Borcal session 2019-04

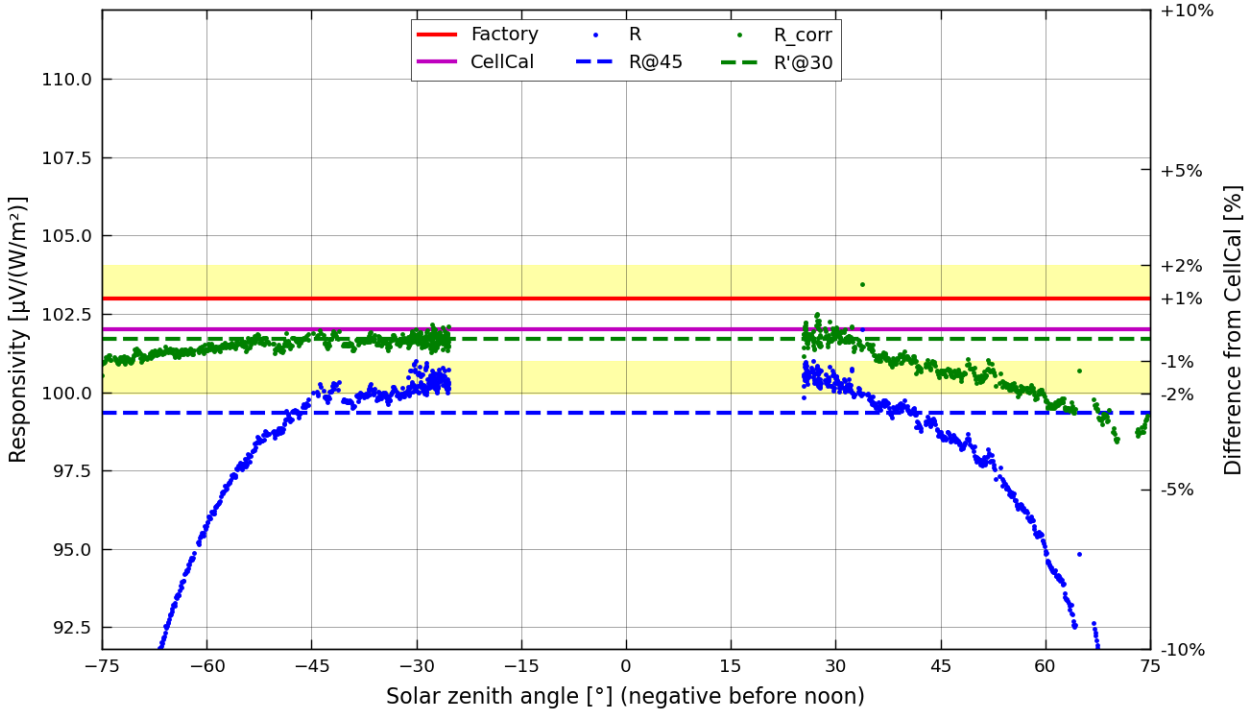

Figure B-59 Detailed results for NES SOZ-03 s/n 14312
obtained during Borcal session 2019-05

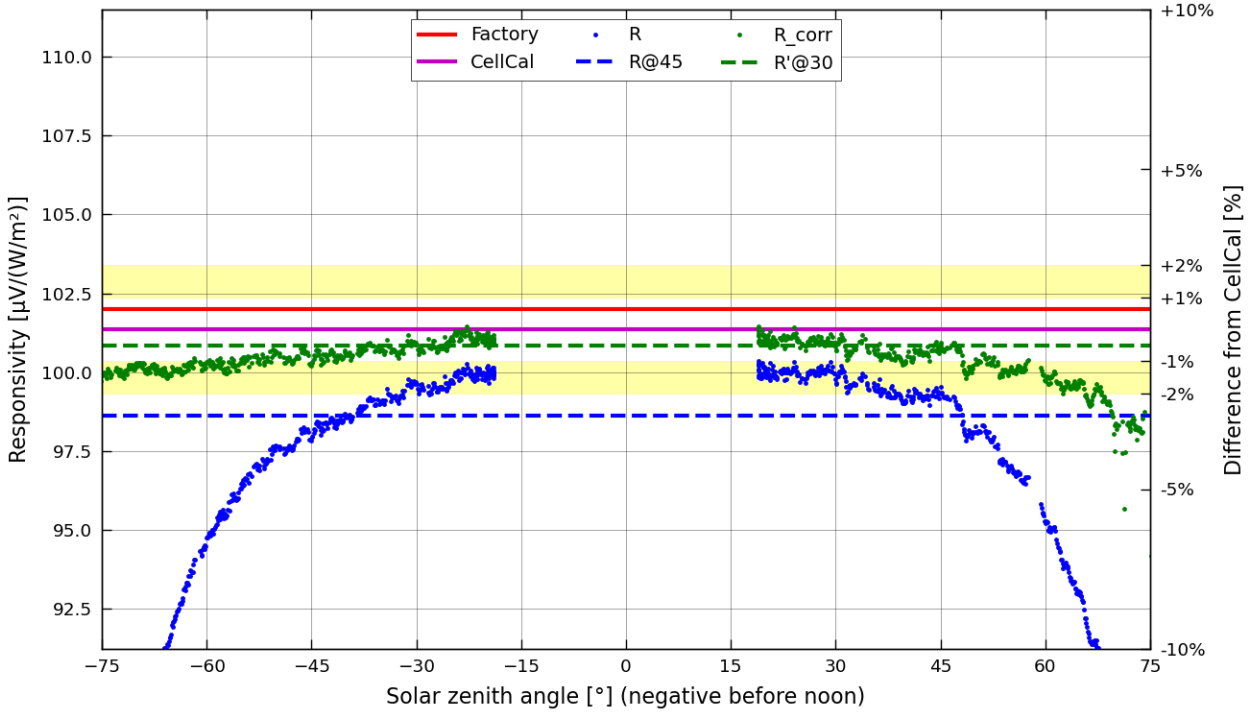

Figure B-60 Detailed results for NES SOZ-03 s/n 14313
obtained during Borcal session 2019-04

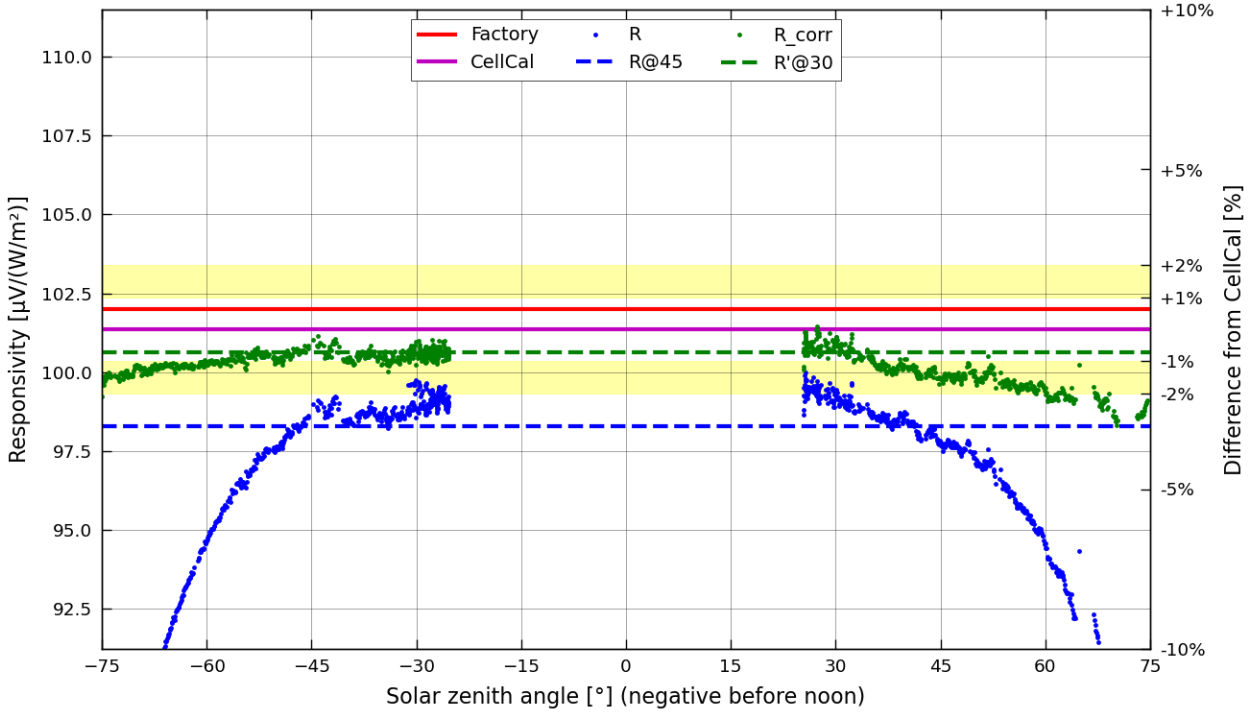

Figure B-61 Detailed results for NES SOZ-03 s/n 14313
obtained during Borcal session 2019-05

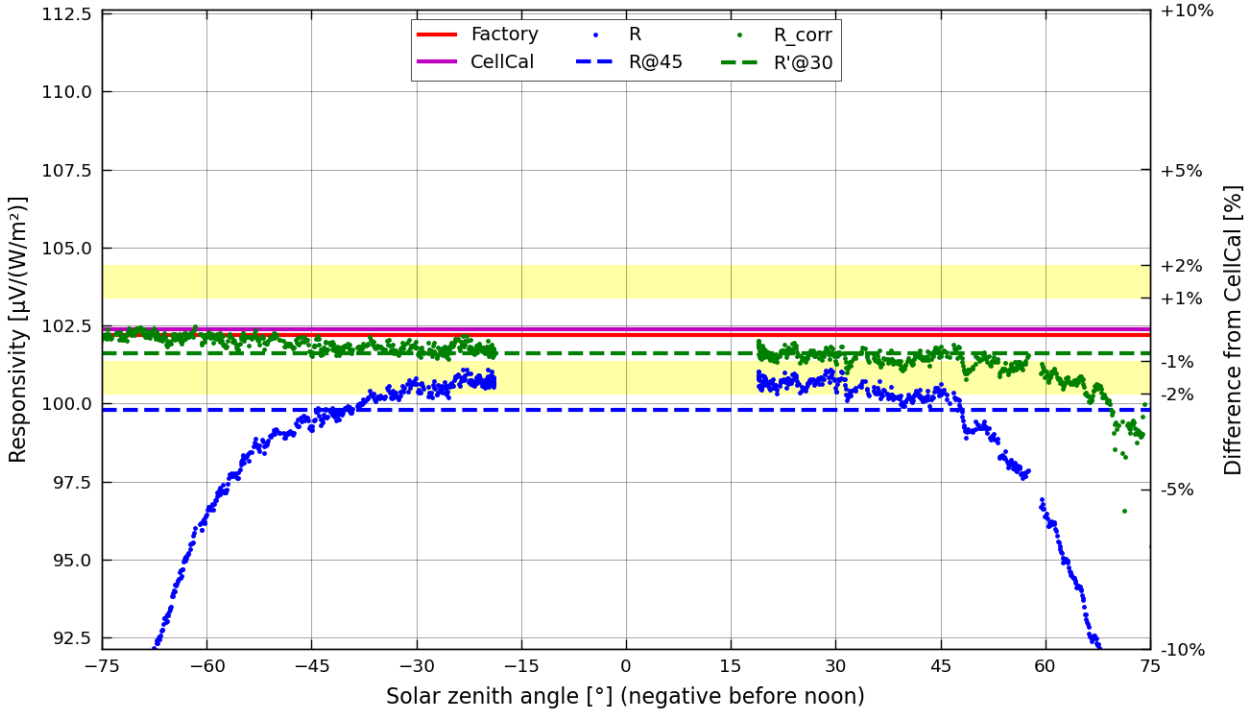

Figure B-62 Detailed results for NES SOZ-03-P s/n 14422
obtained during Borcal session 2019-04

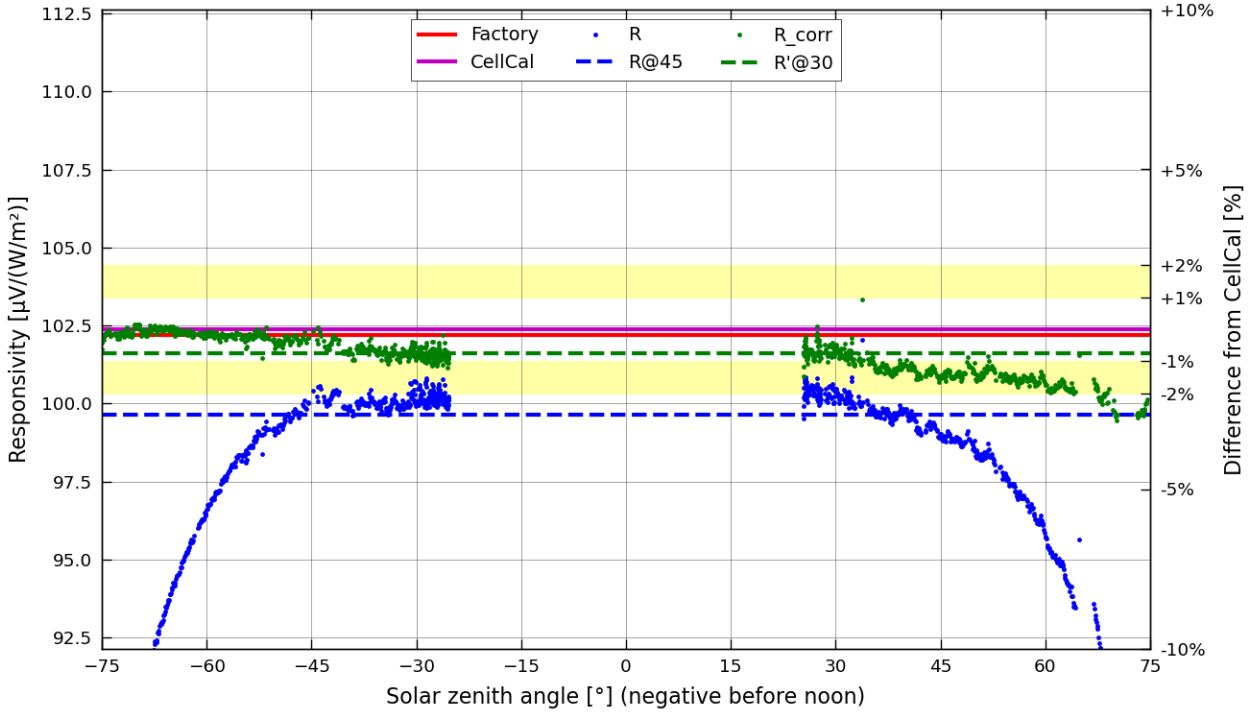

Figure B-63 Detailed results for NES SOZ-03-P s/n 14422
obtained during Borcal session 2019-05

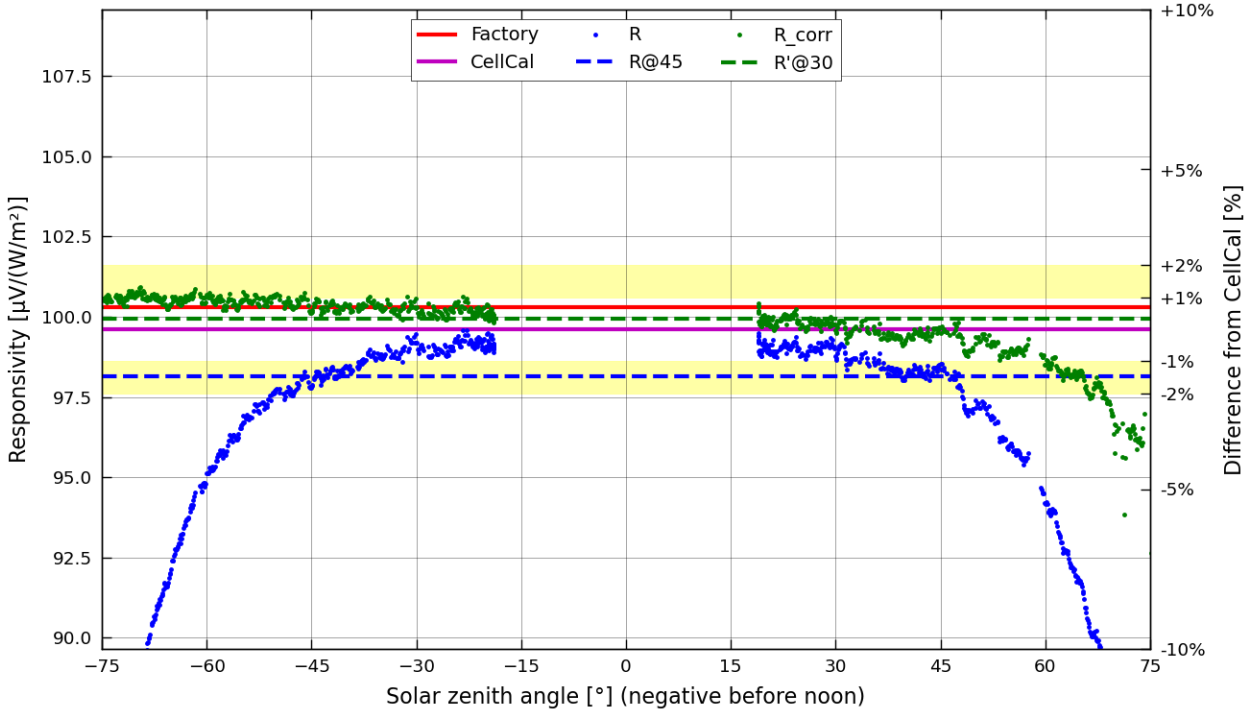

Figure B-64 Detailed results for NES SOZ-03-P s/n 14423
obtained during Borcal session 2019-04

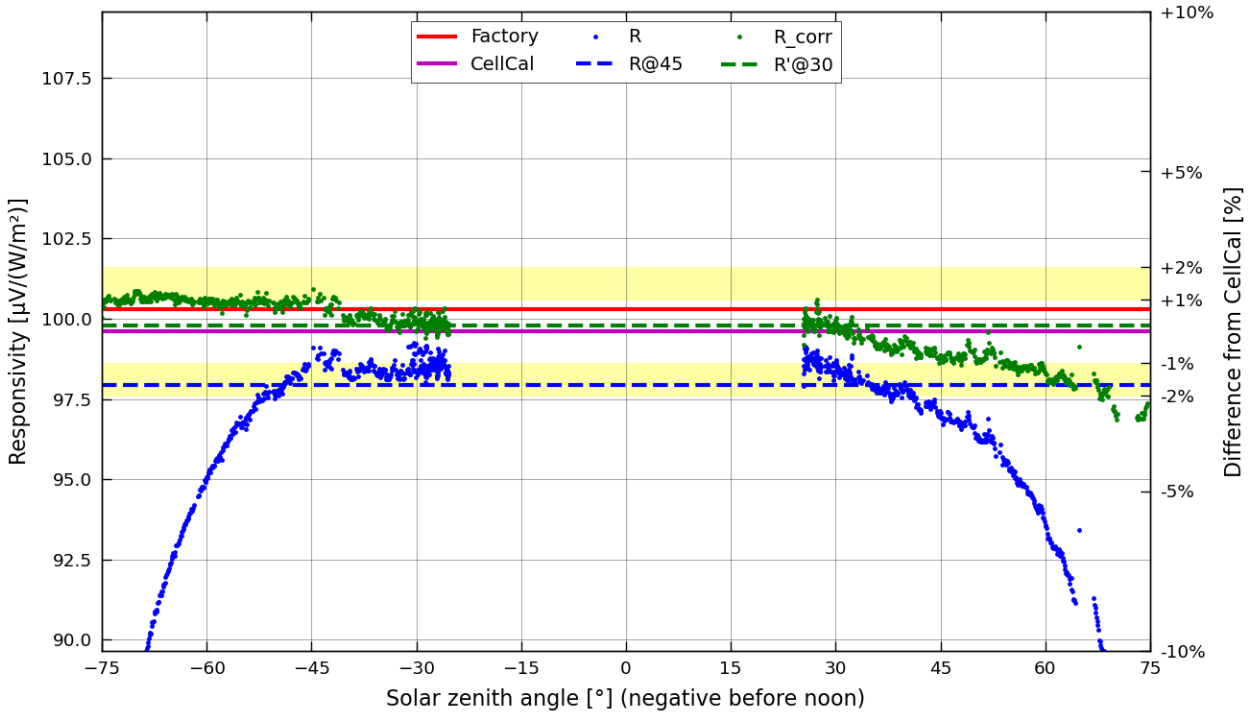

Figure B-65 Detailed results for NES SOZ-03-P s/n 14423
obtained during Borcal session 2019-05